SANDIA REPORT

SAND2007-2327
Unlimited Release
Printed April 2007

Collective Systems: Physical and Information Exergies

Rush D. Robinett, III and David G. Wilson

Prepared by
Sandia National Laboratories
Albuquerque, New Mexico 87185 and Livermore, California 94550

Sandia is a multiprogram laboratory operated by Sandia Corporation,
a Lockheed Martin Company, for the United States Department of Energy's
National Nuclear Security Administration under Contract DE-AC04-94-AL85000.

Issued by Sandia National Laboratories, operated for the United States Department of Energy by Sandia Corporation.

Available to DOE and DOE contractors from
U.S. Department of Energy
Office of Scientific and Technical Information
P.O. Box 62
Oak Ridge, TN 37831

Telephone: (865) 576-8401
Facsimile: (865) 576-5728
E-Mail: reports@adonis.osti.gov
Online ordering: http://www.osti.gov/bridge

Available to the public from
U.S. Department of Commerce
National Technical Information Service
5285 Port Royal Rd
Springfield, VA 22161

Telephone: (800) 553-6847
Facsimile: (703) 605-6900
E-Mail: orders@ntis.fedworld.gov
Online ordering: http://www.ntis.gov/help/ordermethods.asp?loc=7-4-0#online

SAND2007-2327
Unlimited Release
Printed April 2007

Collective Systems: Physical and Information Exergies

Rush D. Robinett, III
Energy & Infrastructure Future Group

David G. Wilson
Energy Systems Analysis Department

Sandia National Laboratories
P.O. Box 5800
Albuquerque, NM 87185-1108

Abstract

Collective systems are typically defined as a group of agents (physical and/or cyber) that work together to produce a collective behavior with a value greater than the sum of the individual parts. This amplification or synergy can be harnessed by solving an inverse problem via an information-flow/communications grid: given a desired macroscopic/collective behavior find the required microscopic/individual behavior of each agent and the required communications grid. The goal of this report is to describe the fundamental nature of the Hamiltonian function in the design of collective systems (solve the inverse problem) and the connections between and values of physical and information exergies intrinsic to collective systems. In particular, physical and information exergies are shown to be equivalent based on thermodynamics and Hamiltonian mechanics.

Acknowledgment

The authors would like to thank Steven Goldsmith, Department 05633, Barry Spletzer, Group 06470, John Wagner, Department 06341, and John Feddema, Department 06473 for their insights into these concepts involving collective systems. Thanks to Al Reed, Department 06852 for his original contribution [1] associated with the "nonlinear satellite exergy analysis." The authors would also like to thank Robert Glass, Randall LaViolette, and George Barr of Department 06326, and Walt Beyeler, Department 06322 for their technical review of this report.

Last but not least, the authors thank Tim Berg, Department 05624 for his original contributions associated with Fisher Information [2] and technical review of this report.

The authors also realize that there may be multiple meanings and interpretations of many of the definitions in this report such as; self organization, criticality, self-organized criticality, complexity, complex systems, adaptation, complex adaptive systems, etc. Our hope is that in this report the definitions may be acceptable within the context of their usage and that in the future, we may strive to establish a more robust common set of definitions and understanding, leading to some form of standardization.

Contents

List of Figures

Chapter 1

Introduction to Collective Systems

One way to describe collective systems is by way of a mechanics-based analogy. For example, the aerodynamic coefficients (lift, drag, etc.) for a re-entry vehicle, such as the Space Shuttle, moving from the exoatmosphere (which is modeled using rarified gas dynamics) to sea level (which is modeled using continuum mechanics) are analogous to the parameters that describe the dynamics of small numbers of robots to millions. Figure 1.1 depicts a fluid mechanics analogy of a swarm of robotic agents. The basic controlling parameter is

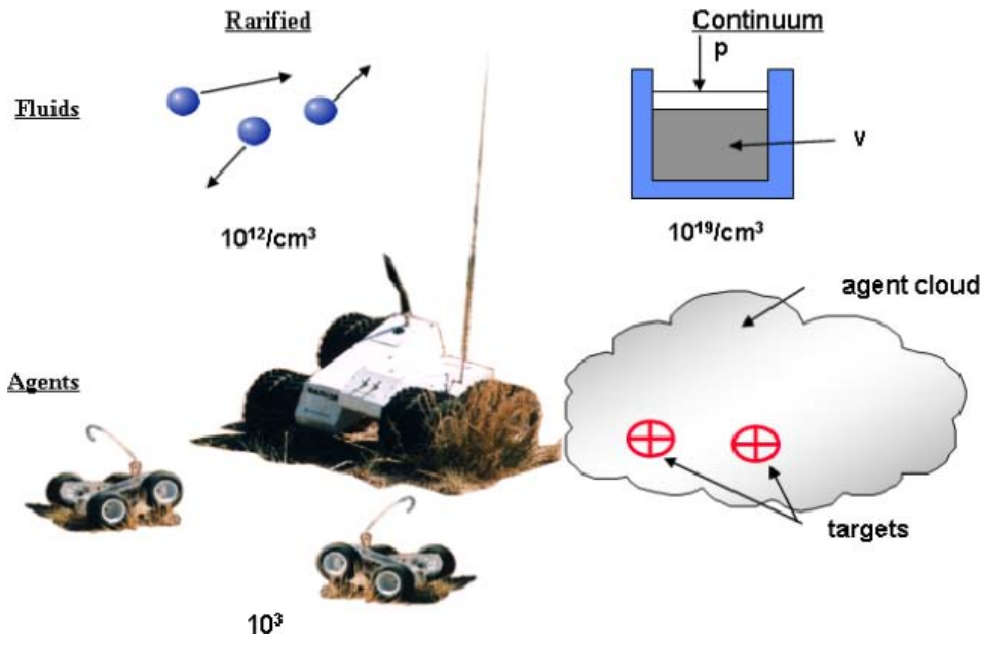

Figure 1.1. Transition from discrete to continuum models (illustrative example)

the mean free path between collisions of molecules, which relates to the size of particles (or robots) and density. To be specific, the mean free path is defined as [3]

$$\lambda = \frac{1}{\sqrt{2}\pi d^2 \bar{n}}$$

where

d = diameter of the molecule
$\bar{n}$ = number of molecules per unit volume.

The mean free path determines the method used to calculate the aerodynamic coefficients from rarified gas dynamics which models many individual molecules in a Monte Carlo setting, through a transitional phase which mixes individual molecule models with continuum models, to continuum mechanics. This analogy, robot diameter and robot density, leads directly to the applications of statistical mechanics, continuum mechanics, calculus of variations, chemical kinetics, and quantum mechanics, which address the analysis of a single particle (agent) to millions of particles (agents).

The basic mechanics-based strategy of analyzing and designing collective systems is presented in Figure 1.2. The fundamental building block is the Hamiltonian function which is

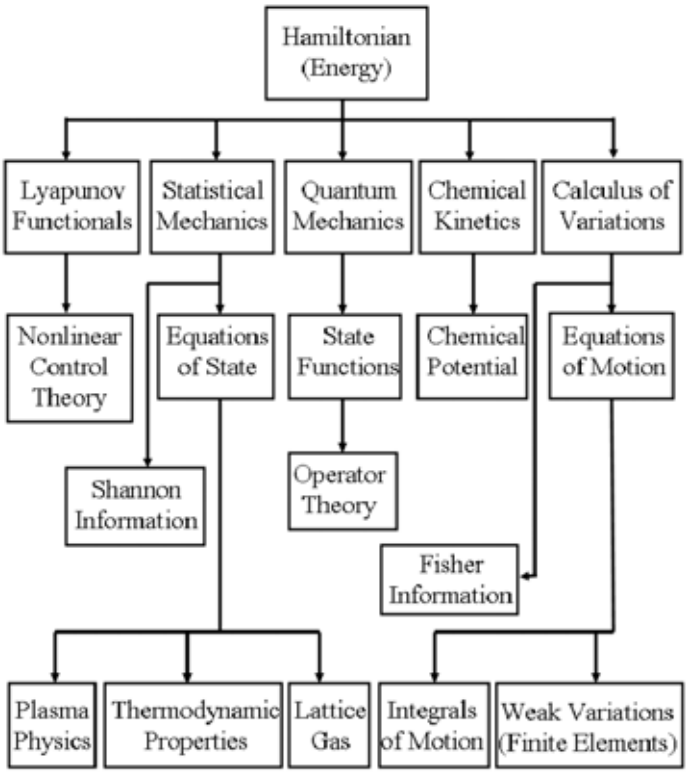

Figure 1.2. Flowchart describing mechanics based approaches for collective systems

the total energy for conservative systems (i.e., external forces can be modeled as potential

functions) [4]. In section B.2, the Hamiltonian will be redefined as the stored exergy in a system based on an irreversible thermodynamics interpretation.

In general, these techniques can be divided into microscopic and macroscopic tools. Calculus of variations and quantum mechanics are typically used for microscopic analysis, whereas statistical mechanics and chemical kinetics are used for macroscopic analysis, even though there exists some overlap among these techniques. Microscopic tools are necessary to complete the inverse problem: transform the desired or designed macroscopic/collective behavior into the microscopic/individual behavior of each agent.

To be more specific, at the core of the mechanics-based strategy is Hamilton's principle. The Hamiltonian is a scalar function that is used to develop the evolution of dynamical systems; these dynamical systems can be either deterministic or statistical. Hamilton's principle assumes that the systems under consideration are characterized by two energy (stored exergy) functions: a kinetic energy and a potential energy. This paper utilizes the extended Hamilton's principle [5] which accounts for nonconservative forces to connect Hamiltonian mechanics, irreversible and nonequilibrium thermodynamics, nonlinear control theory (from Lyapunov functionals), and self-organizing systems to collective systems by way of information theory. The rest of this report develops the statistical mechanics and calculus of variations pathways which culminate in equivalences between physical and information exergies for equilibrium and non-equilibrium collective systems.

This report is divided up into 4 chapters and 4 appendices. In Chapter 1 collective systems as well as microscopic and macroscopic tools were introduced. Chapter 2 applies these techniques to equilibrium systems. Chapter 3 applies these techniques to time-dependent and nonequilibrium systems. Chapter 4 provides a summary and recommendations for future work. Appendix A presents Fisher Information. Appendix B defines exergy based on thermodynamics, describes the connections between thermodynamics and Hamiltonian mechanics, and then derives the necessary and sufficient conditions for stability, control, and performance of nonlinear systems. Appendix C extends the nonlinear exergy/entropy control design in Appendix B to collective systems. Appendix D introduces and defines the concept of limit cycles for both linear and nonlinear systems and gives a new concept for the investigation of extended eigen analysis for nonlinear systems as: "the power flow principle of stability for nonlinear systems."

Chapter 2

Equilibrium Collective Systems

Statistical and continuum mechanics involve the analysis of the collective behavior of large groups of objects, usually molecules, by relatively simple macroscopic means. Many mathematical and intuitive rules have been developed that allow relatively easy handling of problems that would become quickly intractable if particles were to be analyzed individually.

One of the simplest examples of these relationships is the ideal gas law, which provides a simple algebraic relationship between the pressure, volume, and temperature of an ideal gas. In reality, an ideal gas consists of many individual particles, on the order of 10^{20} molecules per cubic centimeter, with the particles following much more complex relationships than the ideal gas law itself. However, the application of statistical mechanics to derive a continuum approximation, allows this otherwise intractable problem to be handled easily. This is accomplished by generating a Hamiltonian, forming a partition function, and calculating the mean values. This framework is used to solve an inverse control problem. The inverse control problem involves envisioning a collective behavior of a swarm of robots that is desirable, and from this, determining the set of rules that individual robots must follow to produce the desired swarm behavior in the form of interaction potential fields.

To demonstrate these concepts with an example, it is given that a swarm of robots will be used to search a volume for a target (see Fig. 2.1). One can analyze the long term (as $t \rightarrow \infty$) collective behavior of the robot swarm by analogy with equilibrium thermodynamics. The application of statistical mechanics begins with generating a Hamiltonian for an ideal gas of non-interacting (non-communicating) robots within an empty volume (see Fig. 2.2).

$$\mathcal{H} = \mathcal{T} + \mathcal{V} = E = \sum_{i=1}^{N} \frac{p_i^2}{2m} + \mathcal{V}(\mathbf{r}) \tag{2.1}$$

followed by forming a partition function [8]

$$Z = \int\int e^{-\beta E} \frac{d^f \mathbf{p} d^f \mathbf{r}}{h^f} = \frac{1}{N!} \left[\int\int e^{-\beta(\mathbf{p}^2/2m + \mathcal{V})} \frac{d^3\mathbf{p} d^3\mathbf{r}}{h^3} \right]^N \tag{2.2}$$

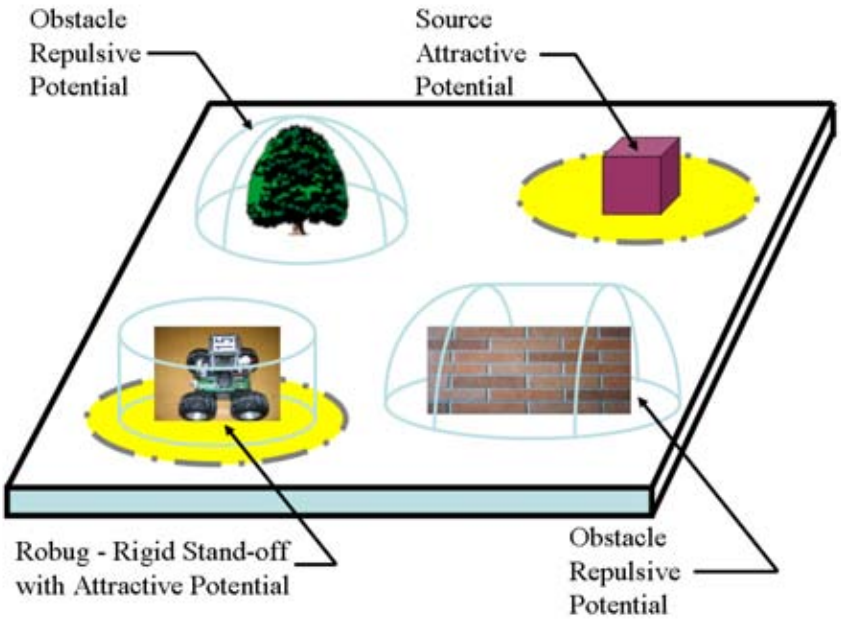

Figure 2.1. Source/target detection and localization

where $\mathcal{V} = 0, \beta = \frac{1}{kT}, T =$ temperature which implies

$$Z = \frac{1}{N!}\left[\left(\frac{2\pi m}{h^2\beta}\right)^{3/2} V\right]^N$$

culminating in the calculation of the ideal gas law from the mean values

$$\begin{aligned} \bar{p} &= \frac{1}{\beta}\frac{\partial ln}{\partial Z}Z = \frac{1}{\beta}\frac{\partial}{\partial V}\left[ln(\tfrac{1}{N!}) + ln\left(\frac{2\pi m}{h^2\beta}\right)^{3N/2} + NlnV\right] \\ &= \frac{1}{\beta}\frac{N}{V} \\ \bar{p} &= NkT/V \end{aligned} \tag{2.3}$$

where $\bar{p}$ is pressure, N is the number of robots, k is the Boltzmann constant (scaled for our robot problem), V is the volume, and T is the temperature. For this application, the search space is equivalent to the volume, and the temperature is equivalent to information flow (rate) being derived from the sensors on the individual robots. The temperature equivalent can be derived in at least two ways.

The first way is to recognize that the kinetic energy is proportional to temperature at equilibrium which can be simplified to one-dimension (1D) as [3]

$$\mathcal{T}_{ave} = \frac{1}{2}m\dot{x}_{ave}^2 = \frac{1}{2}kT$$

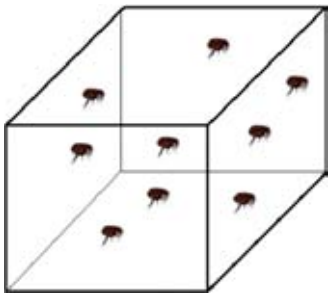

Figure 2.2. Collection of non-interacting robots in limited volume box

which leads to

$$T = \frac{m}{k}\dot{x}_{ave}^2$$

and

$$\dot{x}_{ave} = \sqrt{\frac{kT}{m}}.$$

The obstacle detection sensor systems on each robot must have a sampling rate and channel capacity (Shannon information/entropy) sufficient to detect the walls of the search volume and redirect each robot to produce an emulation of an elastic impact. Figure 2.1 presents the layout of obstacles, walls, and sources/targets that will be used throughout this section. Figure 2.3 shows a simplified 1D model to support the determination of the bandwidth (Δf), number of bits (n), channel capacity (C_{ave}), and Shannon information/entropy rate ($\dot{H}_{ave}$) [6]. This results in

$$\begin{aligned} \Delta f &= \tfrac{1}{\tau} = \tfrac{\dot{x}}{\text{range}} = \tfrac{\dot{x}}{10\,\text{meter}} = 0.1\,\dot{x}\,\text{Hz} \\ n &= \frac{\text{range}}{\text{resolution}} = \frac{10\,\text{meter}}{1\,\text{meter}} = 10\,\text{bits} \\ C_{ave} &= \tfrac{1}{\tau}\log_2 n = \dot{H}_{ave}\,(\text{bits/sec}). \end{aligned} \tag{2.4}$$

The second way is to utilize Fisher information. From (A.7) in Appendix A, it is observed that

$$I_{ave} = \frac{8}{m}\mathcal{T}_{ave} = 4\dot{x}_{ave}^2 \tag{2.5}$$

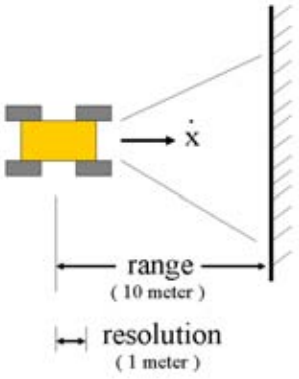

Figure 2.3. Sensor system requirements

and

$$I_{ave} = \frac{8}{m}\left[\frac{1}{2}kT\right] = 4\frac{kT}{m} \tag{2.6}$$

which gives

$$T = \frac{m}{4k}I_{ave} \tag{2.7}$$

where I_{ave} is the average Fisher information. Also, Frieden [7] provides another set of relationships for Fisher "temperature" as

$$\frac{1}{T_\theta} \equiv -k_\theta \frac{\partial I_{ave}}{\partial \theta} \tag{2.8}$$

where θ is any parameter under measurement and Fisher information per molecule for an ideal gas in a volume is

$$\frac{I_{ave}}{N} = \frac{kT}{k_E T_E} \tag{2.9}$$

with $\theta = E$ and $\frac{1}{T} \equiv \partial S/\partial E$.

For a volume, $\mathcal{T}_{ave} = \frac{3}{2}kT$ and $I_{ave} = \frac{12}{m}kT$ which produces

$$T = \frac{m}{12k}I_{ave}$$

and

$$\frac{I_{ave}}{N} = \frac{12}{mN}kT \quad \Rightarrow \quad \frac{1}{k_E T_E} = \frac{12}{mN} = -\frac{\partial I_{ave}}{\partial E}.$$

Returning to the ideal gas law, it is time to investigate the implications for the robot swarm. A necessary condition for all of the robots to swarm the target is for the pressure to be zero ($\bar{p} = 0$). This condition means that no robots hit the "walls" of the search volume. From (2.3) it is observed that the condition of $\bar{p} = 0$ is possible if $T = 0$, meaning no information is being derived from the sensors since the robot is not moving. The pressure will also be zero if $V = \infty$, meaning an infinite search space exists.

The next step in the equilibrium analysis is to add a limited range attractive source/target (i.e., chemical plume) in the search volume (see Fig. 2.4). Following the same process

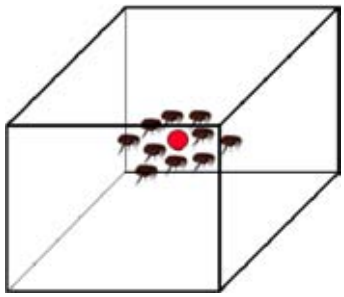

Figure 2.4. Collection of non-interacting robots (non-communicating) in limited volume box with a limited range attractive source

above, the Hamiltonian is generated for an *ideal gas* of non-interacting (non-communicating) robots within a volume containing a target

$$\mathcal{H} = \mathcal{T} + \mathcal{V} = E = \sum_{i=1}^{N} \frac{p_i^2}{2m} + \mathcal{V}(\mathbf{r}) \tag{2.10}$$

followed by forming a partition function

$$Z = \frac{1}{N!}\left[\left(\frac{2\pi m}{h^2\beta}\right)^{3/2} \int e^{-\beta\mathcal{V}(\mathbf{r})} d^3\mathbf{r}\right]^N$$

$$\mathcal{V}(\mathbf{r}) = \begin{cases} -\mathcal{V}_o + \gamma\,\mathbf{r} & , \quad 0 \le \mathbf{r} \le \mathbf{r}_s \\ 0 & , \quad \mathbf{r}_s \le \mathbf{r} \le \mathbf{R} \end{cases}$$

$$\gamma = \frac{\mathcal{V}_o}{\mathbf{r}_s}$$

(see Fig. 2.5 for plot of $\mathcal{V}(\mathbf{r})$ versus $\mathbf{r}$)

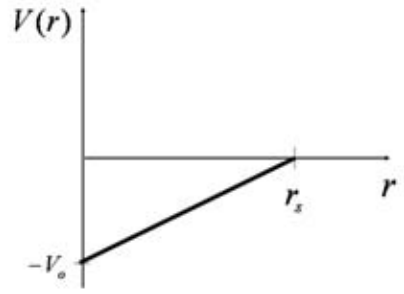

Figure 2.5. Limited range attractive source/target

$$\begin{aligned} \int_o^R e^{-\beta\mathcal{V}(\mathbf{r})} d^3\mathbf{r} &= \int_o^{\mathbf{r}_s} e^{\beta(\mathcal{V}_o - \gamma\mathbf{r})} 4\pi\mathbf{r}^2 d\mathbf{r} + \int_{\mathbf{r}_s}^{\mathbf{R}} 4\pi\mathbf{r}^2 d\mathbf{r} \\ &= 4\pi e^{\beta\mathcal{V}_o} \int_o^{\mathbf{r}_s} \mathbf{r}^2 e^{-\beta\gamma\mathbf{r}} d\mathbf{r} + V - V_s \end{aligned}$$

where

$$\int \mathbf{r}^2 e^{\alpha\mathbf{r}} d\mathbf{r} = e^{-\beta\gamma\mathbf{r}} \left[-\frac{\mathbf{r}^2}{\beta\gamma} - \frac{2\mathbf{r}}{\beta^2\gamma^2} - \frac{2}{\beta^3\gamma^3} \right]$$

which implies

$$\int_o^{\mathbf{r}_s} \mathbf{r}^2 e^{\beta\gamma\mathbf{r}} d\mathbf{r} = -\frac{e^{-\beta\gamma\mathbf{r}_s}}{\beta\gamma} \left[\mathbf{r}_s^2 + \frac{2\mathbf{r}_s}{\beta\gamma} + \frac{2}{\beta^2\gamma^2} \right] + \frac{2}{\beta^3\gamma^3} = \nabla.$$

The resulting partition function is

$$Z = \frac{1}{N!} \left[\left(\frac{2\pi m}{h^2\beta} \right)^{3/2} (\Delta + V - V_s) \right]^N$$

$$\Delta = 4\pi e^{\beta\mathcal{V}_o} \nabla$$

culminating in the calculation of the mean values

$$\begin{aligned} \bar{p} &= \frac{1}{\beta}\frac{\partial ln}{\partial V}Z \\ &= \frac{1}{\beta}\frac{N}{(\Delta+V-V_s)} \\ &= \frac{NkT}{(\Delta+V-V_s)} \end{aligned}$$

where Δ is the source strength, and V_s is the volume of the attractive force potential. Once again, $\bar{p} = 0$ may be imposed which implies that the robots do not hit the "walls." This means that $T = 0$, or $V = \infty$, as before; and that $\Delta = \infty$ which is equivalent to having an infinite source strength. For

$\Delta \to \infty$:

$$\Delta = 4\pi\left[-\frac{1}{\beta\gamma}\left(\mathbf{r}_s^2 + \frac{2\mathbf{r}_s}{\beta\gamma} + \frac{2}{\beta^2\gamma^2}\right) + \frac{2e^{\beta\mathcal{V}_o}}{\beta^3\gamma^3}\right]$$

$\mathcal{V}_0 \to \infty$:

$$lim_{\mathcal{V}_o\to\infty}\left(\frac{e^{\beta\mathcal{V}_o}}{\mathcal{V}_o^3}\right) = lim_{\mathcal{V}_o\to\infty}\left(\frac{\beta^3 e^{\beta\mathcal{V}_o}}{6}\right) = \infty \qquad \text{by L'Hôpital's Rule.}$$

This ideal gas formulation implies that the robots do not cooperate and perform target location independently as well as being able to take up the same position simultaneously (Bose-Einstein particles [8]).

The next step is to add cooperation (communication, sensing other robots, and taking up finite space) which can be accomplished by adding "real gas effects." Real gas effects can be modeled using van der Waal's equation and more generally, by the "virial expansion" of the equation of state [8]

$$\frac{\bar{p}}{kT} = n + B_2(T)n^2 + B_3(T)n^3 + \ldots$$

where $n = N/V$ is the number of molecules (robots) per unit volume, $B_2 = B_3 = \ldots = 0$ is the ideal gas law, and $B_2 \neq 0$ provides for the van der Waal's equation which will be derived next. The higher order terms enable the designer/analyst to evaluate and optimize different cooperation strategies.

The interaction potential fields presented in Fig. 2.1 are mathematical constructs of the microscopic/individual behaviors of each robot to produce the macroscopic/collective behaviors described by the virial expansion of the equation of state. This provides one step in the design/optimization of collective behaviors. A second step in the design/optimization

process will be described in Chapter 3 where non-equilibrium techniques are employed to ensure the time evolution of the collective behaviors meet the system constraints. Also, these potential fields can be treated as probability density functions in order to determine the likelihood of target detection and localization as well as inter-robot communication and cooperation by propagating them over time using Fisher information (Appendix A) and the Fisher Lagrangian.

The Hamiltonian is generated for a non-ideal gas of communicating/interacting robots within an empty search volume

$$\mathcal{H} = \mathcal{T} + \mathcal{V} = E = \sum_{i=1}^{N} \frac{p_i^2}{2m} + \mathcal{V}(\mathbf{r}) \tag{2.11}$$

followed by forming a partition function

$$Z = \frac{1}{N!}\left[\left(\frac{2\pi m}{h^2\beta}\right)^{3/2} \int e^{-\beta \mathcal{V}_B(\mathbf{r})} d^3\mathbf{r}\right]^N$$

$$\mathcal{V}_B(\mathbf{r}) = \begin{cases} \infty & \mathbf{r} \leq \mathbf{R}_o \\ -\mathcal{V}_1\left(\frac{\mathbf{R}_o}{\mathbf{r}}\right)^q & \mathbf{r} > \mathbf{R}_o \end{cases}$$

with a diagram of the interaction potential plotted in Fig. 2.6. This interaction potential which accounts for real gas effects requires an increase in sampling rate and channel capacity (Shannon entropy) due to the increase in closing speeds between robots. Basically, one can replace $\dot{x}$ with $2\dot{x}$ in equations (2.4) as a starting point.

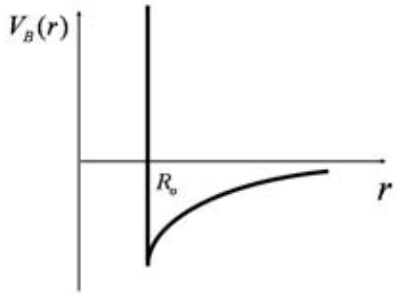

Figure 2.6. Simplified Lennard-Jones potential

Assume $\mathcal{V}_B(\mathbf{r}) = \bar{\mathcal{V}}_B$ except within V_x where $\mathcal{V}_B(\mathbf{r}) = \infty$ which implies

$$Z = \frac{1}{N!}\left[\left(\frac{2\pi m}{h^2\beta}\right)^{3/2} (V - V_x)\, e^{-\beta \bar{\mathcal{V}}_B}\right]^N$$

where

$$\begin{aligned}\bar{\mathcal{V}}_B &= \tfrac{1}{2}N\bar{U} \\ \bar{U} &= \tfrac{1}{V}\int_{\mathbf{R}_o}^{\mathbf{R}} \mathcal{V}_B(\mathbf{r})4\pi\mathbf{r}^2 d\mathbf{r} \\ &= -\tfrac{4\pi}{3}\tfrac{\mathbf{R}_o^3}{V}\left(\tfrac{3}{q-3}\right)\mathcal{V}_1\end{aligned}$$

$$\bar{\mathcal{V}}_B = -\tilde{a}\frac{N}{V}, \quad \tilde{a} = \frac{2\pi}{3}\mathbf{R}_o^3\left(\frac{3}{q-3}\right)\mathcal{V}_1, \quad q > 3$$

and

$$V_x = \tilde{b}N, \quad \tilde{b} = 4\left[\frac{4\pi}{3}\left(\frac{\mathbf{R}_o}{2}\right)^3\right]$$

culminating in the calculation of the mean values

$$\bar{p} = \frac{1}{\beta}\frac{\partial ln}{\partial V}Z = \frac{1}{\beta}\frac{\partial}{\partial V}\left[Nln(V - V_x) - N\beta\bar{\mathcal{V}}_B\right]$$

or

$$\bar{p} = \frac{NkT}{(V - \tilde{b}N)} - \tilde{a}\left(\frac{N^2}{V^2}\right) \tag{2.12}$$

where $\tilde{a}$ and $\tilde{b}$ determine the degree of interaction between the particles (i.e., the amount of communication and interaction between robots.) Again, $\bar{p} = 0$ is imposed which leads to some new results and the old result of $V = \infty$.

One new result is that $T = 0$ does not satisfy $\bar{p} = 0$ which implies this equation will have to be modified near $T = 0$. A second new result is that $\bar{p} = 0$ when

$$kT\frac{V^2}{N^2} - \tilde{a}\frac{V}{N} + \tilde{a}\tilde{b} = 0 \tag{2.13}$$

then

$$V = \frac{N}{2kT}\left[\tilde{a} \pm \sqrt{\tilde{a}(\tilde{a} - 4\tilde{b}kT)}\right]$$

which defines a phase transition or "emergent behavior." The robot swarm "condenses into a robot molecule." This result is potentially problematic if the "robot molecule" inhibits

the collective search process. On the other hand, the alpha-beta approach of reference [9] utilizes a robot molecule to conserve energy usage.

The final step in this example is to add a limited range attractive source in the search volume. A Hamiltonian is generated for a non-ideal gas of communicating/interacting robots within a search volume containing a target

$$\mathcal{H} = \mathcal{T} + \mathcal{V} = E = \sum_{i=1}^{N} \frac{p_i^2}{2m} + \mathcal{V}(\mathbf{r}) \tag{2.14}$$

followed by forming a partition function

$$Z = \frac{1}{N!}\left[\left(\frac{2\pi m}{h^2\beta}\right)^{3/2}(\Delta + V - V_s - V_x)\, e^{-\beta\bar{\mathcal{V}}_B}\right]^N$$

where

$$\begin{array}{ll} \bar{\mathcal{V}}_B = -\tilde{a}\frac{N}{V}, & \tilde{a} = \frac{2\pi}{3}\mathbf{R}_o^3\left(\frac{3}{q-3}\right)\mathcal{V}_1, \quad q > 3 \\ V_x = \tilde{b}N, & \tilde{b} = \frac{2\pi}{3}\mathbf{R}_o^3 \end{array}$$

culminating in the calculation of the mean values

$$\begin{array}{rcl} \bar{p} & = & \frac{1}{\beta}\frac{\partial lnZ}{\partial V} = \frac{1}{\beta}\frac{\partial}{\partial V}\left[Nln(\Delta + V - V_s - V_x) - N\beta\bar{\mathcal{V}}_B\right] \\ & = & NkT/(\Delta + V - V_s - V_x) - \tilde{a}N^2/V^2 \end{array}$$

which implies

$$\bar{p} = \frac{NkT}{(\Delta + V - V_s - \tilde{b}N)} - \tilde{a}\frac{N^2}{V^2}.$$

Once again, $\bar{p} = 0$ is imposed which leads to new results and the old result of $V = \infty$. The result that $T = 0$ does not satisfy $\bar{p} = 0$ continues to be a problem.

A new result is $\Delta = \infty$ does not satisfy $\bar{p} = 0$ which implies that the robots cannot take up the same position simultaneously (Fermi-Dirac particles [8]). A second new result is that $\bar{p} = 0$ when

$$NkTV^2 = \tilde{a}N^2(\Delta + V - V_s - \tilde{b}N)$$

$$kTV^2 - \tilde{a}NV + \tilde{a}N(\tilde{b}N + V_s - \Delta) = 0$$

which implies

$$\begin{aligned} V &= \frac{\tilde{a}N \pm \left[(\tilde{a}N)^2 - 4kT\tilde{a}N(\tilde{b}N + V_s - \Delta)\right]^{1/2}}{2kT} \\ &= V_{1,2}. \end{aligned}$$

This is a modified phase transition or emergent behavior that reference [9] exploits in alpha-beta variants.

Chapter 3

Nonequilibrium Collective Systems

The main goal of applying nonequilibrium analyses to collective systems is to understand and design the time-dependent macroscopic and microscopic behaviors as well as the evolution of a system through time. An effective way to meet this goal is to utilize particle physics models and codes that are presented and applied to robot collectives in references [10, 11, 12]. An additional goal is to demonstrate the equivalence between physical and information exergies based on Hamiltonian mechanics and nonequilibrium thermodynamics. Exergy is defined and the Hamiltonian is related to exergy in Appendix B. For completeness, Hamiltonian mechanics for an individual agent will be reviewed next followed by the extension to collective systems which directly leads into the discussion of physical and information exergies with respect to Fisher information.

The derivation of the Hamiltonian [5] begins with the Lagrangian for a system defined as

$$\mathcal{L} = \mathcal{T}(\mathbf{q}, \dot{\mathbf{q}}, t) - \mathcal{V}(\mathbf{q}, t) \tag{3.1}$$

where

t = time explicitly
$\mathbf{q}$ = N-dimensional generalized coordinate vector
$\dot{\mathbf{q}}$ = N-dimensional generalized velocity vector
$\mathcal{T}$ = Kinetic energy
$\mathcal{V}$ = Potential energy.

The Hamiltonian is defined in terms of the Lagrangian as

$$\mathcal{H} \equiv \sum_{i=1}^{n} \frac{\partial \mathcal{L}}{\partial \dot{q}_i} \dot{q}_i - \mathcal{L}(\mathbf{q}, \dot{\mathbf{q}}, t) = \mathcal{H}(\mathbf{q}, \dot{\mathbf{q}}, t). \tag{3.2}$$

The Hamiltonian in terms of the canonical coordinates $(\mathbf{q}, \mathbf{p})$ is

$$\mathcal{H}(\mathbf{q}, \mathbf{p}, t) = \sum_{i=1}^{n} p_i \dot{q}_i - \mathcal{L}(\mathbf{q}, \dot{\mathbf{q}}, t) \tag{3.3}$$

where the canonical momentum is defined as

$$p_i = \frac{\partial \mathcal{L}}{\partial \dot{q}_i}. \tag{3.4}$$

Then Hamilton's canonical equations of motion become

$$\begin{array}{rcl} \dot{q}_i & = & \frac{\partial \mathcal{H}}{\partial p_i} \\ \dot{p}_i & = & -\frac{\partial \mathcal{H}}{\partial q_i} + Q_i \end{array} \tag{3.5}$$

where Q_i is the generalized force vector. Next taking the time derivative of (3.3) gives

$$\dot{\mathcal{H}} = \sum_{i=1}^{n} \left(\dot{p}_i \dot{q}_i + p_i \ddot{q}_i - \frac{\partial \mathcal{L}}{\partial t} - \frac{\partial \mathcal{L}}{\partial q_i} \dot{q}_i - \frac{\partial \mathcal{L}}{\partial \dot{q}_i} \ddot{q}_i \right). \tag{3.6}$$

Then substitute (3.5) and simplifying gives

$$\dot{\mathcal{H}} = \sum_{i=1}^{n} Q_i \dot{q}_i - \frac{\partial \mathcal{L}}{\partial t}. \tag{3.7}$$

Hamiltonians for most natural systems are not explicit functions of time (or $\partial \mathcal{L}/\partial t = 0$). Then for

$$\mathcal{L} = \mathcal{L}(\mathbf{q}, \dot{\mathbf{q}}) \tag{3.8}$$

the power (work/energy) equation becomes

$$\dot{\mathcal{H}}(\mathbf{q}, \mathbf{p}) = \sum_{i=1}^{n} Q_i \dot{q}_i. \tag{3.9}$$

The collective Lagrangian is

$$\mathcal{L} = \sum_{i=1}^{N} \mathcal{L}_i = \sum_{i=1}^{N} \mathcal{T}_i - \sum_{i=1}^{N} \mathcal{V}_i \tag{3.10}$$

and the collective Hamiltonian is

$$\mathcal{H} = \sum_{i=1}^{N} \mathcal{H}_i = \sum_{i=1}^{N} \sum_{j=1}^{M} \left[\frac{\partial \mathcal{L}_i}{\partial \dot{q}_{ij}} \dot{q}_{ij} - \mathcal{L}_i \right]. \tag{3.11}$$

The equations of motion can also be generated from the Lagrangian,

$$\frac{d}{dt}\left(\frac{\partial \mathcal{L}_i}{\partial \dot{q}_{ji}}\right) - \frac{\partial \mathcal{L}_i}{\partial q_{ji}} = Q_{ji} \tag{3.12}$$

and related to Fisher information [7] to propagate a mean value and/or a probability distribution function for sensing and communication

$$I = 8\int \bar{\mathcal{T}}\, dt \tag{3.13}$$

where $\bar{\mathcal{T}} = \sum_{i=1}^{N} \frac{1}{m_i}\mathcal{T}_i$.

Now, exergy/entropy control [13] (presented in Appendices B and C) may be applied to help expand the discussion of the equivalence between physical exergy and information exergy as described in Appendices A and B where the Hamiltonian surface determines the accessible states of the system. One can explain by expanding on (A.4) through bound Fisher information [7] as

$$J = 8\int \left[\bar{\mathcal{V}} + \bar{\mathcal{V}}_c\right] dt \tag{3.14}$$

with the collective potential field as

$$\bar{\mathcal{V}} = \sum_{i=1}^{N} \frac{1}{m_i}\mathcal{V}_i$$

and the collective control potential as

$$\bar{\mathcal{V}}_c = \sum_{i=1}^{N} \frac{1}{m_i}\mathcal{V}_{c_i}.$$

Specifically, Fisher and bound Fisher informations can be combined to produce a Lagrangian functional from which equations of motion can be generated using calculus of variations [7]. This approach provides insight into the value of physical and information exergies since it directly tells one the physical and/or information flow structures necessary to complete the operation. These abstract concepts can be made more clear by solving several examples.

Example 3.1. Radar guided missile
The first example is a radar guided missile attacking a ground target while being jammed.

The Hamiltonian of the missile is simplified to a point mass in one degree of freedom (1 DOF)

$$\mathcal{H} = \mathcal{T} + \mathcal{V} = \frac{1}{2}m\dot{x}^2 + \mathcal{V} \tag{3.15}$$

where $\mathcal{V}$ is presented in Fig. 3.1 for an unjammed single ground target represented as a potential function similar to reference [14] and Fig. 3.2 for a jammed double target, then

$$\begin{aligned} \mathcal{V}_u &= \tfrac{1}{2}kx^2 + \tfrac{1}{4}k_{NL}x^4 \\ \mathcal{V}_j &= -\tfrac{1}{2}kx^2 + \tfrac{1}{4}k_{NL}x^4. \end{aligned} \tag{3.16}$$

The equivalence of physical and information exergies becomes more clear when the jamming is suppressed. In this case, the jamming is suppressed by a proportional feedback term to deform the Hamiltonian surface

$$\mathcal{V}_c + \mathcal{V} = \frac{1}{2}[K_P - k]x^2 + \frac{1}{4}k_{NL}x^4 \tag{3.17}$$

that eliminates the false targets. This can be accomplished by modulating the radar (information exergy), increasing the radar power (physical exergy), getting closer to the target, etc. In any case, the cost of each option can be evaluated with respect to the required exergy rate (power) and exergy to hit the target as well as the risk to the pilot and aircraft.

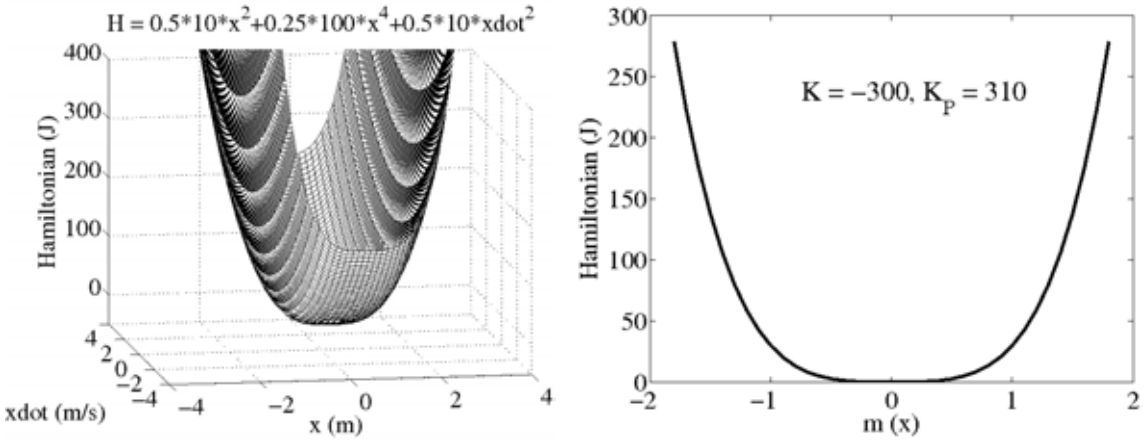

Figure 3.1. Three dimensional (left) Hamiltonian phase plane plot where the net positive stiffness produces a positive bowl surface. The two-dimensional cross-section plot (right) is at $\dot{x} = 0$.

Example 3.2. Teams of robots locating a chemical plume
A second example is locating the source of a chemical plume. A chemical sensor provides

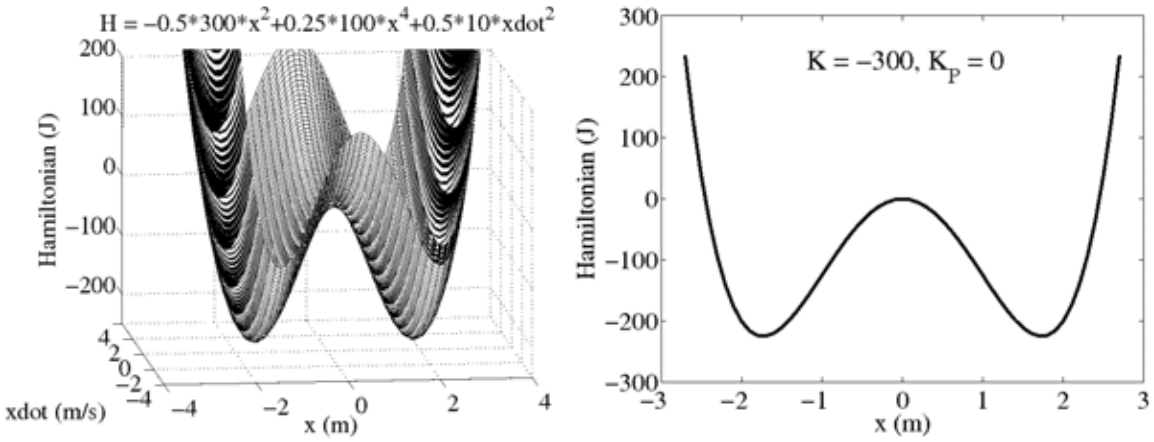

Figure 3.2. Three dimensional (left) Hamiltonian phase plane plot negative stiffness produces a saddle surface. The two-dimensional cross-section plot (right) is at $\dot{x} = 0$.

a measurement of the chemical concentration at a point, x, and at a time, t. How do you get range and bearing to a target using only chemical sensors? An answer is to create a "virtual potential field" with a team of robots by flowing information through a distributed decentralized sensor and feedback control network in order to synthesize range and bearing to a target.

The team of robots in [14] created a "virtual potential field" by flowing information through a distributed decentralized sensor and feedback control network. In the present context, the Hamiltonian of the robot collective is deformed by a virtual potential field

$$\mathcal{H} = \sum_{i=1}^{N} \mathcal{H}_i = \sum_{i=1}^{N} [\mathcal{T}_i + \mathcal{V}_{c_i}]$$

and the Lagrangian becomes

$$\mathcal{L} = \sum_{i=1}^{N} \mathcal{L}_i = \sum_{i=1}^{N} [\mathcal{T}_i - \mathcal{V}_{c_i}]$$

where

$$\begin{aligned} \mathcal{T}_i &= \tfrac{1}{2} m_i \mathbf{x}_i^T \mathbf{x}_i \\ \mathcal{V}_{c_i} &= G_i(\mathbf{x}_i) - G_i(\mathbf{x}_i^*) = \tfrac{1}{2} \mathbf{G_{x_i}}^T \mathbf{G_{xx_i}}^{-1} \mathbf{G_{x_i}} + \mathbf{x}_i^T \mathbf{G_{x_i}} + \tfrac{1}{2} \mathbf{x}_i^T \mathbf{G_{xx_i}} \mathbf{x}_i \end{aligned}$$

where $\mathcal{V}_{c_i}$ is positive definite about the estimated minimum $\mathbf{x}_i^*$ for all $\mathbf{x}_i$ in the domain of $\mathbf{x}$. The equations of motion are derived from the Lagrangian as (3.12) which gives

$$m_i \ddot{\mathbf{x}}_i = \mathbf{u}_i \tag{3.18}$$

Therefore, the time derivative of the collective Hamiltonian becomes

$$\begin{aligned} \dot{\mathcal{H}} &= \sum_{i=1}^{N} \dot{\mathcal{H}}_i \\ &= \sum_{i=1}^{N} \left[m_i \ddot{\mathbf{x}}_i + \frac{\partial \mathcal{V}_{c_i}}{\partial \mathbf{x}_i} \right]^T \dot{\mathbf{x}}_i \\ &= \sum_{i=1}^{N} \left[\mathbf{u}_i + \frac{\partial \mathcal{V}_{c_i}}{\partial \mathbf{x}_i} \right]^T \dot{\mathbf{x}}_i \end{aligned}$$

where the individual estimator/guidance algorithm for finding the source/target is

$$G_i(\mathbf{x}_i) = G_{o_i} + \mathbf{x}_i^T \mathbf{G}_{\mathbf{x}i} + \frac{1}{2} \mathbf{x}_i^T \mathbf{G}_{\mathbf{x}\mathbf{x}i} \mathbf{x}_i.$$

The feedback controller is

$$\mathbf{u}_i = -\left[\frac{\partial \mathcal{V}_{c_i}}{\partial \mathbf{x}_i} \right] - \mathbf{K}_{\mathbf{I}i} \int \mathbf{x}_i d\tau - \mathbf{K}_{\mathbf{D}i} \dot{\mathbf{x}}_i \tag{3.19}$$

and the collective stability boundary becomes

$$\sum_{i=1}^{N} \left[\left[-\mathbf{K}_{\mathbf{I}i} \int \mathbf{x}_i d\tau \right]^T \dot{\mathbf{x}}_i \right]_{ave} = \sum_{i=1}^{N} \left[\left[\mathbf{K}_{\mathbf{D}i} \dot{\mathbf{x}}_i \right]^T \dot{\mathbf{x}}_i \right]_{ave} \tag{3.20}$$

which determines the limit cycle behavior (see Appendix D for more details on limit cycles) constrained to the deformed Hamiltonian surface. The collective performance is analyzed using the following Lyapunov function which is an extension of reference [14]

$$V = \sum_{i=1}^{N} \rho_i V_i = \frac{1}{2} \sum_{i=1}^{N} \rho_i m_i \dot{\mathbf{x}}_i^T \dot{\mathbf{x}}_i + \sum_{i=1}^{N} \rho_i \mathcal{V}_{c_i}$$

with

$$\begin{aligned} \dot{V} &= \sum_{i=1}^{N} \rho_i \dot{V}_i = \sum_{i=1}^{N} \rho_i m_i \ddot{\mathbf{x}}_i^T \dot{\mathbf{x}}_i + \sum_{i=1}^{N} \rho_i \frac{\partial \mathcal{V}_{c_i}}{\partial \mathbf{x}_i}^T \dot{\mathbf{x}}_i \\ &= \sum_{i=1}^{N} \rho_i \left[m_i \ddot{\mathbf{x}}_i + \frac{\partial \mathcal{V}_{c_i}}{\partial \mathbf{x}_i} \right]^T \dot{\mathbf{x}}_i = \sum_{i=1}^{N} \rho_i \left[\mathbf{u}_i + \frac{\partial \mathcal{V}_{c_i}}{\partial \mathbf{x}_i} \right]^T \dot{\mathbf{x}}_i \end{aligned}$$

where the collective Hamiltonian can be deformed via the collective control potential or bound Fisher information in order to enhance your exergy usage or manipulate your competitor's exergy usage (see Section C.1.3 for exergy usage details).

As a numerical example, a collective team of 8 robots are used to implement the control law (3.19) to find the source of the chemical plume. The dynamical entities are smart loitering autonomous robots. Initially, the eight robots are shown surrounding the chemical plume source (center star) in Fig. 3.3 (upper-left). By making use of one another's sensing to improve individual performance then the overall collective performance results. The

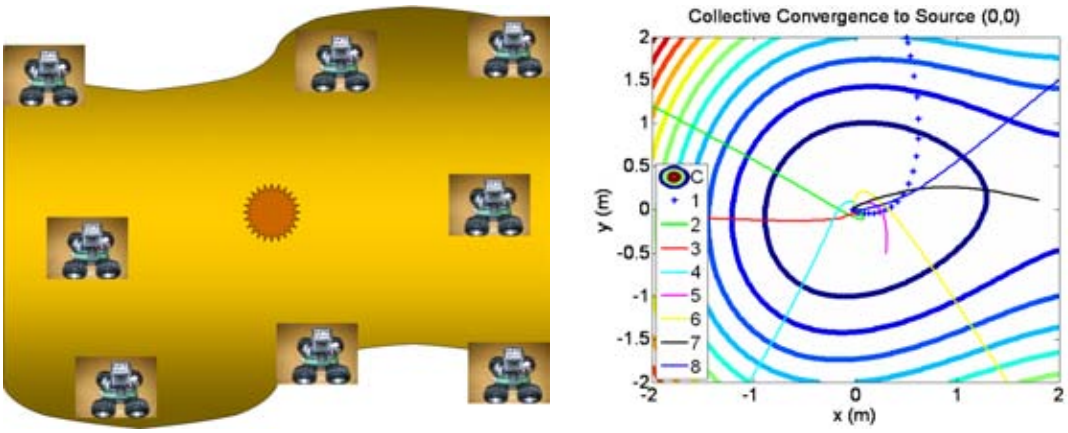

Figure 3.3. The collective system of 8 robots (left) and the cooperative localized convergence to the chemical plume source located at $(x,y) = (0,0)$ (right)

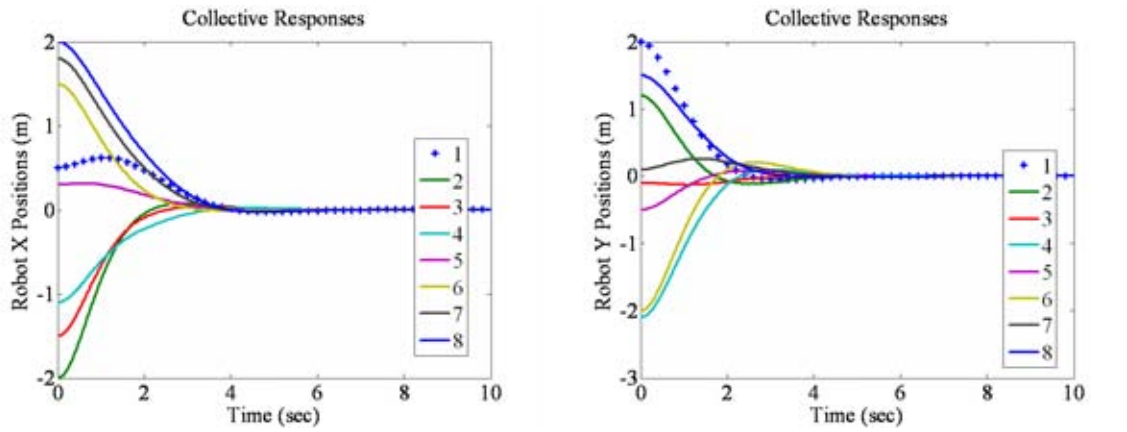

Figure 3.4. Transient responses for dissipative case X-positions (left) and Y-positions (right)

collective system cooperatively localizes the chemical plume source, located at $(x,y) = (0,0)$ (see Fig. 3.3 - right). For this case, the collective dissipative term is greater than the collective generative term as shown by the decaying transient responses (see Fig. 3.4 X-positions - left and Y-positions - right). In addition, the collective system was used to demonstrate the collective neutral boundary condition (3.20) with the corresponding transients shown in Fig. 3.5 (X-positions - left and Y-positions - right). Note that the transient oscillations do not decay. This case also demonstrates a smart loitering robot individual mode that is part of the overall collective control. Each robot was modeled as a unity point mass with the governing dynamic equations of motion given by (3.18).

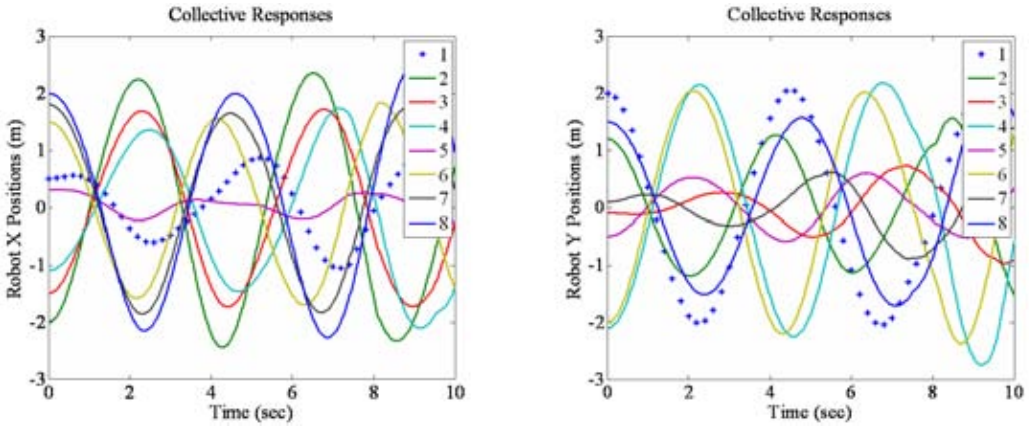

Figure 3.5. Transient responses for neutral boundary case X-positions (left) and Y-positions (right)

At this point in the chapter, it is important to discuss the deformation of the Hamiltonian surface which is implemented as a "static process" versus the exergy flow through the system that defines a "dynamic process." A simple example is to expand on the radar jamming problem by analyzing (3.17) with proportional feedback to reverse the bifurcation of $k < 0$. For

$$V = \mathcal{H} = \mathcal{T} + \mathcal{V} + \mathcal{V}_c$$

then

$$\begin{aligned} \mathcal{V} + \mathcal{V}_c &= -\tfrac{1}{2}kx^2 + \tfrac{1}{4}k_{NL}x^4 + \tfrac{1}{2}K_P x^2 \\ &= \tfrac{1}{2}[K_P - k]x^2 + \tfrac{1}{4}k_{NL}x^4 \end{aligned} \tag{3.21}$$

and $K_P \geq k$. Where the negative sign on k is explicitly accounted for in the equation.

To determine the effect that the proportional controller gain K_P has on the system, Hamiltonian surface plots are generated. By investigating a system with negative stiffness and by adding enough K_P to result in an overall positive net stiffness, one changes the shape of

the Hamiltonian surface from a saddle point surface (see Fig. 3.2) to a positive bowl surface (see Fig. 3.1). A two-dimensional cross-section of the Hamiltonian versus the position shows the characteristics of the overall storage or potential functions. The operating point at $(H,\dot{x},x) = (0,0,0)$ changes from being unstable to stable, for small values of $|x| > 0$, when enough additional K_P is added, a net positive stiffness for the system results.

To formally assess the instability of the negative stiffness, let

$$|k| > K_P \quad \text{for} \quad k < 0 \quad \text{and} \quad K_P > 0 \quad \text{and} \quad K_{NL} = 0.$$

The Lyapunov function can be changed from the Hamiltonian to the Lagrangian, again explicitly accounting for the negative sign on k,

$$\begin{aligned} V &= \mathcal{L} = \mathcal{T} - (\mathcal{V} + \mathcal{V}_c) = \tfrac{1}{2}m\dot{x}^2 + \tfrac{1}{2}(k - K_P)x^2 > 0 \\ \dot{V} &= [m\ddot{x} + (k - K_P)x]\,\dot{x} = [u + (2k - K_P)x]\,\dot{x} \\ &= 2(k - K_P)x\dot{x} > 0 \end{aligned}$$

for $u = -K_P x$. The plots for the Lagrangian and Hamiltonian are shown in Fig. 3.6.

This is called static stability/instability commonly found in re-entry vehicles [15] and aeroelasticity [16], in contrast to dynamic stability/instability defined by the exergy flows into a self-organizing system (see Appendix B and Section D.4). For re-entry vehicles, the static margin determines the static stability. The static margin (SM) is the difference in length between the center-of-mass and the center-of-pressure relative to the nose (see Fig. 3.7) of the re-entry vehicle. For

$$SM = x_{cp} - x_{cm}$$

then the following definitions apply

$$\begin{aligned} x_{cp} &= \text{center-of-pressure location} \\ x_{cm} &= \text{center-of-mass location} \\ \alpha &= \text{angle of attack} \\ V_{fs} &= \text{free stream velocity.} \end{aligned}$$

If $SM < 0$, the re-entry vehicle is statically unstable. If $SM > 0$, the re-entry vehicle is statically stable. The aerodynamic moment for a re-entry vehicle is presented in Fig. 3.8 (left) which upon integration with respect to the angle of attack (α) gives a quadratic potential function (see Fig. 3.8 - right).

For the aeroelasticity of an airplane wing, similar analysis is done for the divergence speed of the wing [16]. In this case, the center of pressure has moved forward of the center of

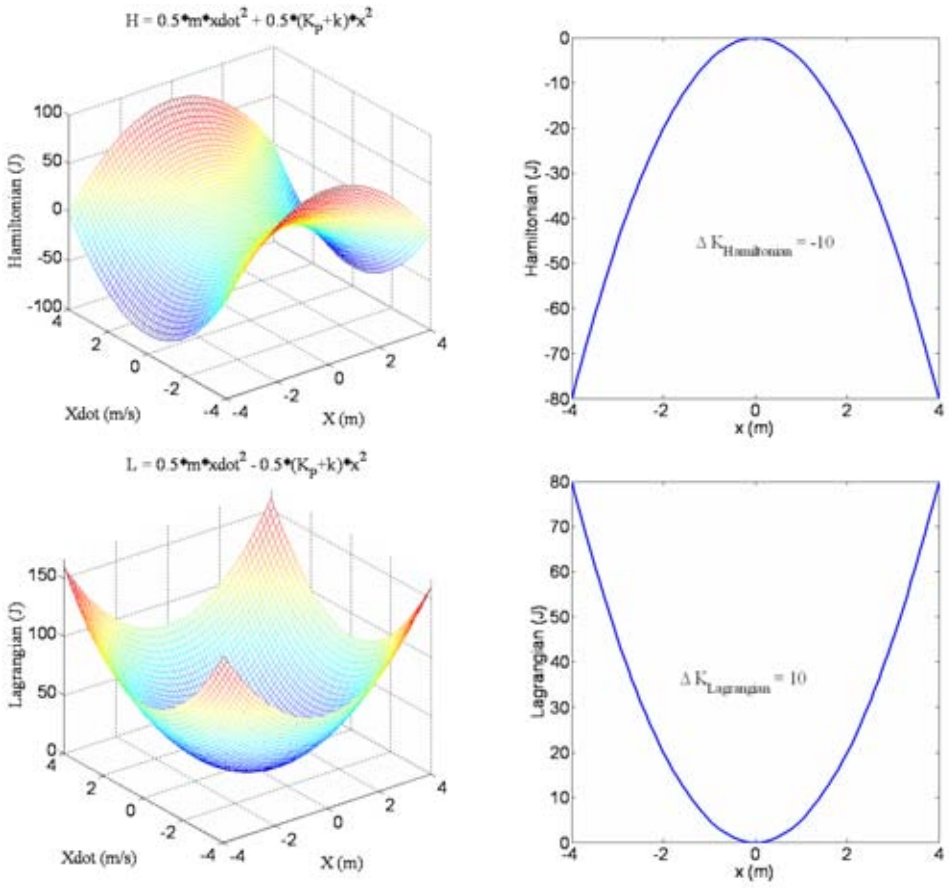

Figure 3.6. Hamiltonian and Lagrangian 3D and 2D plots for $K_P = 290, k = -300$, $\Delta K_{Hamiltonian} = -10$, and $\Delta K_{Lagrangian} = 10$.

twist with respect to the leading edge of the wing, and the aerodynamic moment overwhelms the torsional stiffness to create a static instability. Once again, the Hamiltonian surface is no longer positive definite. But, this condition of static stability provides the designer with additional performance enhancements including limited range repulsive potentials to eliminate collisions between robots and superior longitudinal (pitch) response in high performance aircraft such as the F-16. At any rate, this insight enables a clearer understanding of how stability and performance criteria can be met in nonlinear systems without requiring the typical zero-sum trade-off process , performance versus stability, inherent in linear systems.

Returning to the discussion of physical and information exergies with respect to Fisher information, an interesting way to evaluate the performance of this control design is by

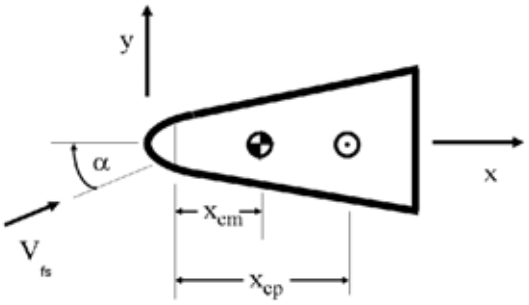

Figure 3.7. Static margin

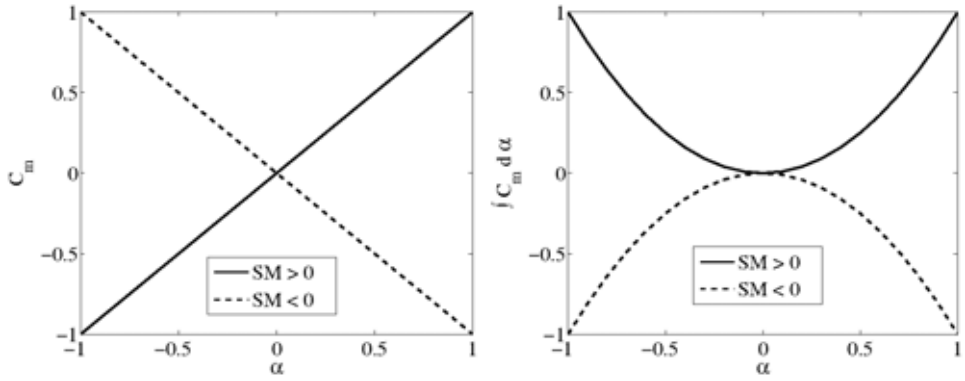

Figure 3.8. Aerodynamic moment (left) and integral of aerodynamic moment with respect to angle of attack (right)

using a modified Fisher information metric [17]

$$I_{cycle} = \frac{1}{\Delta t}\int \frac{\ddot{x}^2}{\dot{x}^4} dt$$

where Δt is the limit cycle period. This metric is another way to find and quantify the limit cycle which is discussed in more detail in Appendix D.

The Fisher information and Fisher Lagrangian are

$$I - J = 8\int \left[\bar{\mathcal{T}} - \left(\bar{\mathcal{V}} + \bar{\mathcal{V}}_c\right)\right] dt$$

which tie the information exergy to the physical exergy. Once again, the derivation of

the equations of motion informs one about the functionality of the physical infrastructure (robots, sensors, etc.) versus the information-driven collective. The whole is greater than the sum of the parts since the sum of the parts in the chemical plume tracing problem is zero [18]. Notice, the Fisher informations are the integrals of physical and information exergies which leads to the general result of

$$\dot{I} - \dot{J} = 8\left[\bar{\mathcal{T}} - \left(\bar{\mathcal{V}} + \bar{\mathcal{V}}_c\right)\right]. \tag{3.22}$$

This provides a constraint on information flow and a disordering rate since $\dot{I} - \dot{J} \leq 0$ (see [7]) as $t \to \infty$. The Fisher Lagrangian can be rewritten as the Fisher Hamiltonian

$$I + J = 8\int \left[\bar{\mathcal{T}} + (\bar{\mathcal{V}} + \bar{\mathcal{V}}_c)\right] dt \tag{3.23}$$

which leads to

$$\ddot{I} + \ddot{J} = 8\left[\dot{\bar{\mathcal{H}}}\right] \tag{3.24}$$

where

$$\bar{\mathcal{H}} = \sum_{i=1}^{N} \frac{1}{m_i}\mathcal{H}_i.$$

Equation (3.24) provides a direct connection between stability and information flow since the physical exergy flow is directly related to the information exergy (virtual potential) flow and the Fisher information flow. Furthermore, the Fisher information flow into a self-organizing collective system becomes a single point of failure (refer to Appendix C for more details) since it is equivalent to the physical and information exergy flows; it keeps track of the order of the system. Also, (3.23) is an ideal optimization functional for solving the minimum information problem (see reference [18] for more details). Appendix C provides a short review of the stability characteristics of self-organizing collective systems.

Example 3.3. Adaptive control as physical and information exergies
As a further example of how physical and information exergies are related, an adaptive control problem is reviewed. Once again, starting with the mass-spring-damper (with a PID tracking controller) problem (also see Fig. D.1)

$$m\ddot{x} + kx = -c\dot{x} + u$$

with the Hamiltonian given as

$$\begin{aligned} \mathcal{H} &= \mathcal{T} + \mathcal{V} + \mathcal{V}_C + \mathcal{V}_I \\ &= \tfrac{1}{2}m(\dot{x} - \dot{x}_r)^2 + \tfrac{1}{2}k(x - x_r)^2 + \tfrac{1}{2}K_P(x - x_r)^2 + \tfrac{1}{2}\tilde{\Phi}^T\Gamma^{-1}\tilde{\Phi} \end{aligned}$$

where the last term is associated with the adaptive parameter estimation terms or the information exergy potential ($\mathcal{V}_I$). In this case, the difference between the estimated and "true" parameters makes up the information flow. The goal is to drive the estimated parameters to the "true" parameters for which specific performance criteria can then be established. Next, the Hamiltonian rate becomes

$$\begin{aligned} \dot{\mathcal{H}} &= [m(\ddot{x}-\ddot{x}_r)+(k+K_P)(x-x_r)]\,(\dot{x}-\dot{x}_r)+\tilde{\Phi}^T\Gamma^{-1}\dot{\tilde{\Phi}} \\ &= [-m\ddot{x}_r-kx_r+K_P(x-x_r)-c\dot{x}+u]\,(\dot{x}-\dot{x}_r)+\tilde{\Phi}^T\Gamma^{-1}\dot{\tilde{\Phi}}. \end{aligned} \tag{3.25}$$

The controller is selected as

$$u = u_{ref} + \Delta u = u_{ref} + u_P + u_G + u_D \tag{3.26}$$

where

$$\begin{aligned} u_{ref} &= \hat{m}\ddot{x}_r+\hat{k}x_r+\hat{c}\dot{x} \\ \Delta u &= u_P+u_G+u_D \\ u_P &= -K_P(x-x_r) \\ u_G &= -K_I\textstyle\int_0^t(x-x_r)d\tau \\ u_D &= -K_D(\dot{x}-\dot{x}_r). \end{aligned}$$

Note that parameters with a hat ($\hat{}$) represent the estimate of the true parameter. Substituting (3.26) into (3.25) yields

$$\begin{aligned} \dot{\mathcal{H}} &= \left[(\hat{m}-m)\ddot{x}_r+(\hat{k}-k)x_r+(\hat{c}-c)\dot{x}-K_I\textstyle\int_0^t(x-x_r)d\tau-K_D(\dot{x}-\dot{x}_r)\right](\dot{x}-\dot{x}_r) \\ &\quad +\tilde{\Phi}^T\Gamma^{-1}\dot{\tilde{\Phi}}. \end{aligned} \tag{3.27}$$

Next identify and set

$$(\hat{m}-m)\ddot{x}_r+(\hat{k}-k)x_r+(\hat{c}-c)\dot{x} = Y\tilde{\Phi}. \tag{3.28}$$

Then substitute (3.28) into (3.27) and simplifying gives

$$\dot{\mathcal{H}} = \left[-K_I\int_0^t(x-x_r)d\tau-K_D(\dot{x}-\dot{x}_r)\right](\dot{x}-\dot{x}_r)+\tilde{\Phi}^T\left[Y^T(\dot{x}-\dot{x}_r)+\Gamma^{-1}\dot{\tilde{\Phi}}\right] \tag{3.29}$$

where

$$\begin{aligned} \tilde{\Phi}^T &= \begin{bmatrix}(\hat{m}-m) & (\hat{k}-k) & (\hat{c}-c)\end{bmatrix} \\ \dot{\tilde{\Phi}}^T &= \dot{\hat{\Phi}}^T = \begin{bmatrix}\dot{\hat{m}} & \dot{\hat{k}} & \dot{\hat{c}}\end{bmatrix} \\ Y &= \begin{bmatrix}\ddot{x}_r & x_r & \dot{x}\end{bmatrix}. \end{aligned}$$

To ensure the information exergy potential is a conservative term, the last term in (3.29) vanishes with

$$\dot{\hat{\Phi}} = -\Gamma Y^T (\dot{x} - \dot{x}_r).$$

This also results in the following adaptive parameter update equations

$$\begin{aligned} \dot{\hat{m}} &= -\gamma_1 \, \ddot{x}_r (\dot{x} - \dot{x}_r) \\ \dot{\hat{k}} &= -\gamma_2 \, x_r (\dot{x} - \dot{x}_r) \\ \dot{\hat{c}} &= -\gamma_3 \, \dot{x} (\dot{x} - \dot{x}_r) \end{aligned}$$

which concludes in the following passively stable condition

$$\oint_\tau \left[-K_I \int_0^t (x - x_r) d\tau' \right] (\dot{x} - \dot{x}_r) dt < \oint_\tau \left[K_D (\dot{x} - \dot{x}_r)^2 \right] dt. \tag{3.30}$$

This derivation demonstrates that when the adaptive parameter estimates or information exergies are driven to the "true" parameters then the system reduces to the actual physical exergy or available storage in the system for which the final constraint (3.30) determines the system performance and passive stability. The inherent trade-off is the additional cost of the adaptive controller hardware and software versus a robust control design.

To summarize the analysis a numerical simulation was performed. The following numerical values were selected for the model: $m = 10$ kg, $k = 10$ N/m, and $c = 1$ N-s/m. The control gains were selected as: $K_P = 550$, $K_I = 20$, $K_D = 31$, $\gamma_1 = 1000$, $\gamma_2 = 2500$, and $\gamma_3 = 1000$. The system was initially at rest $(x_o = 0, \dot{x}_o = 0)$. The control system gains were selected to provide a critically damped response and the adaptive gains used to provide quick convergence to the "true" parameters. As with most standard adaptive control, this provides guaranteed stability, but not necessarily converging to the exact "true" parameters. A standard bang-coast-bang acceleration profile was used to generate the reference inputs and provide rich signal content. The position, velocity and acceleration responses are shown in Fig. 3.9 (left). The corresponding errors for position, velocity, and acceleration, are also shown in Fig. 3.9 (right). The total input force (u), reference force (u_{ref}), and control force (Δu) are shown in Fig. 3.10 (left). The adaptive estimated parameter responses for $\hat{m}$, $\hat{k}$, and $\hat{c}$ are shown in Fig. 3.10 (right).

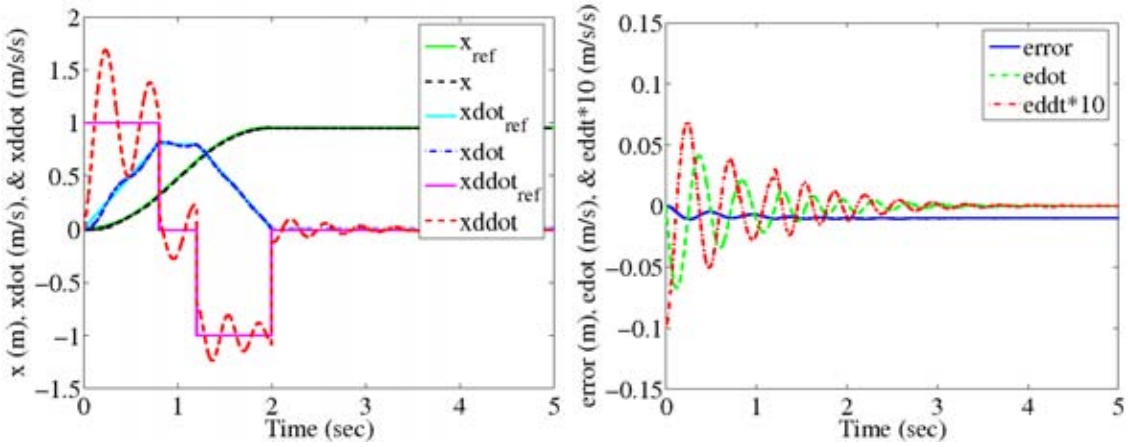

Figure 3.9. Adaptive control mass-spring-damper responses: position, velocity, acceleration (left) and corresponding errors (right)

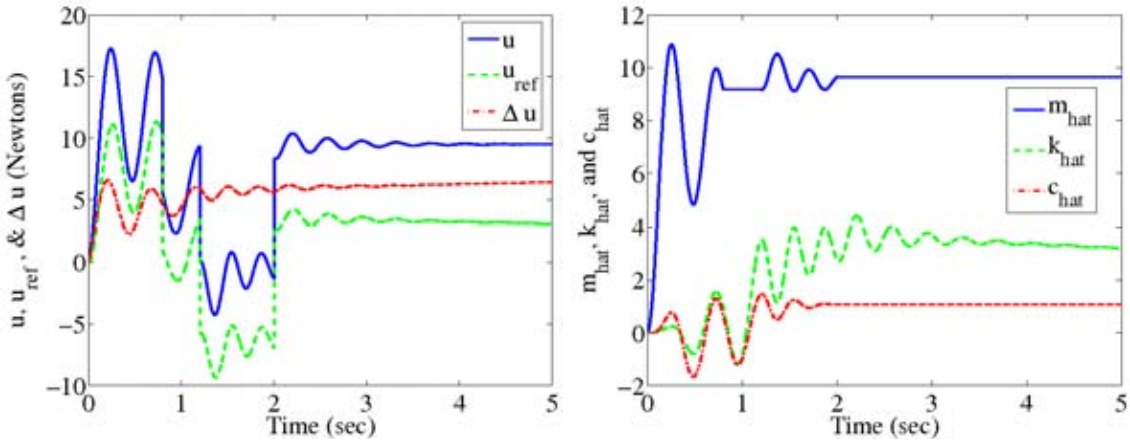

Figure 3.10. Adaptive control mass-spring-damper responses: input force, reference force, and control force are shown (left) with corresponding adaptive parameter estimates (right)

The exergy-rate and exergy responses for the adaptive control mass-spring-damper system are shown in Fig. 3.11. For both responses the passivity terms are greater (in magnitude) than the generative terms which satisfy the inequality in (3.30).

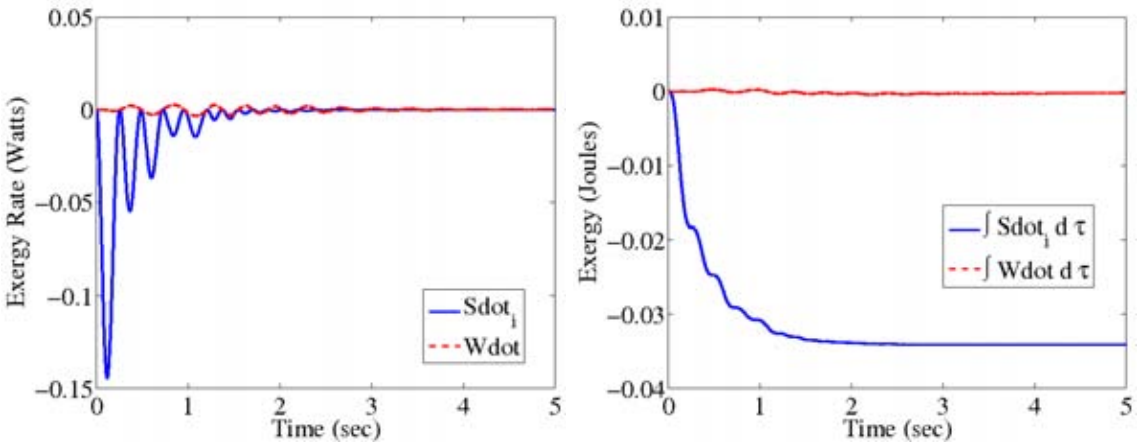

Figure 3.11. Adaptive control mass-spring-damper responses: exergy-rate (left) and exergy (right)

Example 3.4. Performance of electric power grid system

The last example is to enhance the performance of the electric power grid. The goal of the power grid is to distribute electricity from the source to the load with a power factor of 1 (see reference [25]). The power factor[1] is defined as the ratio of the real power to the apparent power and ranges from 0 to 1. Low power factor loads increase losses and energy costs in a power distribution system. The term VAR (volt-amperes reactive) is the unit of reactive power (or VAR support) and represents the power consumed by a reactive load. Power factor correction returns the power factor of an electric AC power transmission system to very near unity by switching in or out banks of capacitors or inductors which act to cancel the inductive or capacitive effects of the load. For example, the inductive effect of motor loads may be offset by locally connected capacitors. An active power factor corrector is a power electronic system that controls the amount of power drawn by a load in order to obtain a power factor as close to unity as possible. In the following paragraphs a simple RLC network that represents several key components in an electric power grid will be analyzed with respect to power flow.

The Hamiltonian and corresponding Hamiltonian rate are

$$\begin{aligned} \mathcal{H} &= \tfrac{1}{2}L\dot{q}^2 + \tfrac{1}{2}\tfrac{1}{C}q^2 \\ \dot{\mathcal{H}} &= [L\ddot{q} + \tfrac{1}{C}q]\dot{q} = [v\dot{q} - R\dot{q}^2]. \end{aligned} \tag{3.31}$$

[1] *Power factor, VAR, power factor correction,* and *active power factor corrector* terms have been defined from the Wikipedia encyclopedia.

which arise from the Thevinen equivalent circuit (which is an intrinsic collective electrical network) as shown in Fig. 3.12.

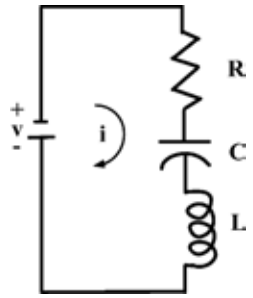

Figure 3.12. Thevinen equivalent RCL circuit

The general *RCL* network dynamics are given as

$$v = L\ddot{q} + R\dot{q} + \frac{1}{C}q$$

where

$$\begin{array}{rcl} q & = & \text{charge} \\ i & = & \dot{q} = \text{current} \\ R & = & \text{Equivalent resistance} \\ C & = & \text{Equivalent capacitance} \\ L & = & \text{Equivalent inductance} \\ v & = & \text{Applied voltage (generator) .} \end{array}$$

The power factor of 1 occurs when the sinusoid input frequency matches the natural frequency of the circuit or

$$\Omega^2 = \frac{1}{LC} = \omega^2$$

for $v = v_o \cos \Omega t$. A simple strategy to achieve a power factor of 1 is to have capacitor banks available to provide "VAR support" where needed on the grid, since most loads and generators are heavily inductive. A potentially more flexible approach is to use power electronics to provide proportional feedback to do real-time VAR support or

$$v = v_o \cos \Omega t - K_p q$$

which leads to

$$\begin{array}{rcl} \mathcal{H} & = & \frac{1}{2}L\dot{q}^2 + \frac{1}{2}[\frac{1}{C} + K_P]q^2 \\ \dot{\mathcal{H}} & = & [L\ddot{q} + (\frac{1}{C} + K_P)q]\dot{q} = [(v_o \cos \Omega t)\dot{q} - R\dot{q}^2]. \end{array} \tag{3.32}$$

Clearly, the cost of K_P (power electronics) versus $\frac{1}{C}$ (capacitor banks) can be evaluated with respect to exergy, exergy rate, flexibility, reliability, etc.

A more general, and possibly clearer, understanding of the trade-offs between information and physical exergies can be described by rewriting (3.32) as a tracking controller

$$\begin{array}{rcl} \mathcal{H} & = & \frac{1}{2}L(\dot{q} - \dot{q}_R)^2 + \frac{1}{2}\frac{1}{C}(q - q_R)^2 \\ \dot{\mathcal{H}} & = & \left[L(\ddot{q} - \ddot{q}_R) + \frac{1}{C}(q - q_R)\right](\dot{q} - \dot{q}_R) \end{array}$$

where

$$L\ddot{q} = -R\dot{q} - \frac{1}{C}q + v.$$

Next, modify $\mathcal{H}$ to account for K_P as

$$\begin{array}{rcl} \hat{\mathcal{H}} & = & \frac{1}{2}L(\dot{q} - \dot{q}_R)^2 + \frac{1}{2}[\frac{1}{C} + K_P](q - q_R)^2 \\ \dot{\hat{\mathcal{H}}} & = & \left[L(\ddot{q} - \ddot{q}_R) + [\frac{1}{C} + K_P](q - q_R)\right](\dot{q} - \dot{q}_R) \\ & = & [\Delta v + K_P(q - q_R) - R(\dot{q} - \dot{q}_R)](\dot{q} - \dot{q}_R) \end{array}$$

where

$$\begin{array}{rcl} v & = & v_R + \Delta v \\ v_R & = & L\ddot{q}_R + R\dot{q}_R + \frac{1}{C}q_R. \end{array}$$

If one designs v_R for $\omega^2 = \Omega^2 = 1/LC$ then $v_R\dot{q}_R = R\dot{q}_R^2$ which requires feedback control if $\omega^2 = 1/LC \neq \Omega^2$ to get a power factor of 1 then

$$\Delta v = -K_p(q - q_R) - K_I \int (q - q_R)dt - K_D(\dot{q} - \dot{q}_R).$$

By choosing $K_I = K_D = 0$, then the control strategy becomes

$$\dot{\hat{\mathcal{H}}} = \left[L(\ddot{q} - \ddot{q}_R) + [\frac{1}{C} + K_P](q - q_R)\right](\dot{q} - \dot{q}_R) = -R(\dot{q} - \dot{q}_R)^2$$

where

$$R\dot{q}_R^2 = v_o \cos \Omega t \; \dot{q}_R$$

and

$$\frac{1}{\bar{C}} = \left[\frac{1}{C} + K_P \right].$$

In this example, the clear tradeoff is between a physical capacitor bank and a power flow control device. The capacitor is simple, reliable, and fixed capacity. The control device is flexible, adaptable, and presently more expensive and possibly less reliable. Also, there are a couple of major issues with this approach that should be addressed in future studies:

1. Does it actually get closer to a power factor of 1 since one is expending exergy to run power electronics?
2. Does closing the control loop locally destabilize the collective grid especially when K_I and K_D are nonzero? In particular, does the controlled system performance result in a stable linear limit cycle (refer to Appendix D).

Chapter 4

Summary and Conclusions

This report has demonstrated the fundamental nature of the Hamiltonian function in the design of collective systems. Specifically, this report has mathematically explained the concept of "far from thermodynamic equilibrium on the basis of exergy dissipation" for self-organizing collective systems: the continuous compensation of irreversible entropy production in an open system with an impedance and capacity-matched persistent exergy source (refer to Appendix C). This mathematical explanation has tied irreversible thermodynamics and Hamiltonian systems together to enhance the analysis of self-organizing collective systems. In particular, equivalences between physical and information-based exergies have been developed based on Shannon information, Fisher information, and virtual fields. These equivalences were and can be used to evaluate the performance trade-offs and values (i.e., economic, etc.) of physical versus information-driven infrastructures to enhance one's economic competitiveness and/or performance on the battlefield. Finally, equilibrium and non-equilibrium thermodynamics and information theory were used to analyze and design self-organizing collective systems. New emergent behaviors, phase transitions, from microscopic/individual behaviors were discovered such as "robot molecules" that can both enhance and degrade the macroscopic/collective behaviors.

The final example of Chapter 3 provides some very interesting open questions and research issues in self-organizing collective systems. These questions and issues are partially driving our present research agenda.

Appendix D develops and presents new and innovative insights into the significance of limit cycles. In particular, limit cycles are shown to be generalized stability boundaries and the linear limit cycle behavior of the electric power grid is the generalization of a unity power factor. Also, limit cycles are the result of a balanced power flow which leads to far from thermodynamic equilibrium on the basis of exergy dissipation. Finally, an extension of eigen analysis to nonlinear systems, deemed, "power flow principle of stability for nonlinear systems," was developed via limit cycle analysis.

References

[1] R.D. Robinett, III, D.G. Wilson, and A.W. Reed, *Exergy Sustainability*, Sandia National Laboratories, SAND2006-2759, May 2006.

[2] T. Berg, *Fisher Information: Its Flow, Fusion, and Coordination,* Sandia National Laboratories, SAND2002-1969 Report, June 2002.

[3] W.G. Vincenti and C.H. Kruger, Jr., *Introduction to Physical Gas Dynamics,* Robert E. Krieger Publishing, 1982.

[4] R.Weinstock, *Calculus of Variations with Applications to Physics and Engineering*, Dover Publications, 1974.

[5] L. Meirovitch, *Methods of Analytical Dynamics*, McGraw-Hill, New York, 1970.

[6] M. Schwartz, *Information Transmission, Modulation, and Noise - A Unified Approach to Communication Systems*, McGraw-Hill, 1959.

[7] B.R. Frieden, *Physics from Fisher Information: A Unification*, Cambridge University Press, 1999.

[8] F. Reif, *Fundamentals of Statistical and Thermal Physics*, McGraw-Hill, 1965.

[9] S.Y. Goldsmith and R.D. Robinett, III, *Collective Search by Mobile Robots Using Alpha-Beta Coordination*, Collective Robotics Workshop, Agent World 98, May 1998.

[10] M.W. Trahan, J.S. Wagner, K.M. Stantz, P.C. Gray, and R.D. Robinett, III, *Swarms of UAV's and Fighter Aircraft*, ICNPAA-98, Second International Conference on Nonlinear Problems in Aviation and Aerospace, April 1998.

[11] K.M. Stantz, S.M. Cameron, R.D. Robinett, III, M.W. Trahan, and J.S. Wagner, *Dynamical Behavior of Multi-robot Systems Using Lattice Gas Automata*, Proceedings of SPIE's 13^{th} Annual International Symposium on Aerospace/Defense Sensing, Simulation, and Controls, Vol. 3693, March 1999.

[12] S.M. Cameron, G.M. Loubriel, R.D. Robinett, III, K.M. Stantz, M.W. Trahan, and J.S. Wagner, *Adaptive Remote-Sensing Techniques Implementing Swarms of Mobile Agents*, Proceedings of SPIE's 13^{th} Annual International Symposium on Aerospace/Defense Sensing, Simulation, and Controls, Vol. 3693, March 1999.

[13] R.D. Robinett, III and D.G. Wilson, *Exergy and Entropy Thermodynamic Concepts for Control System Design: Slewing Single Axis*, AIAA Guidance, Navigation, and Control Conference and Exhibit, Keystone, CO., August 2006.

[14] R.D. Robinett, III and J.E. Hurtado, *Stability and Control of Collective Systems,* Journal of Intelligent and Robotic Systems, Vol. 39, 2004, pp. 43-55.

[15] R.D. Robinett, III, *A Unified Approach to Vehicle Design, Control, and Flight Path Optimization,* Stratech Studies SS87-1, College Station, TX, December, 1987.

[16] E.H. Dowell, et.al., *A Modern Course in Aeroelasticity*, Sijthoff & Noordhoff, 1978.

[17] C.W. Pawlowski, B.D. Fath, A.L. Mayer, and H. Cabezas, *Towards a Sustainability Index Using Information Theory*, Journal of Energy, Vol. 30, 2005.

[18] R.D. Robinett, III and D.G. Wilson, *Collective Plume Tracing: A Minimum Information Approach to Collective Control*, Accepted for publication, Invited paper, IEEE 2007 American Control Conference, New York, NY, July 11-13, 2007.

[19] J.A. Cooper and R.D. Robinett, III, *Structured Communication and Collective Cohesion Measured by Entropy,* Journal of System Safety, Electronic Edition, Vol. 41, No. 4, 2005.

[20] R.D. Robinett, III and D.G. Wilson, *Exergy and Irreversible Entropy Production Thermodynamic Concepts for Control System Design: Robotic Servo Applications*, Proceedings of the 2006 IEEE International Conference on Robotics and Automation, Orlando, Florida, May 2006.

[21] R.D. Robinett, III, D.G. Wilson, and A.W. Reed, *Exergy Sustainability for Complex Systems*, International Conference on Complex Systems, Boston, Ma., June 2006.

[22] D.S. Scott, *Links and Lies*, International Journal of Hydrogen Energy, Vol. 28, 2003, pp. 473-476.

[23] D. Kondepudi and I. Prigogine, *Modern Thermodynamics: From Heat Engines to Dissipative Structures*, John Wiley & Sons, New York, N.Y., 1999.

[24] D.S. Scott, *Exergy*, International Journal of Hydrogen Energy, Vol. 28, 2003, pp. 369-375.

[25] R.J. Smith, *Circuits, Devices, and Systems: A First Course in Electrical Engineering*, John Wiley & Sons, Third Edition, 1976.

[26] T.L. Saaty and J. Bram, *Nonlinear Mathematics*, McGraw-Hill, New York, 1964.

[27] B. van der Pol, *Radio Rev.* **1**, 704-754, 1920 and B. van der Pol, *Phil. Mag.*, **3**, 65, 1927.

[28] F. Heylighen, *The Science of Self-Organization and Adaptivity*, Principia Cybernetic Web, http://perspmcl.vub.ac.be/

[29] H. Haken, *Advanced Synergetics: Instability Hierarchies of Self-Organizing Systems and Devices*, Springer-Verlag, New York, NY, 1983.

[30] G. Buenstorf, *Self-Organization and Sustainability: Energetics of Evolution and Implications for Ecological Economics*, Ecological Economics, Vol. 33, 2000, pp. 119-134.

[31] A. Cooper and R.D. Robinett, III, *Deriving Sustainable Ordered Surety by Overcoming Persistent Disorder Pressures*, Journal of System Safety, Vol. 42, No. 4, July-August 2006.

[32] H. Haken, *Synergetics: An Introduction*, 3^{rd} Edition, Springer-Verlag, New York, NY, 1983.

[33] P.M. Allen, *Cities and Regions as Self-Organizing Systems,* Models of Complexity, Gordon and Breach, Amsterdam, 1997.

[34] P. Bak, *How Nature Works: The Science of Self-Organized Criticality,* Springer, Berlin, 1996.

[35] E.P. Gyftopoulos and G. P. Beretta, *Thermodynamics: Foundations and Applications*, Macmillan Publishing Company, New York, 1991.

[36] F.J. Flanigan, *Complex Variables - Harmonic and Analytic Functions*, Dover Publications, 1983.

[37] M.L. Boas, *Mathematical Methods in the Physical Sciences*, John Wiley and Sons, 1966.

[38] W.E. Boyce and R.C. DiPrima, *Introduction to Differential Equations*, John Wiley and Sons, 1970.

[39] M. Sabatini, *Limit Cycle's Uniqueness for a Class of Plane Systems*, Technical Report UTM 662, February 2004, Mathematica, University of Trento, Italy.

[40] K. Ogata, *Modern Control Engineering*, Prentice-Hall, Inc., Englewood Cliff, N.J., 1970.

Appendix A

Fisher Information

This Appendix describes the basic concepts of Fisher information necessary for the discussion of physical and information exergies that enable the deformation of the potential field and enable the kinetic energy state. From a communications point of view, Fisher information is a measure of how well the receiver can estimate the message from the sender where as Shannon information/entropy is a measure of the sender's transmission efficiency over a communications channel [7, 19]. Fisher information is defined as [7]

$$I = 4 \int \dot{q}^2(x) dx \tag{A.1}$$

where $q^2(x) = p(x)$ is a "real amplitude" function of the probability density function $p(x)$. Equation (A.1) can be interpreted as the "mean kinetic energy" and for the purposes of this discussion as

$$I = 4 \int \dot{q}^2 dt = 4 \int \frac{2}{m} \mathcal{T} dt \tag{A.2}$$

where $\mathcal{T} = \frac{1}{2} m \dot{q}^2$.

I is the scaled integral of the mean kinetic energy portion of both the Lagrangian and the Hamiltonian and is referred to as the Fisher data information. The second part, the potential energy, is referred to as the phenomenological or bound Fisher information, J. The Lagrangian is

$$\mathcal{L} = \mathcal{T} - \mathcal{V} \tag{A.3}$$

where

$$I - J = \frac{8}{m} \int [\mathcal{T} - \mathcal{V}] dt \tag{A.4}$$

and the equations of motion are

$$\frac{d}{dt} \left(\frac{\partial \mathcal{L}}{\partial \dot{q}_i} \right) - \frac{\partial \mathcal{L}}{\partial q_i} = Q_i \tag{A.5}$$

or equivalently from Hamilton's equations

$$\begin{aligned} \dot{q}_i &= \frac{\partial \mathcal{H}}{\partial p_i} \\ \dot{p}_i &= -\frac{\partial \mathcal{H}}{\partial q_i} + Q_i. \end{aligned} \tag{A.6}$$

This formulation of the "Fisher" Lagrangian provides an intimate relationship between physical and information exergies. It shows the equivalence relationship and how to evaluate the effectiveness of physical and information solutions relative to stability and performance requirements. Furthermore, it shows that physical exergy is a result of information exergy in the form of "knowledge" about the system when turning energy flows into work.

One final note, Fisher information is a time-dependent, gradient information metric that generates a differential equation when operated on by calculus of variations, but (A.2) can be rewritten for $t \to \infty$ as an average

$$I_{ave} = \frac{8}{m}\mathcal{T}_{ave} = \frac{8}{m}\left[\frac{1}{2}m\dot{q}_{ave}^2\right] = \frac{8}{m}\left[\frac{1}{2}kT\right] \tag{A.7}$$

where $\frac{1}{2}kT$ is the equivalent mean kinetic energy of a molecule in a one-dimension equilibrium condition [3]. This equation is used in Chapter 2 when evaluating the information flow in an ideal gas of robot agents.

Appendix B

Exergy/Entropy Control Design

In this appendix which is a modification of reference [13] the first and second laws of thermodynamics are used to define exergy. Hamiltonian systems as described in Chapter 3 are used to define connections between thermodynamics and Hamiltonian mechanics. Finally, stability conditions are derived for nonlinear systems with respect to Lyapunov's direct method. Further details on this methodology can be found in references [1, 13, 20, 21].

B.1 Thermodynamic Concepts

One interpretation of the first law of thermodynamics states energy is conserved. The second law of thermodynamics implies that the entropy of the universe always increases. The first law is a conservation equation while the second law is an inequality. Mathematically, a result of the first law can be written in terms of it's time derivatives or energy rate for a system [22] as (see Fig. B.1)

$$\dot{\mathcal{E}} = \sum_i \dot{Q}_i + \sum_j \dot{\mathcal{W}}_j + \sum_k \dot{m}_k \left(h_k + ke_k + pe_k + \ldots\right). \tag{B.1}$$

The term on the left is the rate at which energy is changing within the system. The heat entering or leaving the system is given by $\dot{Q}_i$ and the work entering or leaving the system is given by $\dot{\mathcal{W}}_j$. Material can enter or leave the system by $\dot{m}_k$ that includes enthalpy, h, kinetic and potential energies, ke, pe, etc. In addition, each term is "summed" over an arbitrary number of entry and exit locations i, j, k.

The second law or entropy rate equation for a system [22] is given as

$$\dot{\mathcal{S}} = \sum_i \frac{\dot{Q}_i}{T_i} + \sum_k \dot{m}_k s_k + \dot{\mathcal{S}}_i = \dot{\mathcal{S}}_e + \dot{\mathcal{S}}_i. \tag{B.2}$$

Where the left hand term is the rate entropy changes within the system and the right hand terms represent, in order, entropy change due to heat interactions to and from the system

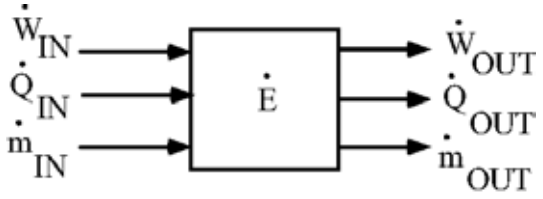

Figure B.1. Energy flow control volume

and the rate material carries it in or out. These two terms can be combined into one term $\dot{S}_e$, the entropy exchanged (either positive or negative) with the environment and $\dot{S}_i$ is the irreversible entropy production rate within the system. Figure B.2 shows the entropy exchanges and production within the system [23].

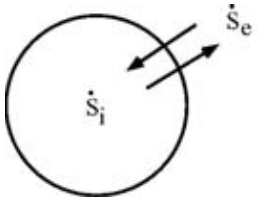

Figure B.2. Entropy with flux exchange system

The irreversible entropy production rate can be written as the sum of the thermodynamic forces, $\mathcal{F}_k$, and the thermodynamic flows, $\dot{\mathcal{X}}_k$, [23]

$$\dot{\mathcal{S}}_i = \sum_k \mathcal{F}_k \dot{\mathcal{X}}_k \geq 0. \tag{B.3}$$

Next, for systems with a constant environmental temperature (T_o), a thermodynamic quantity called the availability function is defined as [22, 23, 24]

$$\Xi = \mathcal{E} - T_o \mathcal{S}. \tag{B.4}$$

The availability function is described as the maximum theoretically available energy that can do work which we call exergy. Exergy is also known as negative-entropy [22, 24]. Taking the time derivative of the availability function (B.4) and substituting in the expressions for (B.1) and (B.2) results in the exergy rate equation

$$\dot{\Xi} = \sum_i \left(1 - \frac{T_o}{T_i}\right) \dot{Q}_i + \sum_j \left(\dot{\mathcal{W}}_j - p_o \frac{d\bar{V}}{dt}\right) + \sum_k \dot{m}_k \zeta_k^{flow} - T_o \dot{\mathcal{S}}_i. \tag{B.5}$$

Where $\dot{\Xi}$ is the rate at which exergy stored within the system is changing. The terms on the right, in order, define the rate exergy is carried in/out by; i) heat, ii) work (less any work the system does on the environment at constant environmental pressure p_o if the system volume $\bar{V}$ changes), and iii) by the material (or quantity known as flow exergy). The final term, $T_o\dot{\mathcal{S}}_i$, is the rate exergy is destroyed within the system or exergy consumption rate.

B.2 Thermo-Mechanical Relationships

This section discusses the concepts of conservative systems and forces, reversible and irreversible thermodynamic systems, average power and power flow, and the connections between Hamiltonian mechanics and thermodynamics required to support the concepts of necessary and sufficient conditions for stability of nonlinear systems. It is worth noting at this point that, by definition, electrical power is "pure exergy rate" and the Hamiltonian is stored exergy.

B.2.1 Conservative Mechanical Systems

A system is conservative if

$$\dot{\mathcal{H}} = 0 \qquad \text{and} \qquad \mathcal{H} = \text{constant.}$$

A force is conservative if

$$\oint F \cdot dx = \oint F \cdot \mathrm{v} dt = \oint Q_j \dot{q}_j dt = 0$$

for any closed path where F is the force, dx the displacement, and v the velocity. Basically, all of the forces can be modeled as potential force fields which are exergy storage devices.

B.2.2 Reversible Thermodynamic Systems

A thermodynamic system is reversible if

$$\begin{aligned} d\mathcal{S} &= \tfrac{dQ}{T} \\ \oint d\mathcal{S} &= \oint \tfrac{dQ}{T} = 0 \\ \oint d\mathcal{S} &= \oint \left[d\mathcal{S}_i + d\mathcal{S}_e \right] = \oint \left[\dot{\mathcal{S}}_i + \dot{\mathcal{S}}_e \right] dt = 0 \end{aligned}$$

which implies that $\dot{\mathcal{S}}_e = \dot{Q}/T$ since by definition the second law gives $\dot{\mathcal{S}}_i = 0$.

B.2.3 Irreversible Thermodynamic Systems

For

$$\oint d\mathcal{S} = \oint \left[\dot{\mathcal{S}}_i + \dot{\mathcal{S}}_e\right] dt = 0$$

then $\dot{\mathcal{S}}_e \leq 0$ and $\dot{\mathcal{S}}_i \geq 0$.

B.2.4 Analogies and Connections

Now the connections between thermodynamics and Hamiltonian mechanics are investigated.

1. The irreversible entropy production rate can be expressed as

$$\dot{\mathcal{S}}_i = \sum_k \mathcal{F}_k \dot{\mathcal{X}}_k = \frac{1}{T_o} \sum_k Q_k \dot{q}_k \geq 0. \tag{B.6}$$

2. The time derivative of the Hamiltonian is equivalent to the exergy rate since the Hamiltonian for a conservative system is stored exergy, then

$$\begin{array}{rcl} \dot{\mathcal{H}} & = & \sum_k Q_k \dot{q}_k \\ \dot{\Xi} & = & \dot{W} - T_o \dot{\mathcal{S}}_i = \sum_{j=1}^{N} Q_j \dot{q}_j - \sum_{l=N+1}^{M+N} Q_l \dot{q}_l. \end{array} \tag{B.7}$$

   Where N is the number of generators, M the number of dissipators, and let $\dot{W} = \sum_j \dot{\mathcal{W}}_j$. The following assumptions apply when utilizing the exergy rate equation (B.5) for *Hamiltonian systems*:

   (a) No substantial heat flow:

$$\dot{Q}_i \approx 0.$$

   (b) No substantial exergy flow or assume T_i is only slightly greater than T_o:

$$1 - \frac{T_o}{T_i} \approx 0.$$

   (c) No $p_o \bar{V}$ work on the environment:

$$p_o \frac{d\bar{V}}{dt} = 0.$$

   (d) No mass flow rate:

$$\sum_k \dot{m}_k \zeta_k^{flow} = 0.$$

(e) Then define:

$$\begin{array}{rcll} \dot{W} & \geq & 0 & \text{power input/generated} \\ T_o\dot{S}_i & \geq & 0 & \text{power dissipated.} \end{array}$$

3. A conservative system is equivalent to a reversible system when

$$\dot{\mathcal{H}} = 0 \quad \text{and} \quad \dot{S}_e = 0$$

then

$$\dot{S}_i = 0 \quad \text{and} \quad \dot{W} = 0.$$

4. A system that "appears to be conservative", but is not reversible is defined as:

$$\begin{array}{rcll} \dot{\mathcal{H}}_{ave} & = & 0 & = \frac{1}{\tau}\oint[\dot{W} - T_o\dot{S}_i]dt \\ & = & (\dot{W})_{ave} - (T_o\dot{S}_i)_{ave} & = \frac{1}{\tau}\oint[\sum_{j=1}^{N} Q_j\dot{q}_j - \sum_{l=N+1}^{M+N} Q_l\dot{q}_l]dt \\ & = & \text{average power over a cycle} & \end{array}$$

where τ is the period of the cycle. To be more specific about the average power calculations, the AC power factor [25] provides an excellent example. For the general case of alternating current supplied to a complex impedance the voltage and current differ in phase by an angle θ. The time responses for power, voltage, and current are shown for a general AC circuit in Fig. B.3 with

$$\begin{array}{rcl} \dot{W} & = & P = Q\dot{q} = v\,i = \sqrt{2}\bar{v}\cos(\omega t + \theta)\cdot\sqrt{2}\bar{i}\cos\omega t \\ & = & \bar{v}\bar{i}[\cos\theta + \cos(2\omega t + \theta)] \end{array}$$

where P is power, v is voltage ($\bar{v}$), i is current ($\bar{i}$), θ is the phase angle, and ω is the frequency. Integrating over a cycle gives

$$(\dot{W})_{ave} = \bar{v}\bar{i}\cos\theta$$

where for the second term

$$\oint \cos(2\omega t + \theta)dt = 0.$$

This is an important set of conditions that will be used in the next section to find the generalized stability boundary.

5. Finally, the power terms are sorted into three categories:

   (a) $(\dot{W})_{ave}$ - power generators; $(Q_j\dot{q}_j)_{ave} > 0$

   (b) $(T_o\dot{S}_i)_{ave}$ - power dissipators; $(Q_l\dot{q}_l)_{ave} < 0$

   (c) $(T_o\dot{S}_{rev})_{ave}$ - reversible/conservative exergy storage terms; $(Q_k\dot{q}_k)_{ave} = 0$.

These three categories are fundamental terms in the following definitions and design procedures.

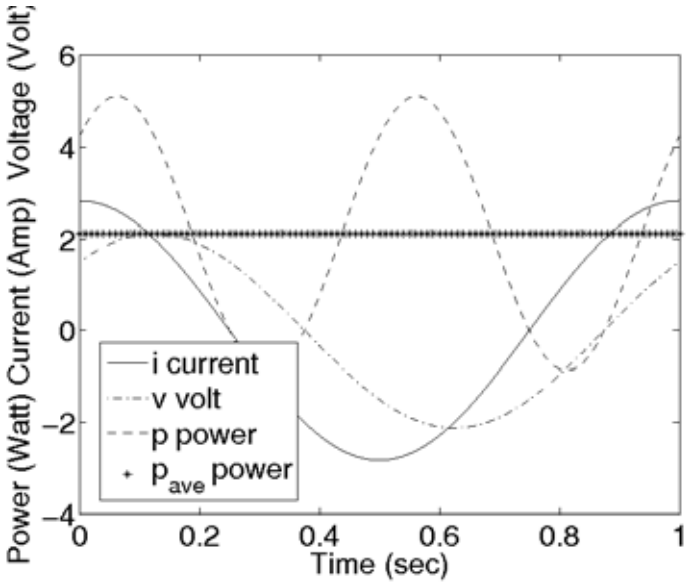

Figure B.3. Time response for power in a general AC circuit with $\omega = 2\pi, \bar{v} = 1.5, \bar{i} = 2.0$, and $\theta = \pi/4$

B.3 Necessary and Sufficient Conditions for Stability

This section describes the concepts from nonlinear control theory that will be used to assess the balance of exergy flows into versus the exergy consumption/destruction (irreversible entropy production) inside an open, self-organizing system. Open, self-organizing systems are the class of collective systems emphasized in this report and described in more detail in Appendix C. The balance of these exergy flows determines a fundamental necessary condition for sustainability of a self-organizing system: a limit cycle (see Appendix D).

The Lyapunov function is defined as the total energy (stored exergy by our definition) which for most mechanical systems is equivalent to an appropriate Hamiltonian function

$$V = \mathcal{H} \tag{B.8}$$

which is positive definite. The time derivative is

$$\begin{aligned} \dot{V} &= \dot{\mathcal{H}} = \textstyle\sum_k Q_k \dot{q}_k = \sum_{j=1}^{N} Q_j \dot{q}_j - \sum_{l=N+1}^{M+N} Q_l \dot{q}_l \\ &= \dot{W} - T_o \dot{\mathcal{S}}_i. \end{aligned} \tag{B.9}$$

B.3.1 Stability and Instability Theorems

To describe a nonlinear self-organizing system's behavior two theorems [26] help to characterize the essential features of their motion. In addition, by bounding the Lyapunov function between these Theorems, both necessary and sufficient conditions are a result of the transition of the time derivative of the Lyapunov function from stable to unstable.

1. **Lyapunov Theorem for Stability** Assume that there exists a scalar function V of the state $\mathbf{x}$, with continuous first order derivatives such that

   $$\begin{array}{ll} V(\mathbf{x}) & \text{is positive definite} \\ \dot{V}(\mathbf{x}) & \text{is negative definite} \\ V(\mathbf{x}) & \to \infty \quad \text{as} \quad \|\mathbf{x}\| \to \infty \end{array}$$

   Then the equilibrium at the origin is globally asymptotically stable.

2. **Chetaev Theorem for Instability** Considering the equations of disturbed motion, let V be zero on the boundary of a region R which has the origin as a boundary point, and let both V and $\dot{V}$ be positive-definite in R; then the undisturbed motion is unstable at the origin.

B.3.2 Stability Lemma for Nonlinear Self-Organizing Systems

Based on the relationships between thermodynamic exergy and Hamiltonian systems a Fundamental Stability Lemma can be formulated.

Fundamental Stability Lemma for Hamiltonian Systems The stability of Hamiltonian systems is bounded between Theorems 1 and 2. Given the Lyapunov derivative as a decomposition and sum of exergy generation rate and exergy dissipation rate then:

$$\dot{V} = \dot{W} - T_o \dot{\mathcal{S}}_i = \sum_{j=1}^{N} Q_j \dot{q}_j - \sum_{l=N+1}^{M+N} Q_l \dot{q}_l \tag{B.10}$$

that is subject to the following general necessary and sufficient conditions:

$$\begin{array}{lcll} T_o \dot{\mathcal{S}}_i & \geq & 0 & \text{Positive semi-definite, always true} \\ \dot{W} & \geq & 0 & \text{Positive semi-definite; exergy pumped into the system.} \end{array}$$

The following corollaries encompass both stability and instability for Hamiltonian systems which utilize AC power concepts [25]:

Corollary 1: For $(T_o\dot{S}_i)_{ave} = 0$ and $(\dot{W})_{ave} = 0$ then $\dot{V} = 0$ the Hamiltonian system is neutrally stable, conservative and reversible.

Corollary 2: For $(T_o\dot{S}_i)_{ave} = 0$ and $(\dot{W})_{ave} > 0$ then $\dot{V} > 0$ the Hamiltonian system is unstable.

Corollary 3: For $(T_o\dot{S}_i)_{ave} > 0$ and $(\dot{W})_{ave} = 0$ then $\dot{V} < 0$ the Hamiltonian system is asymptotically stable and a passive system in the general sense (passivity controllers).

Corollary 4: Given apriori $(T_o\dot{S}_i)_{ave} > 0$ and $(\dot{W})_{ave} > 0$ then the Hamiltonian system is further subdivided into:

4.1: For $\left(T_o\dot{S}_i\right)_{ave} > \left(\dot{W}\right)_{ave}$ with $\dot{V} < 0$ yields asymptotic stability

4.2: For $\left(T_o\dot{S}_i\right)_{ave} = \left(\dot{W}\right)_{ave}$ with $\dot{V} = 0$ yields neutral stability

4.3: For $\left(T_o\dot{S}_i\right)_{ave} < \left(\dot{W}\right)_{ave}$ with $\dot{V} > 0$ yields an unstable system.

The bottom line is that stability is defined in terms of power flow which determines whether the system is moving toward or away from its minimum energy and maximum entropy state.

B.3.3 Classic van der Pol Equation Example

Before moving on to collective self-organizing systems, it is instructive to provide a couple of simple examples. Example 1 is the classic van der Pol's equation [27] which is analyzed using the techniques of this section. Originally, the "van der Pol equation" is credited to van der Pol, and is a model of an electronic circuit for early radio vacuum tubes of a triode electronic oscillator [27]. The tube acts like a normal resistor when the current is high, but acts as a negative resistor if the current is low. The main feature is that electrical circuits that contain these elements pump up small oscillations due to a negative resistance when currents are small, but drag down large amplitude oscillations due to positive resistance when the currents are large. This behavior is known as a *relaxation oscillation*, as each period of the oscillation consists of a slow buildup of energy ('stress phase') followed by a phase in which energy is discharged ('relaxation phase'). This particular system has played a large role in nonlinear dynamics and has been used to study limit cycles (see Appendix D) and self-sustained oscillatory phenomena in nonlinear systems.

Consider the van der Pol equation which includes a non-linear damping term:

$$\ddot{x} - \mu(1 - x^2)\dot{x} + x = 0.$$

Next include the actual mass and stiffness values (other than unity) or

$$m\ddot{x} - \mu(1 - x^2)\dot{x} + kx = 0.$$

The appropriate Hamiltonian/Lyapunov function is defined as:

$$\mathcal{H} = V = \frac{1}{2}m\dot{x}^2 + \frac{1}{2}kx^2 > 0.$$

Then the corresponding time derivative of the Lyapunov function becomes

$$\begin{aligned} \dot{V} &= [m\ddot{x} + kx]\dot{x} \\ &= \left[\mu\dot{x}(1-x^2)\right]\dot{x} \\ &= \mu\dot{x}^2 - \mu x^2\dot{x}^2. \end{aligned}$$

Identifying generator and dissipator terms yields

$$\begin{aligned} \dot{W} &= \mu\dot{x}^2 \\ T_o\dot{S}_i &= \mu x^2\dot{x}^2 \end{aligned}$$

The stability boundary can be determined as

$$\begin{aligned} \left[\dot{W}\right]_{ave} &= \left[T_o\dot{S}_i\right]_{ave} \\ \left[\mu\dot{x}^2\right]_{ave} &= \left[\mu x^2\dot{x}^2\right]_{ave} \end{aligned}$$

By investigating several initial conditions both inside, on, and outside the limit cycle then three separate conditions can be observed. Figure B.4 shows these conditions with the corresponding numerical values given in Table B.1.

Table B.1. Van der Pol model numerical values

Case	description	x_o	$\dot{x}_o$	μ	m	k
		(m)	(m/s)	(kg/s)	(kg)	(kg/s^2)
1	generate	0.1	-0.1	1.5	1.0	1.0
2	neutral	1.0	-1.0	1.5	1.0	1.0
3	dissipate	2.0	-2.0	1.5	1.0	1.0

The responses are plotted on the Hamiltonian 3D surface (left) with the projection onto the phase plane shown on the 2D plot (right). The system trajectories are constrained to move along the Hamiltonian surface as a function of exergy flow into the system versus the exergy dissipation rate. For the case outside the limit cycle (case 3), the dissipator term dominates and for the case inside the limit cycle (case 1) the generator term dominates. For both cases

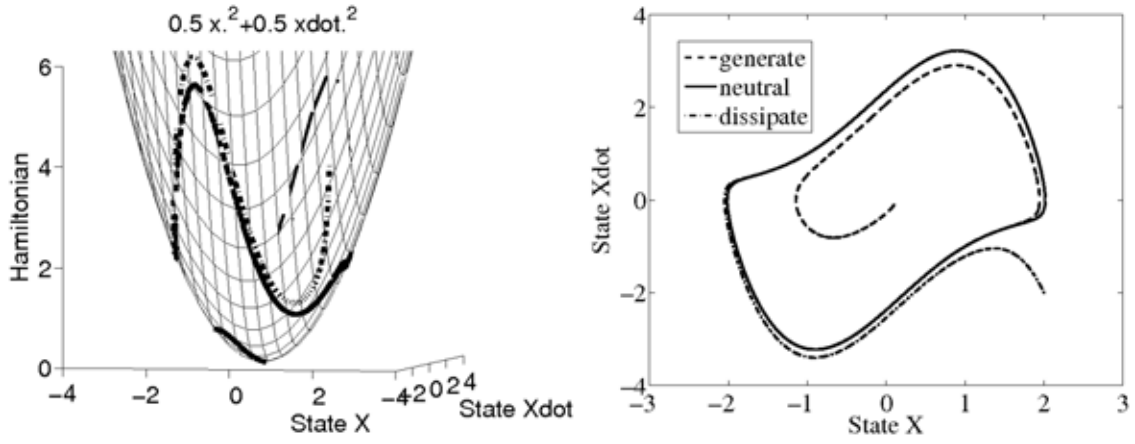

Figure B.4. Van der Pol responses: Hamiltonian 3D surface (left) and phase plane 2D projection (right)

inside and outside the limit cycle, the system migrates back to the stability boundary. For the case already on the limit cycle (case 2) then the system is already at neutral stability. The generative case exergy-rate (left) and exergy (right) plots are shown in Fig. B.5. The neutral case exergy-rate (left) and exergy (right) plots are shown in Fig. B.6. The dissipative case exergy-rate (left) and exergy (right) plots are shown in Fig. B.7. The cycle is defined at approximately $\tau = 3.5$ seconds. For the neutral pair the terms cancel each other out at the end of the cycle or $[\dot{W}]_{ave} = [T_o \dot{S}_i]_{ave}$. For the generator case then $[\dot{W}]_{ave} > [T_o \dot{S}_i]_{ave}$ and for the dissipator case then $[\dot{W}]_{ave} < [T_o \dot{S}_i]_{ave}$, respectively. Eventually, given enough cycles both the generator and dissipator cases will converge to the neutral case.

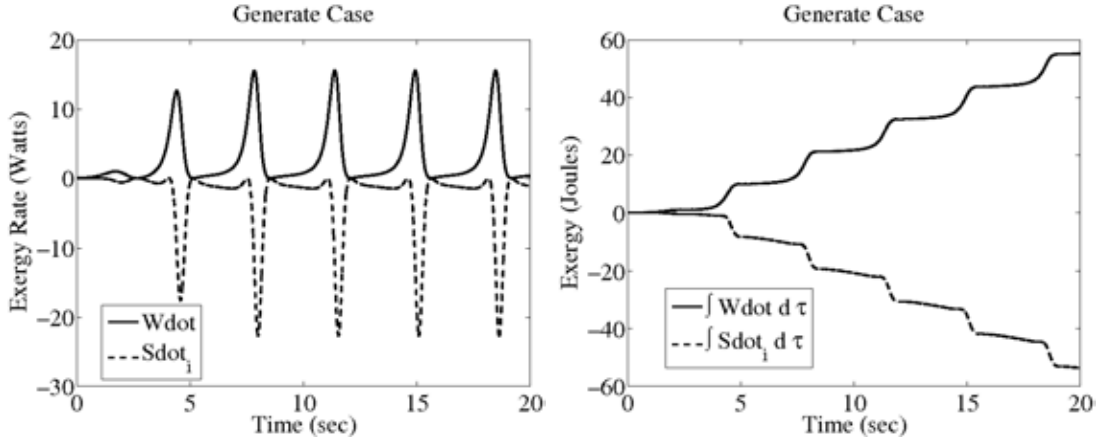

Figure B.5. Van der Pol exergy-rate (left) and exergy (right) responses - generative case

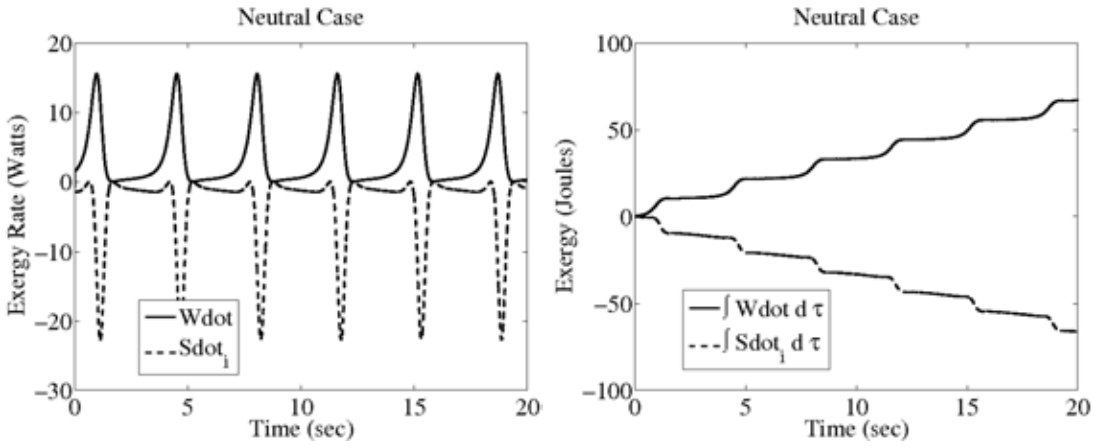

Figure B.6. Van der Pol exergy-rate (left) and exergy (right) responses - neutral case

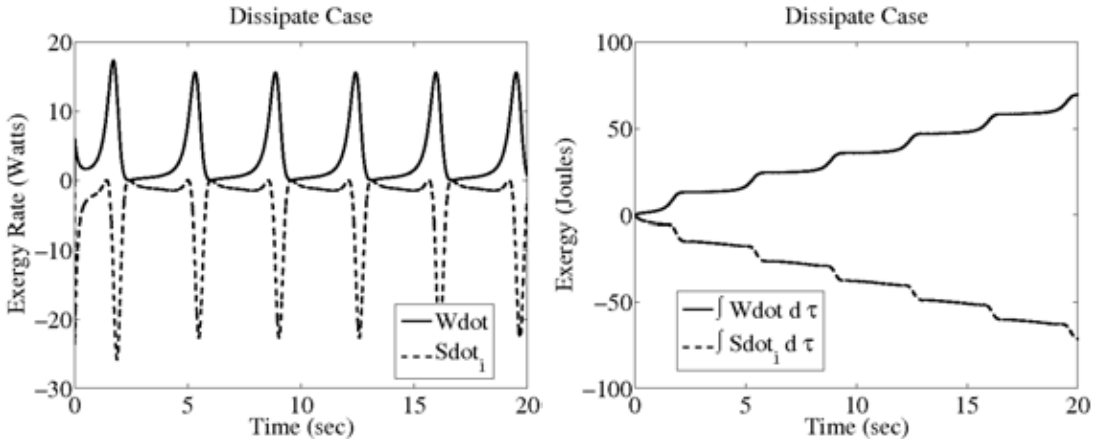

Figure B.7. Van der Pol exergy-rate (left) and exergy (right) responses - dissipative case

As an interesting analogy to a Proportional-Integral-Derivative (PID) control system, replace the power generator term with an integral term as

$$\dot{W} = \mu \dot{x}^2 = -K_I \left[\int_0^t x d\tau \right] \dot{x}.$$

The equivalence of the integral term as a power generator is analyzed and proved in reference [13]. Since the negative damping term is nonlinear, the dynamic response to initial conditions and resulting limit cycle will be slightly different due to the build-up of the integrator.

The same three test cases used in the previous van der Pol analysis were used with integral action with the numerical values given in Table B.2. Both the Hamiltonian 3D surface (left) with the projection onto the phase plane (right) are shown in Fig. B.8. It is interesting to note for the neutral Case 2, that the integral action has a delayed response which enables the system trajectory to "dissipate" below the limit cycle boundary before it begins to build back up and eventually end up on the neutral boundary. Again Cases 1 and 3 are the generative and dissipative cases. The corresponding exergy and exergy-rate plots for each case are given in Fig. B.9, for the generative case exergy-rate (left) and exergy (right) responses. The neutral case exergy-rate (left) and exergy (right) plots are shown in Fig. B.10. The dissipative case exergy-rate (left) and exergy (right) plots are shown in Fig. B.11.

Table B.2. Van der Pol model with integral action numerical values

Case	description	x_o	$\dot{x}_o$	μ	m	k	K_I
		(m)	(m/s)	(kg/s)	(kg)	(kg/s^2)	(kg/s)
1	generate	0.1	-0.1	1.5	1.0	1.0	1.02
2	neutral	1.0	-1.0	1.5	1.0	1.0	1.02
3	dissipate	2.0	-2.0	1.5	1.0	1.0	1.02

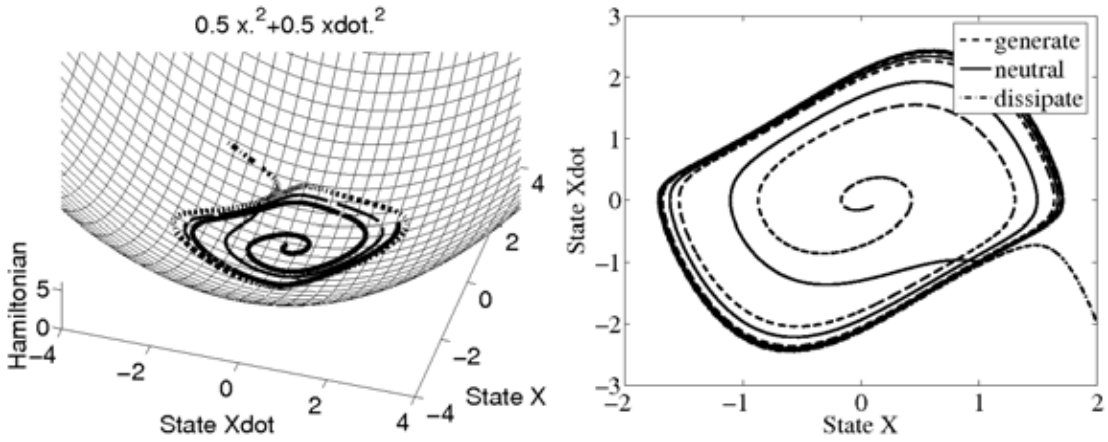

Figure B.8. Van der Pol with integral action responses: Hamiltonian 3D surface (left) and phase plane 2D projection (right)

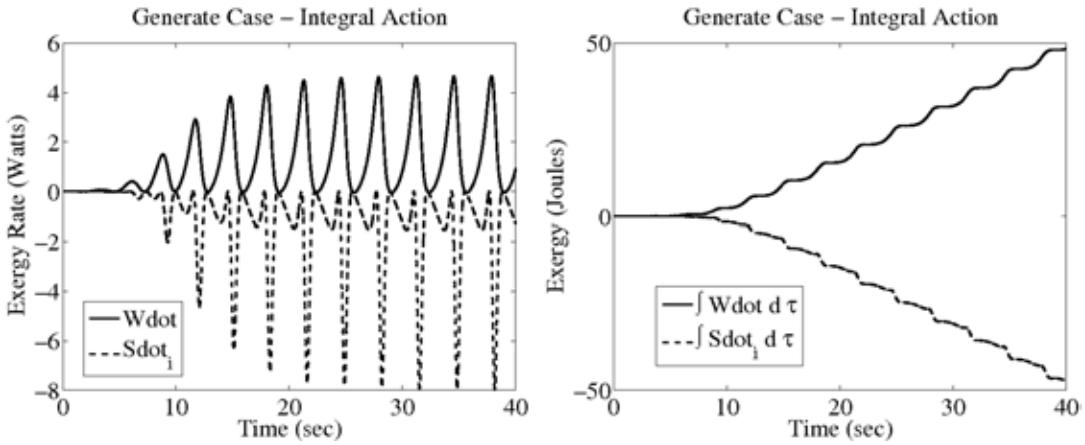

Figure B.9. Van der Pol exergy-rate (left) and exergy (right) responses - generative case with integral action

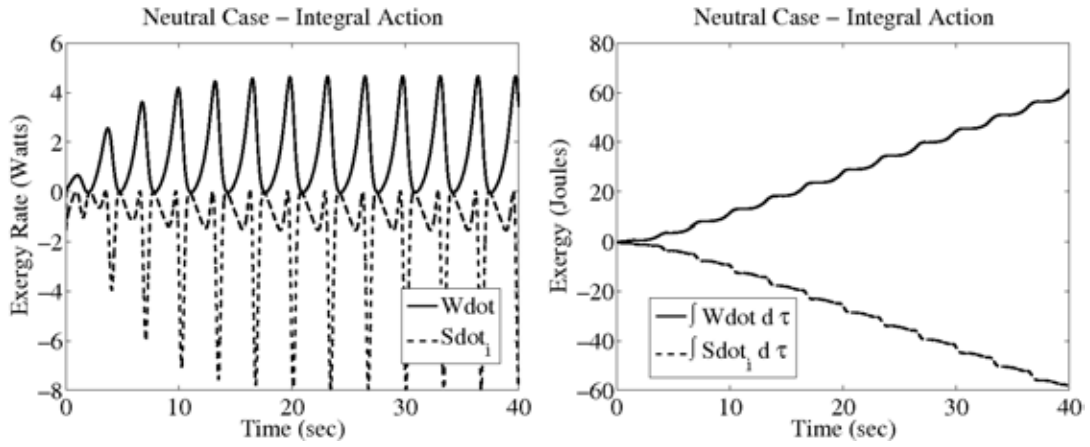

Figure B.10. Van der Pol exergy-rate (left) and exergy (right) responses - neutral case with integral action

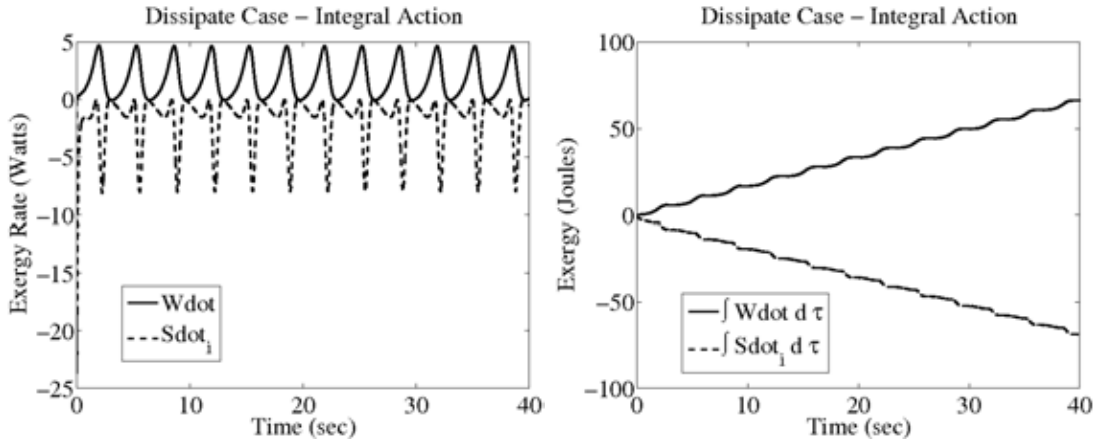

Figure B.11. Van der Pol exergy-rate (left) and exergy (right) responses - dissipative case with integral action

Appendix C

Necessary and Sufficient Conditions for Stability of Collective Systems

In this Appendix which is a modification of references [1, 21], the concepts of Appendix B are extended to self-organizing systems. Self-organizing systems, an important class of collective systems, are reviewed with the assistance of a simplified example to explain the importance of exergy flows. These concepts are applied to several nonequilibrium collective system examples in Chapter 3.

C.1 Self-Organization and Adaptability Concepts

In this section self-organizing system concepts are discussed that will be used to analyze the sustainability of a simplified nonlinear system model which represents a satellite in space. The basic format from Heylighen [28] will be followed with support from Haken [29] and Buenstorf [30].

C.1.1 Background

The Achilles heel or single point of failure of self-organizing systems is the requirement that exergy continuously flow into the system. The self-organizing system is continuously "shedding" entropy to the environment to keep itself organized and living as it consumes or dissipates the exergy flow.

Schrödinger (1945) suggested that all organisms need to import "negative entropy" from their environment and export high entropy (for example, heat) into their environment in order to survive. This idea was developed into a general thermodynamic concept by Prigogine and his co-workers who coined the notion of "dissipative structures" (Prigogine, 1976; Prigogine and Stengers, 1984), structures of increasing complexity developed by open systems on the basis of energy exchanges with the environment. In the self-organization of dissipative structures, the environment serves both as a source of low-entropic energy and as a sink for the high-entropic energy which is necessarily pro-

duced [28].

Basically, self-organizing systems are attempting to balance and perform dialectic synthesis on evolving disordering and ordering pressures [31]. Said another way, life is exergy dissipation (increasing entropy; disorder) and order production in an open system simultaneously. This process which is the evolution of a complex adaptive system is irreversible: the future is fundamentally different from the past, and it is impossible to reconstruct the past from the present [28].

Dissipation is the disordering power flow which is better known as consumption in economics and irreversible entropy production in thermodynamics. Exergy flow into a system is the ordering power flow that is better known as production in economics and exergy rate into an open system in thermodynamics. Balance between these competing power flows is key because these terms are relative to a goal and path through time which means they can "flip over" or reverse roles. For example, the exergy flow into a system by a nuclear weapon is not "matched." It deposits exergy at a rate that destroys the system, which means it is a disordering power flow increasing entropy. So, a mechanism must be inserted to "match" the input to the system if the goal is sustainability instead of destruction. Nuclear power is an attempt to match the exergy source to the exergy sink to move toward exergy sustainability [1].

The balance between these opposing power flows creates a sort of "equilibrium condition" for a self-organizing system. Ilya Prigogine described this as "far from thermodynamic equilibrium on the basis of energy dissipation" and, in cybernetics, it's often called an attractor [28]. Most nonlinear self-organizing systems have several attractors and the system moves between these attractors (reordering) due to variations (perturbations; noise; disorder) in the exergy flow and the system parameters. These system parameters are often called "control parameters" because their values determine the "static" stability characteristics of the system. Static stability and deforming the potential field will be discussed in more detail in Chapter 3. For example, the potential force field [29, 32] for a nonlinear spring system can be written in kinematic form (no dynamics) as

$$\dot{q} = kq + k_{NL}q^3$$

where k is the linear stiffness coefficient and k_{NL} is the nonlinear stiffness coefficient. The potential function is defined as

$$\mathcal{V}(q) = \frac{1}{2}kq^2 + \frac{1}{4}k_{NL}q^4. \tag{C.1}$$

This system changes its fundamental static stability structure (i.e., accessible state space) by changing $k > 0$ to $k < 0$ and $k_{NL} > 0$. Figure C.1 shows how the stable equilibrium state at $q = 0$ bifurcates into two symmetrical stable equilibrium states and becomes an unstable state.

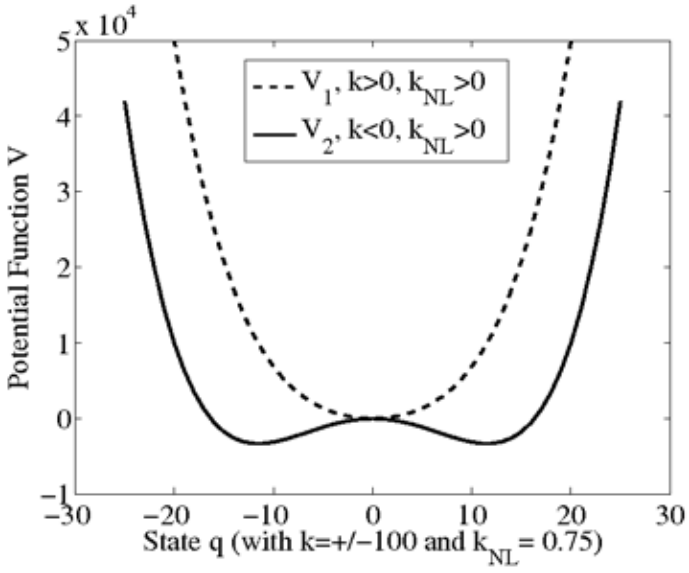

Figure C.1. Nonlinear spring potential function characteristics

These attractors are defined relative to a "fitness index." Some attractors are more likely to survive, and be "more fit," than others. In the previous example, one attractor turned into two attractors which appear to be equally fit if the potential function is interpreted as the fitness surface. In fact, it is possible for the system to jump back and forth between these two attractors by varying the exergy flow and the control parameter through perturbations and noise.

As described earlier, nonlinear systems have several attractors and variations or "fluctuations" that reside between attractors that will push the system to one or the other of the attractors. Positive feedback is necessary for random fluctuations to be amplified (generative) [30, 33]. Maintenance of the structured state in the presence of further fluctuations implies that some negative feedback is also present that dampens (dissipates) these effects [30, 33]. In Appendix B, these are called a power generator and a power dissipator. Self-organization results from the interplay of positive and negative feedback [33]. In Section B.3, this is defined as the stability boundary and/or limit cycle. Appendix D provides several numerical examples. In more complex self-organizing systems, there will be several interlocking positive and negative feedback loops, so that changes in some directions are amplified while changes in other directions are suppressed [28, 30]. At the transition between order and disorder, a large number of bifurcations may be in existence which are analogous to the bifurcations of the previous potential function. Bifurcations may be arranged in a "cascade" where each branch of the fork itself bifurcates further and further, characteristic of the onset of the chaotic regime [28, 23, 30]. The system's behavior on this edge is typically governed by a "power law" where large adjustments are possible, but are much less probable than small adjustments [28]. These concepts enable us to better under-

stand nonlinear systems, also known as *complex adaptive systems*, that are on the "edge of chaos" or those systems that are in a domain between frozen constancy (equilibrium) and turbulent, chaotic activity [28]. The mechanism by which complex systems tend to maintain on this critical edge has also been described as *self-organized criticality* [28, 34]. By appropriately utilizing the preceding concepts, one can design closed-loop nonlinear systems that can exploit this concept of on the edge of chaos.

C.1.2 Simple Nonlinear Satellite System

With this brief background, it's time to analyze a simplified nonlinear satellite system (see Fig. C.2) to mathematically demonstrate the concept of "far from thermodynamic equilibrium on the basis of energy dissipation" for self-organizing (collective) systems. The thermodynamic analysis follows [35]. For purposes of clarity, each control volume is subdivided into two subregions that contain the physical components. The component mass is constant. A single constant temperature characterizes each component. The component subregion is surrounded by an outer zone that characterizes the interaction between the component (at temperature T) and the environment (reservoir) characterized by temperature T_o. Only control volume 2 will be analyzed in this paper (see reference [1] for more control volume detail).

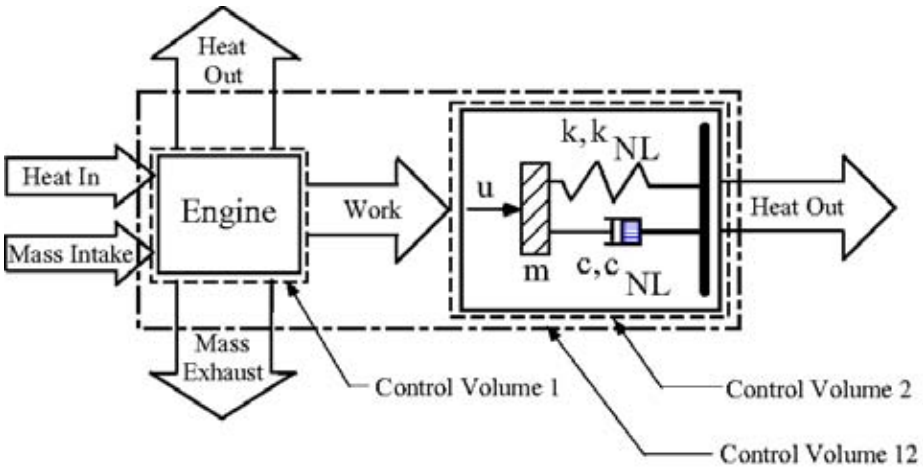

Figure C.2. Simplified nonlinear satellite model

Conservation Equations for the Machine (Control Volume 2):

Control Volume 2 consists of a nonlinear mass/spring/damper system (with Duffing oscillator/Coulomb friction contributing to the nonlinear effects). Work is supplied to the system which results in the acceleration of the mass. The work is dissipated by the damper. This increases the temperature of the components of the system, which is characterized by a single temperature, T_2. The thermal energy is then transferred to the environment, which has

a temperature of T_0. The transfer is realized solely by a heat interaction. No mass enters or leaves Control Volume 2. Performing the energy, entropy, and exergy analyses [35] yields:

$$\begin{aligned}
\dot{\mathcal{E}}_{2_{component}} &= \dot{W} - \dot{Q}_{out_2} \\
\dot{\mathcal{S}}_{2_{component}} &= \dot{\mathcal{S}}_{irr_2} - \frac{\dot{Q}_{out_2}}{T_2} \\
\dot{\Xi}_{2_{component}} &= \dot{W} - T_o \dot{\mathcal{S}}_{irr_2} - \left(1 - \frac{T_o}{T_2}\right) \dot{Q}_{out_2}
\end{aligned}$$

For the surface heat interaction(s) the energy, entropy, and exergy equations are:

$$\begin{aligned}
\dot{\mathcal{E}}_{2_{interact_Q}} &= 0 \quad = [\dot{Q}_{out_2} - \dot{Q}_{out_2}] \\
\dot{\mathcal{S}}_{2_{interact_Q}} &= 0 \quad = \dot{Q}_{out_2} \left[\frac{1}{T_2} - \frac{1}{T_o}\right] + \dot{\mathcal{S}}_{irr_{2_{interact_Q}}} \\
\dot{\Xi}_{2_{interact_Q}} &= 0 \quad = \left[\left(1 - \frac{T_o}{T_2}\right) \dot{Q}_{out_2} - \left(1 - \frac{T_o}{T_o}\right) \dot{Q}_{out_1}\right] - T_o \dot{\mathcal{S}}_{irr_{2_{interact_Q}}} \\
&\qquad = \left(1 - \frac{T_o}{T_2}\right) \dot{Q}_{out_2} - T_o \dot{\mathcal{S}}_{irr_{2_{interact_Q}}}.
\end{aligned}$$

Adding the interaction fluxes to the component fluxes produces the complete equations for Control Volume 2 as:

$$\begin{aligned}
\dot{\mathcal{E}}_{2_{total}} &= \dot{W} - \dot{Q}_{out_2} \\
\dot{\mathcal{S}}_{2_{total}} &= \dot{\mathcal{S}}_{irr_2} - \frac{\dot{Q}_{out_2}}{T_2} + \dot{Q}_{out_2} \left[\frac{1}{T_2} - \frac{1}{T_o}\right] + \dot{\mathcal{S}}_{irr_{2_{interact_Q}}} \\
\dot{\Xi}_{2_{total}} &= \dot{W} - T_o \dot{\mathcal{S}}_{irr_2} - \left(1 - \frac{T_o}{T_2}\right) \dot{Q}_{out_2} + \left(1 - \frac{T_o}{T_2}\right) \dot{Q}_{out_2} - T_o \dot{\mathcal{S}}_{irr_{2_{interact_Q}}}
\end{aligned}$$

and simplifying yields:

$$\begin{aligned}
\dot{\mathcal{E}}_{2_{total}} &= \dot{W} - \dot{Q}_{out_2} \\
\dot{\mathcal{S}}_{2_{total}} &= -\frac{\dot{Q}_{out_2}}{T_o} + \left[\dot{\mathcal{S}}_{irr_2} + \dot{\mathcal{S}}_{irr_{2_{interact_Q}}}\right] \\
\dot{\Xi}_{2_{total}} &= \dot{W} - T_o \left[\dot{\mathcal{S}}_{irr_2} + \dot{\mathcal{S}}_{irr_{2_{interact_Q}}}\right]
\end{aligned}$$

where

$$\dot{\mathcal{S}}_{irr_{2_{interact\_Q}}} = \dot{Q}_{out_2} \left[\frac{1}{T_0} - \frac{1}{T_2}\right].$$

By following earlier derivations, this simplified nonlinear model reduces within Control Volume 2 to

$$\begin{aligned}
V = \mathcal{H} &= \tfrac{1}{2} m\dot{x}^2 + \tfrac{1}{2} k x^2 + \tfrac{1}{4} k_{NL} x^4 \\
\dot{V} = \dot{\mathcal{H}} &= \left[m\ddot{x} + kx + k_{NL} x^3\right] \dot{x} \\
&= \dot{W} - T_o \dot{\mathcal{S}}_i \\
&= u\dot{x} - C\dot{x}^2 - C_{NL} \mathrm{sgn}(\dot{x}) \dot{x} \\
&= \dot{x} \left[-K_P x - K_I \int_0^t x d\tau - K_D \dot{x} - C\dot{x} - C_{NL} \mathrm{sgn}(\dot{x})\right]
\end{aligned}$$

where

$$\begin{aligned} u &= \text{PID feedback controller (Implemented force input)} \\ &= -K_P x - K_I \int_0^t x d\tau - K_D \dot{x}. \end{aligned}$$

Then the following exergy terms are identified as

$$\begin{aligned} \dot{W} &= \left[-K_I \int_0^t x d\tau\right] \dot{x} \\ T_o \dot{\mathcal{S}}_i &= \left[-K_D \dot{x} - C\dot{x} - C_{NL}\text{sgn}(\dot{x})\right] \dot{x} \\ T_o \dot{\mathcal{S}}_{rev} &= \left[m\ddot{x} + kx + K_P x + k_{NL} x^3\right] \dot{x}. \end{aligned}$$

The generalized stability boundary (i.e., far from thermodynamic equilibrium on the basis of energy dissipation) is given as a balance between "positive and negative feedback" (exergy generation and exergy dissipation)

$$\begin{aligned} [\dot{W}]_{ave} &= [T_o \dot{\mathcal{S}}_i]_{ave} \\ \left[-K_I \int_0^t x d\tau \cdot \dot{x}\right]_{ave} &= \left[(K_D + C)\dot{x}^2 + C_{NL}\text{sgn}(\dot{x}) \cdot \dot{x}\right]_{ave}. \end{aligned} \tag{C.2}$$

The "shape" of the resulting limit cycle (see Appendix D) is constrained to the Hamiltonian surface which determines the accessible bifurcated structure as a function of exergy level (see Fig. C.3).

C.1.3 Lifestyle Definition

Next the concept of far from thermodynamic equilibrium on the basis of energy dissipation is interpreted in terms of a "lifestyle" of the mass-spring-damper system within the satellite. The lifestyle is defined by a cyclic path, attractor, or limit cycle in the phase plane that is constrained to the Hamiltonian surface $\mathcal{H} = V$, (left) projected onto the phase plane (right) in Fig. C.3. This path occurs as a result of satisfying (C.2). This interpretation directly provides a means to ensure a sustainable form of far from thermodynamic equilibrium on the basis of energy dissipation: the continuous compensation of irreversible entropy production in an open system with an impedance and capacity-matched persistent exergy source. In other words, the cyclic lifestyle will persist indefinitely as long as (C.2) is satisfied and m, k, K_P, and k_{NL} are constants. Adaptivity can occur when these parameters are varied in a controlled fashion.

One final observation on this topic of impedance and capacity matching, the goal of war and economic competition is to create a production/consumption rate which is sustainable for you and generates an impedance mismatch that is unsustainable for your enemy/competitor. The ultimate goal is to cut-off, destroy, and/or dissipate your competitor's exergy reserves by changing/deforming your competitor's Hamiltonian surface (infrastructure - including population of the work force). This can be accomplished in several ways including: 1)

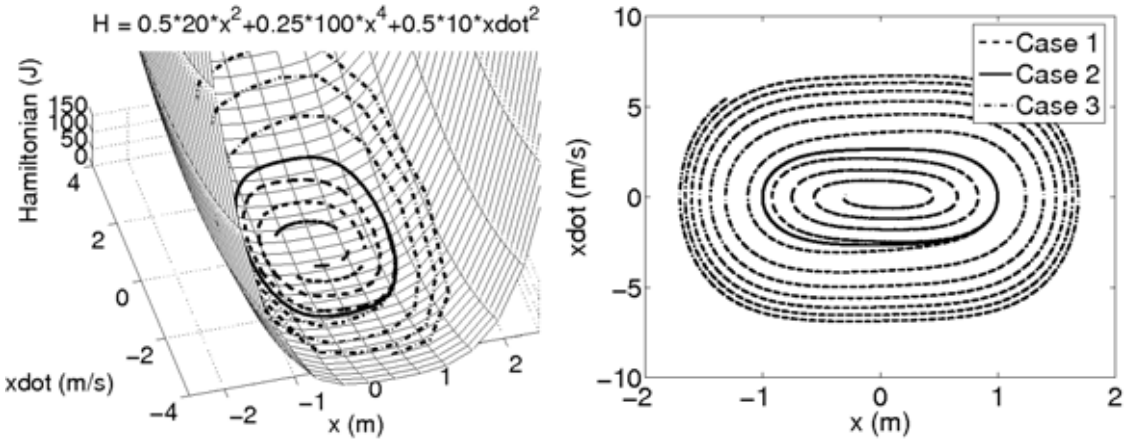

Figure C.3. All cases: mass-spring-damper with Duffing oscillator/Coulomb friction model numerical results: Hamiltonian 3D surface (left) and phase plane 2D projection (right)

pick-up the pace by increasing the limit cycle frequency (i.e., less mass), 2) accelerate the exergy consumption of your competitor by using more efficient technologies, 3) deform the potential field with information flow, and 4) enable the energy state through Fisher information. Topics 3) and 4) are discussed in more detail in Chapter 3.

Appendix D

What is a Limit Cycle?

D.1 Limit Cycle Analyses

The primary goal of this section is to describe several characteristics of limit cycles which include being the stability boundary for linear and nonlinear control systems. A secondary goal is to demonstrate the fundamental nature of the Hamiltonian and power flow control in control system design. In particular, the combination of Hamiltonian mechanics, thermodynamics, and nonlinear control theory described in Appendix B is used to define necessary and sufficient conditions for stability of nonlinear systems: the limit cycle is the generalized stability boundary.

D.2 Linear Limit Cycles

This section describes the concept of *linear limit cycles.* A linear limit cycle is a strange concept to most people since limit cycles are typically associated with nonlinear systems. A limit cycle is defined by Wikipedia as a closed trajectory in phase space having the property that at least one other trajectory spirals into it either as time approaches infinity or as time approaches minus - infinity. By the end of this section, it will be shown how a center [40] of a second-order system can be interpreted as a linear limit cycle, for example, the goal of power engineering.

The mass-spring-damper system of Fig. D.1 will be utilized throughout this discussion by methodically adding more complexity as the discussion progresses.

The Lagrangian and Hamiltonian of this system are

$$\mathcal{L} = \mathcal{T} - \mathcal{V} = \frac{1}{2}m\dot{x}^2 - \frac{1}{2}kx^2 \tag{D.1}$$

and

$$\mathcal{H} = \mathcal{T} + \mathcal{V} = \frac{1}{2}m\dot{x}^2 + \frac{1}{2}kx^2 \tag{D.2}$$

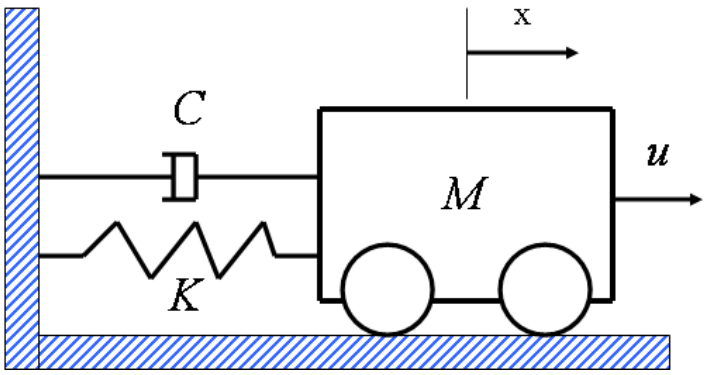

Figure D.1. Mass-spring-damper system

where

$$\begin{array}{lcll} \mathcal{T} & = & \frac{1}{2}m\dot{x}^2 & = \text{ kinetic energy} \\ \mathcal{V} & = & \frac{1}{2}kx^2 & = \text{ potential energy.} \end{array}$$

The equation of motion is derived from Lagrange's equation

$$\frac{d}{dt}\left(\frac{\partial \mathcal{L}}{\partial \dot{q}_i}\right) - \frac{\partial \mathcal{L}}{\partial q_i} = Q_i \tag{D.3}$$

and is determined as

$$m\ddot{x} + kx = -c\dot{x} + u \tag{D.4}$$

where

$$\begin{array}{lcll} q_i & = & x & = \text{ generalized coordinate} \\ \dot{q}_i & = & \dot{x} & = \text{ generalized velocity} \\ Q_i & = & -c\dot{x} + u & = \text{ generalized forces, and} \\ u & = & & \text{control input.} \end{array}$$

The time derivative of the Hamiltonian gives

$$\dot{\mathcal{H}} = [m\ddot{x} + kx]\,\dot{x} = [-c\dot{x} + u]\,\dot{x} \tag{D.5}$$

which for a conservative system is

$$\dot{\mathcal{H}} = 0 \quad \Rightarrow \quad \mathcal{H} = \text{constant}$$

and

$$[-c\dot{x}+u]=0 \tag{D.6}$$

which implies point-by-point cancellation of forces and power flows.

Next (D.5) and (D.6) are investigated in more detail. Equation (D.5) can be rewritten as a line integral

$$\mathcal{H}_{cyclic}=\oint_{\tau}\dot{\mathcal{H}}dt=\oint_{\tau}[m\ddot{x}+kx]\,\dot{x}dt=\oint_{\tau}[-c\dot{x}+u]\,\dot{x}dt \tag{D.7}$$

where

$$\begin{array}{rcl}\tau & = & \text{period of the limit cycle}\\ \oint & = & \text{closed (trajectory) path integral along the Hamiltonian surface .}\end{array}$$

Equation (D.7) is the line integral of the power flow to produce the work per cycle [4, 16, 36, 37] or

$$W_{cyclic}=\oint_{\tau}\mathbf{F}\cdot\dot{\mathbf{x}}dt=\oint_{\tau}Q_i\dot{q}_i dt=\oint_{\tau}\dot{\mathcal{H}}dt \tag{D.8}$$

where

$$\begin{array}{rcl}\mathbf{F} & = & \text{force vector}\\ \dot{\mathbf{x}} & = & \text{velocity vector.}\end{array}$$

Equation (D.7) can be further rewritten as

$$\begin{array}{rcl}\mathcal{H}_{cyclic} & = & \oint_{\tau}[p(x,y)dx+q(x,y)dy]=\oint_{\tau}[\mathcal{H}_x dx+\mathcal{H}_y dy]\\ & = & \oint_{\tau}[kxdx+mydy]=\oint_{\tau}[kx\dot{x}+my\dot{y}]\,dt=0\end{array} \tag{D.9}$$

for $[c\dot{x}-u]=0$, $y=\dot{x}$, $\mathcal{H}_x=\partial\mathcal{H}/\partial x$, since $\mathcal{H}$ is an exact integral, conservative, and path independent. This result can be confirmed by Green's Theorem

$$\mathcal{H}_{cyclic}=\oint_{\tau}[pdx+qdy]=\int\int_{\Omega}[q_x-p_y]\,dxdy=0$$

since

$$\begin{array}{lll}p=\mathcal{H}_x=kx & \Rightarrow & p_y=0\\ q=\mathcal{H}_y=my & \Rightarrow & q_x=0.\end{array}$$

Equation (D.9) describes a center which will be referred to as a linear limit cycle shown in Fig. D.2 (where $m = 10$ kg, $k = 10$ N/m, $\dot{x}_o = 0.0$ m/s, and $x_o = 1.0$ m). The Hamiltonian surface determines the accessible phase space as a function of energy (exergy) level. The power flow, $\dot{\mathcal{H}}$, determines the system trajectory across the Hamiltonian surface as a function of time and initial position.

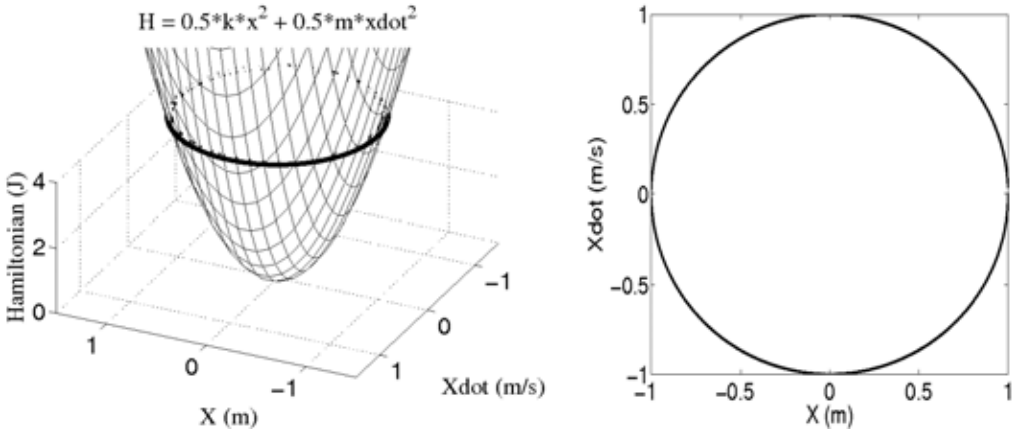

Figure D.2. Linear limit cycle: Hamiltonian 3D surface (left) and phase plane plot (right)

This linear limit cycle defines a constant energy (exergy) orbit in phase space, $\mathcal{H} =$ constant, given some initial condition that defines an initial energy state

$$\mathcal{H} = \frac{1}{2}m\dot{x}_o^2 + \frac{1}{2}kx_o^2 \tag{D.10}$$

Equation (D.10) defines the orbit that is an orthogonal cut across the Hamiltonian manifold and projected onto the phase plane.

Now, one can explore (D.6) further by selecting a Proportional-Integral-Derivative (PID) controller

$$u = -K_P x - K_I \int x dt - K_D \dot{x} \tag{D.11}$$

and rewriting (D.5) as

$$\dot{\mathcal{H}} = [m\ddot{x} + (k + K_P)x]\dot{x} = \left[-(c + K_D)\dot{x} - K_I \int x dt\right]\dot{x} \tag{D.12}$$

which leads to a rewritten version of (D.6) as

$$\left[-(c + K_D)\dot{x} - K_I \int x dt\right] = 0 \tag{D.13}$$

Equation (D.13) was solved in [13] where the integral feedback was shown to be a generative (exergy) term that balances the dissipator terms point-for-point which leads to another linear limit cycle like the one in Fig. D.2. It is as though no forces and power flows are acting on the system. Notice, that if

$$K_I \int x dt\ \dot{x} > -(c + K_D)\dot{x}^2$$

then the system rises to a higher energy state and the system is unstable. On the other hand, if

$$K_I \int x dt\ \dot{x} < -(c + K_D)\dot{x}^2$$

then the system falls to a lower energy state and the system is asymptotically stable. The linear limit cycle is a stability boundary. Equation (D.12) defines an eigenvalue problem that will be discussed in Section D.4.

Next, a particular example of designing linear limit cycles will be explored for a power engineering application [25]. Returning to (D.4), the control input is a sinusoidal voltage and the electrical analogy from Fig. 3.12 gives

$$L\ddot{q} + \frac{1}{C}q = -R\dot{q} + v_o \cos \Omega t \tag{D.14}$$

where $i = \dot{q} =$ current and

$$\begin{array}{lcl} t & = & \text{time} \\ q & = & \text{charge} \\ L & = & \text{inductance} \\ C & = & \text{capacitance} \\ R & = & \text{resistance} \\ v_o & = & \text{voltage} \\ \Omega & = & \text{driving frequency.} \end{array}$$

The Hamiltonian is

$$\mathcal{H} = \frac{1}{2}L\dot{q}^2 + \frac{1}{2}\frac{1}{C}q^2. \tag{D.15}$$

The time derivative of the Hamiltonian is

$$\dot{\mathcal{H}} = \left[L\ddot{q} + \frac{1}{C}q\right]\dot{q} = \left[-R\dot{q} + v_o \cos \Omega t\right]\dot{q} \tag{D.16}$$

where the goals are to make $\dot{\mathcal{H}} = 0$ and obtain a power factor of 1.

The first goal occurs when

$$\dot{\mathcal{H}} = 0 = [v_o \cos \Omega t - R\dot{q}]\, \dot{q}. \tag{D.17}$$

which implies

$$v_o \cos \Omega t = R\dot{q}. \tag{D.18}$$

The second goal occurs when

$$\dot{\mathcal{H}} = 0 = \left[L\ddot{q} + \frac{1}{C}q\right] \dot{q} \tag{D.19}$$

which implies $\omega^2 = 1/LC = \Omega^2$. To verify this (D.14) is solved for the steady-state solution [38]

$$q(t) = \frac{v_o}{[L^2(\omega^2 - \Omega^2)^2 + R^2\Omega^2]^{\frac{1}{2}}} \cos(\Omega t - \delta) \tag{D.20}$$

where

$$\cos \delta = \frac{L(\omega^2 - \Omega^2)}{[L^2(\omega^2 - \Omega^2)^2 + R^2\Omega^2]^{\frac{1}{2}}}.$$

By imposing $\omega^2 = 1/LC = \Omega^2$ then

$$\cos \delta = 0 \quad \Rightarrow \quad \delta = \pi/2$$

which implies

$$\begin{array}{rcl} q & = & \frac{v_o}{R\Omega} \cos(\Omega t - \frac{\pi}{2}) = \frac{v_o}{R\Omega} \sin \Omega t \\ \dot{q} & = & -\frac{v_o}{R} \sin(\Omega t - \frac{\pi}{2}) = \frac{v_o}{R} \cos \Omega t \end{array}$$

which gives (D.18) and for (D.19) then

$$\begin{array}{rcl} -L(\frac{v_o}{R}\Omega) \sin \Omega t + \frac{1}{C}(\frac{v_o}{R\Omega}) \sin \Omega t & = & \left[-L\Omega + \frac{1}{C\Omega}\right] \frac{v_o}{R} \sin \Omega t \\ & = & \left[-\Omega^2 + \frac{1}{LC}\right] \frac{L}{\Omega} \frac{v_o}{R} \sin \Omega t \\ & = & 0. \end{array}$$

Next, the linear limit cycles for this problem, where $\Omega^2 = 1/LC$ and $\Omega^2 \neq 1/LC$ will be investigated. Figure D.3 (upper-left 3D Hamiltonian plot and upper-right phase-plane plot) shows the linear limit cycle for a power factor of 1 or $\Omega^2 = 1/LC$ where "at least one other trajectory spirals into it." It appears like the response of an undamped, unforced linear

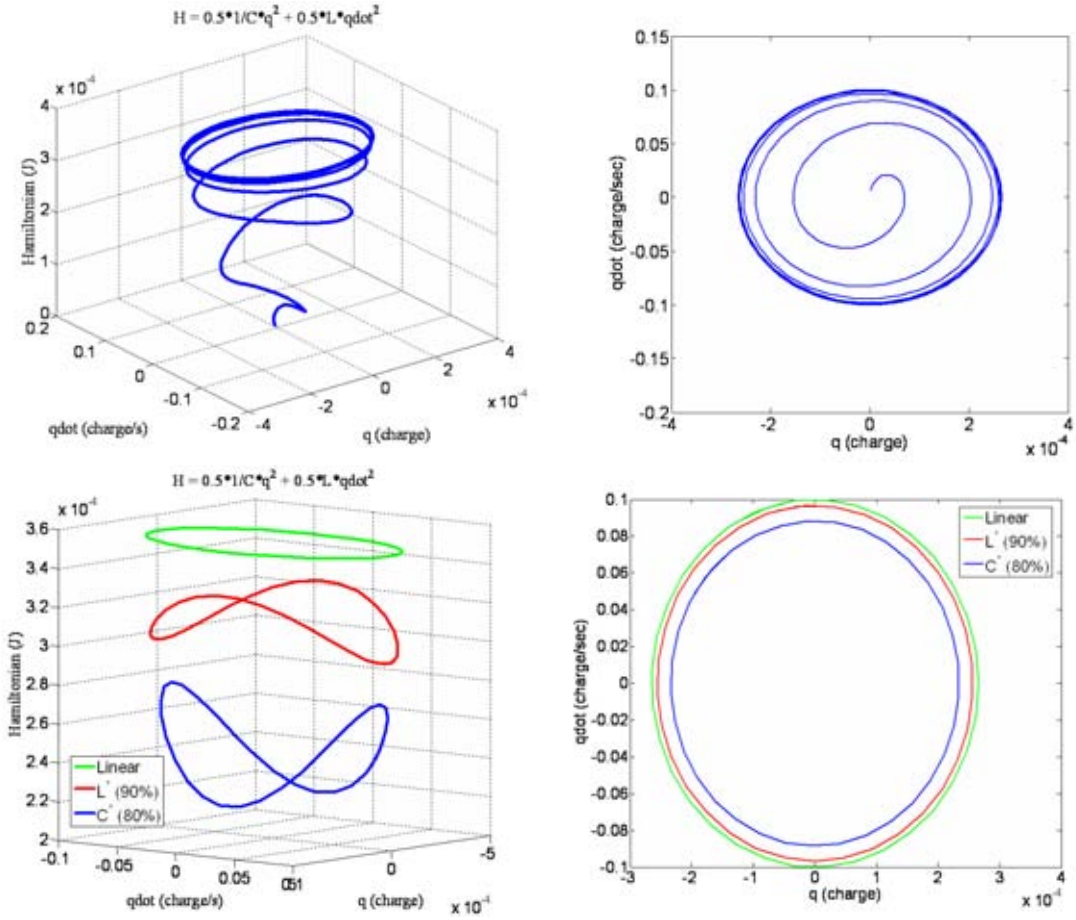

Figure D.3. Linear limit cycle Hamiltonian 3D spiral (upper-left) with corresponding phase plane plot (upper-right). The next 3D plots show the linear, 10% variation in inductance, L or $L' = 90\%$ of L, and 20% variation in capacitance, C or $C' = 80\%$ of C (lower-left) with the corresponding phase plane plots (lower-right)

system. Figure D.3 (linear, 10% variation in L (where $L' = 90\%$ of L), and 20% variation in C (where $C' = 80\%$ of C) are plotted in lower-left along with the phase plane plots lower-right) shows the linear limit cycle for a power factor of less than 1 or $\Omega^2 \neq 1/LC$ (see Table D.1 for numerical values). The energy (exergy) level has dropped and the edges have drooped which results in the concentric ellipses in the phase plane even though the Hamiltonian surface has been deformed by $\Omega^2 \neq 1/LC$. Part of the power flow is being

Table D.1. RLC numerical parameters and results

Case description	L (mH)	C (μF)	R (Ohms)	v_o (Volts)	ω (Hz)	Ω (Hz)	δ (deg)	$\cos(\frac{\pi}{2}-\delta)$ Power Factor
linear	70.362	100.0	10.0	1.0	60.0	60.0	90	1.0
10% variation (L)	63.326	100.0	10.0	1.0	63.25	60.0	75	0.9659
20% variation (C)	70.362	125.0	10.0	1.0	53.67	60.0	118	0.8829

used for "VAR support" or reactive power to ensure a concentric linear limit cycle in the phase plane at a lower energy (exergy) level. Notice that for

$$\oint_{\tau} \dot{\mathcal{H}} dt = \mathcal{H}_{cyclic} = 0$$

implies that $\mathcal{H}(t)$ is cyclic and not constant, where $\tau = 2\pi/\Omega$ and $\Omega^2 \neq \omega^2 = 1/LC$. Note, the goal of power engineering is to generate a power factor of 1 which is equivalent to generating a linear limit cycle. This "out-of-plane" limit cycle behavior is the first hint at how to generalize (D.5) and (D.7) to nonlinear limit cycles.

D.3 Nonlinear Limit Cycles

This section extends the concept of linear limit cycles to nonlinear limit cycles. The linear mass-spring-damper system is extended to a nonlinear system by adding nonlinear stiffness and damping as shown in Fig. D.4.

The Lagrangian and Hamiltonian for this system are

$$\mathcal{L} = \frac{1}{2}m\dot{x}^2 - \frac{1}{2}kx^2 - \frac{1}{4}k_{NL}x^4 \tag{D.21}$$

$$\mathcal{H} = \frac{1}{2}m\dot{x}^2 + \frac{1}{2}kx^2 + \frac{1}{4}k_{NL}x^4 \tag{D.22}$$

with the following equation of motion

$$m\ddot{x} + kx + k_{NL}x^3 = -f(\dot{x}) + u \tag{D.23}$$

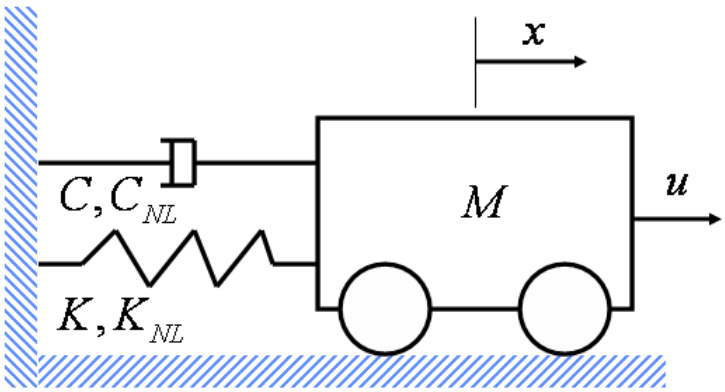

Figure D.4. Nonlinear mass-spring-damper system

where $f(\dot{x})$ is the generalized damping force. The time derivative of the Hamiltonian is

$$\dot{\mathcal{H}} = \left[m\ddot{x} + kx + k_{NL}x^3\right]\dot{x} = \left[-f(\dot{x}) + u\right]\dot{x} \tag{D.24}$$

where the goal is to find the nonlinear limit cycles given by

$$\mathcal{H}_{cyclic} = \oint_{\tau} \dot{\mathcal{H}}dt = \oint_{\tau} \left[m\ddot{x} + kx + k_{NL}x^3\right]\dot{x}dt = \oint_{\tau} \left[-f(\dot{x}) + u\right]\dot{x}dt \tag{D.25}$$

which for a conservative system, $\dot{\mathcal{H}} = 0$ and $\mathcal{H} =$ constant and

$$\left[-f(\dot{x}) + u\right] = 0 \quad \text{(for point-by-point).} \tag{D.26}$$

The more general solution that replaces the point-by-point force balance is a cyclic balance between the power flowing into the system versus the power being dissipated within the system is

$$\mathcal{H}_{cyclic} = \oint_{\tau} \dot{\mathcal{H}}dt = 0 \quad \text{and} \quad \mathcal{H}(t) \quad \text{is cyclic.} \tag{D.27}$$

A familiar example to begin the discussion involving (D.27) is the van der Pol equation

$$\ddot{x} - \mu(1 - x^2)\dot{x} + x = 0. \tag{D.28}$$

The Hamiltonian with non-unity mass and stiffness is

$$\mathcal{H} = \frac{1}{2}m\dot{x}^2 + \frac{1}{2}kx^2 \tag{D.29}$$

with the time derivative of

$$\dot{\mathcal{H}} = [m\ddot{x} + kx]\,\dot{x} = \left[\mu(1-x^2)\dot{x}\right]\dot{x} \tag{D.30}$$

and the nonlinear limit cycle becomes

$$\mathcal{H}_{cyclic} = 0 = \oint_\tau [m\ddot{x} + kx]\,\dot{x}dt = \oint_\tau \left[\mu(1-x^2)\dot{x}\right]\dot{x}dt \tag{D.31}$$

which implies

$$\oint_\tau \left[\mu\dot{x}^2\right] dt = \oint_\tau \left[\mu x^2\dot{x}^2\right] dt. \tag{D.32}$$

Equation (D.32) is satisfied and the numerical results are plotted in Fig. B.4. The exergy balance over a cycle is shown in Fig. B.6 (neutral case). This is a stable limit cycle. Notice, the non-elliptical shape of the nonlinear limit cycle is a result of the cyclic rise and fall of the energy (exergy) level of the system, $\mathcal{H}(t)$, due to the nonlinear damping.

As an interesting analogy to a PID control system, the negative dissipator in the van der Pol system is replaced with an integral term and the nonlinear limit cycle becomes

$$\mathcal{H}_{cyclic} = 0 = \oint_\tau [m\ddot{x} + kx]\,\dot{x}dt = \oint_\tau \left[-K_I \int_0^t x dt_1 - \mu x^2\dot{x}\right]\dot{x}dt \tag{D.33}$$

which implies

$$\oint_\tau \left[-K_I \int_0^t x dt_1\right]\dot{x}dt = \oint_\tau \left[\mu x^2\dot{x}^2\right] dt. \tag{D.34}$$

The numerical results are similar to the discussion of the standard van der Pol case with the numerical results given in Fig. B.8 and the exergy balance over a cycle shown in Fig. B.10 (neutral case).

The second example is a Duffing oscillator equation with Coulomb friction given by

$$m\ddot{x} + kx + k_{NL}x^3 = -c\dot{x} - c_{NL}sign(\dot{x}) + u \tag{D.35}$$

and controlled with a PID controller

$$u = -K_P x - K_I \int x dt - K_D\dot{x}. \tag{D.36}$$

The Hamiltonian is

$$\mathcal{H} = \frac{1}{2}m\dot{x}^2 + \frac{1}{2}(k+K_P)x^2 + \frac{1}{4}k_{NL}x^4 \tag{D.37}$$

with a time derivative of

$$\dot{\mathcal{H}} = \left[m\ddot{x} + (k+K_P)x + k_{NL}x^3\right]\dot{x} = \left[-(c+K_D)\dot{x} - c_{NL}sign(\dot{x}) - K_I\int x dt\right]\dot{x}. \tag{D.38}$$

The nonlinear limit cycle occurs when

$$\oint_\tau \left[-(c+K_D)\dot{x} - c_{NL}sign(\dot{x})\right]\dot{x}dt = \oint_\tau \left[K_I\int x dt\right]\dot{x}dt. \tag{D.39}$$

Numerical simulations were performed to demonstrate where the nonlinear stability boundary lies for the Duffing oscillator/Coulomb friction dynamic model subject to PID control. Twelve separate cases (Cases 1-12) were conducted with the numerical values listed in Table D.2. For Case 1, all the generative/dissipative terms are set to zero which results in

Table D.2. Duffing oscillator/Coulomb friction model and PID control system gains (Note: for all cases $\dot{x}_o = 0.0$)

Case No.	K_P (kg/s^2)	K_I (kg/s^3)	K_D (kg/s)	c (kg/s)	C_{NL} (N)	m (kg)	k (N/m)	k_{NL} (N/m^3)	T_f (sec)	x_o (m)	x_r (m)
1	10	0.0	0.0	0.0	0.0	10	10	100.0	10	1	0
2	10	20.0	2.0	0.1	5.0	10	10	100.0	10	1	0
3	10	40.05	2.0	0.1	5.0	10	10	100.0	10	1	0
4	10	80.0	2.0	0.1	5.0	10	10	100.0	10	1	0
5	−200	20.0	2.0	0.1	5.0	10	10	100.0	36	1	0
6	−200	10.0	2.0	0.1	5.0	10	10	100.0	36	1	0
7	−200	1.0	2.0	0.1	5.0	10	10	100.0	36	1	0
8	−200	1.0	2.0	0.1	5.0	10	10	100.0	100	1	0
9	−200	50.0	2.0	0.1	5.0	10	10	100.0	15	1	0
10	−200	30.0	2.0	0.1	5.0	10	10	100.0	36	−1	0
11	10	20.0	2.0	0.1	5.0	10	−200	100.0	50	0	1
12	10	20.0	2.0	0.1	5.0	10	−200	100.0	50	0	−1

a stable orbit for the nonlinear system (see Fig. D.5 - left). In addition, the sum of the

exergy/energy over a cycle between kinetic and potential is zero as shown in offsetting exergy-rate plots in Fig. D.5 (right). For Case 2 the exergy and exergy rate responses (left) along with the integral of position, position, velocity, and acceleration responses (right) are plotted in Fig. D.6. For this case, the dissipative term is greater than the generative term.

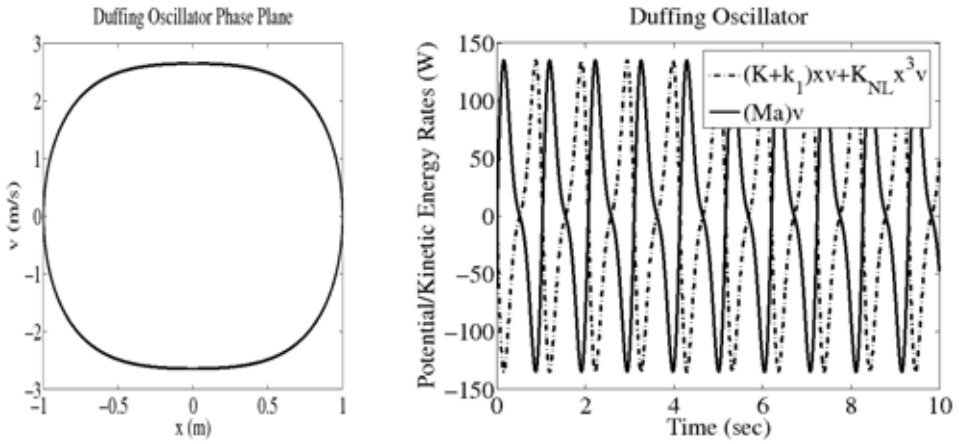

Figure D.5. Case 1 stable phase plane plot (left) and kinetic/potential energy rate responses (right)

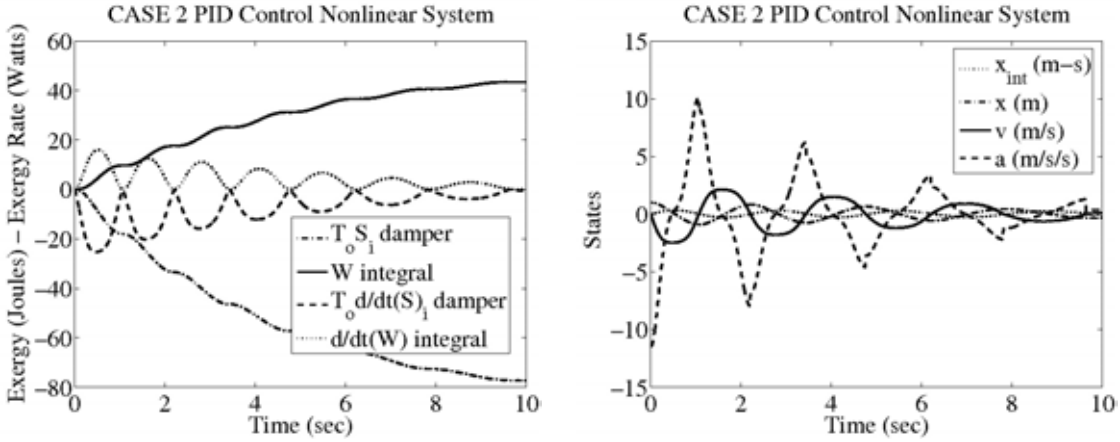

Figure D.6. Case 2 exergy and exerg-rate responses (left) and system responses (right)

This is observed from the decaying system responses. In Case 3 the exergy and exergy rate responses (left) along with the system responses (right) are shown in Fig. D.7. In this case, the average exergy slopes and integrated power areas for the dissipative and generative terms are equivalent which demonstrates (D.39): a nonlinear limit cycle. This results in system responses that do not decay, displaying constant nonlinear oscillatory behavior. In Case 4, the exergy and exergy rate responses (left) along with the system responses (right) are shown in Fig. D.8. In this case, the dissipative term is less than the generative term which results in a system response with increasing nonlinear oscillatory behavior. In

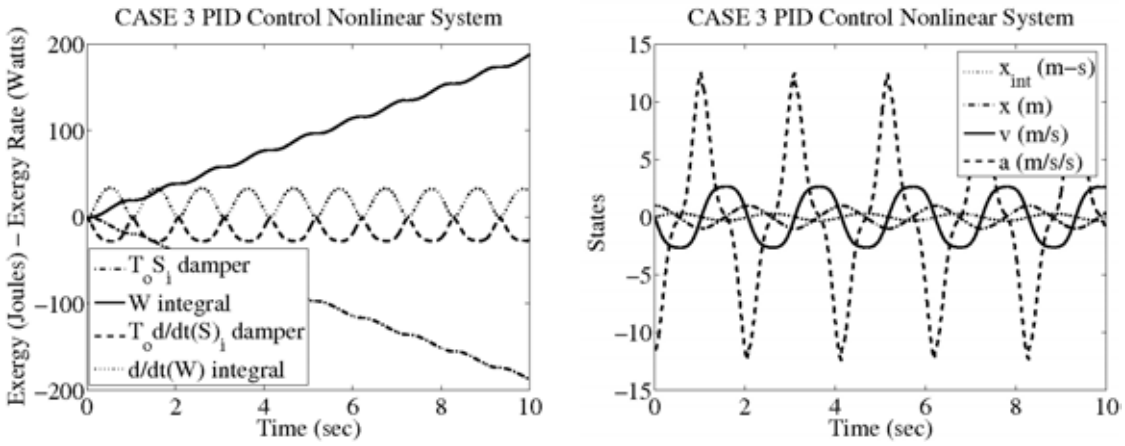

Figure D.7. Case 3 exergy and exergy-rate responses (left) and system responses (right)

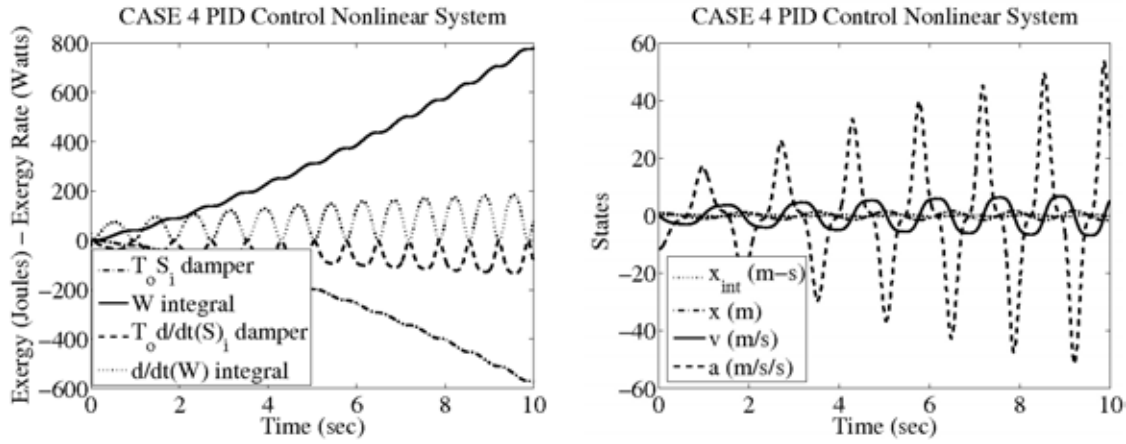

Figure D.8. Case 4 exergy and exergy-rate responses (left) and system responses (right)

summary, Fig. D.9 shows the responses with respect to the Hamiltonian surface with trajectories traversing the surface (left) for each case along with the total exergy responses (right) for the nonlinear system. For Case 3 the nonlinear stability boundary (or neutral stability) is characteristic of an average zero output for the total exergy response or validation of (D.39). For the trajectories on the Hamiltonian surface, Case 2 demonstrates an asymptotically stable decaying response, Case 3 a neutrally stable orbital response, and Case 4 an asymptotically unstable increasing orbit response.

In addition, the stability boundary condition can be used to identify different operating regions for systems that may need to be gain scheduled. For example, the integral gain, in general may be a function of many different parameters

$$K_I = K_I(x_o, \dot{x}_o, C, C_{NL}, K_D).$$

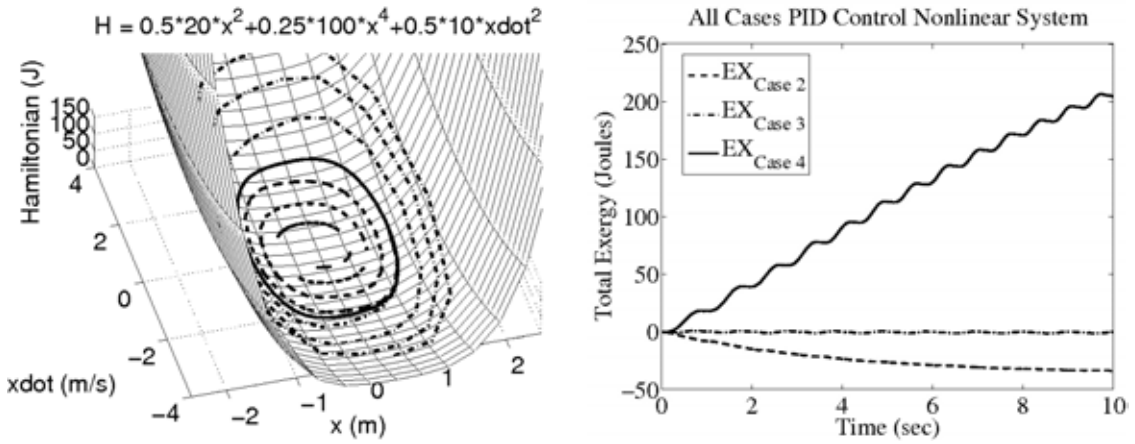

Figure D.9. Cases 2-4: mass-spring-damper with Duffing oscillator/Coulomb friction model numerical results: Hamiltonian 3D surface (left) and total exergy responses (right)

For the purpose of illustration the integral gain was investigated for different initial conditions, x_o, while holding all the other possible parameters constant. The results are shown in Fig. D.10. For several varying initial conditions for x_o, at the stability boundary condition each K_I was determined. The corresponding linear system resulted in constant K_I values which is characteristic of a linear system. The gain scheduling is due to the nonlinear spring. It changes the limit cycle behavior as a function of stored exergy.

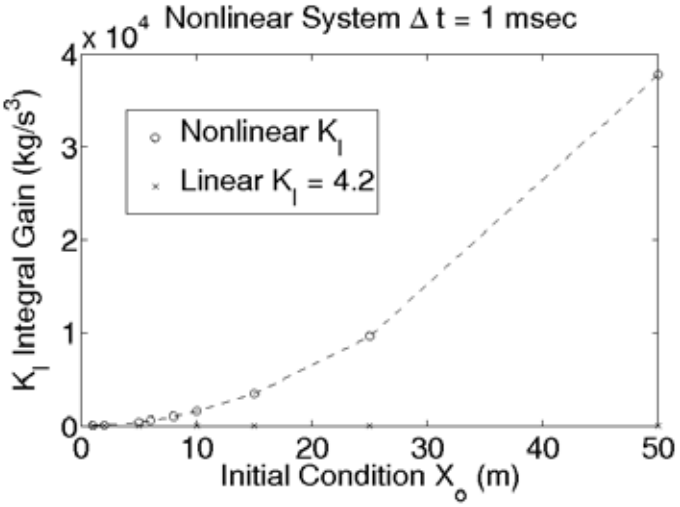

Figure D.10. Gain scheduling with the integral gain as a function of initial conditions

The third example, revisits the previous example of the Duffing oscillator equation with Coulomb friction, however a negative potential or $(K_P + k) < 0$ is investigated (see cases 5-12 in Table D.2). For Cases 5-10, the system is under regulator control, at $(x, \dot{x}) = (0, 0)$

with positive proportional feedback. This causes the point $(x,\dot{x}) = (0,0)$ to be an unstable static node and for the following scenarios, with $(K_P + k) < 0$ the system is forced away from the regulator point.

In Case 5, the system builds up enough energy to transition out of the right well but overshoots into the left well where the process starts again (see Figs. D.11 and D.12). Eventually, the system achieves a balanced equilibrium between both wells, a nonlinear limit cycle. A similar response is shown for Case 6 (see Figs. D.13 and D.14). Note that for a

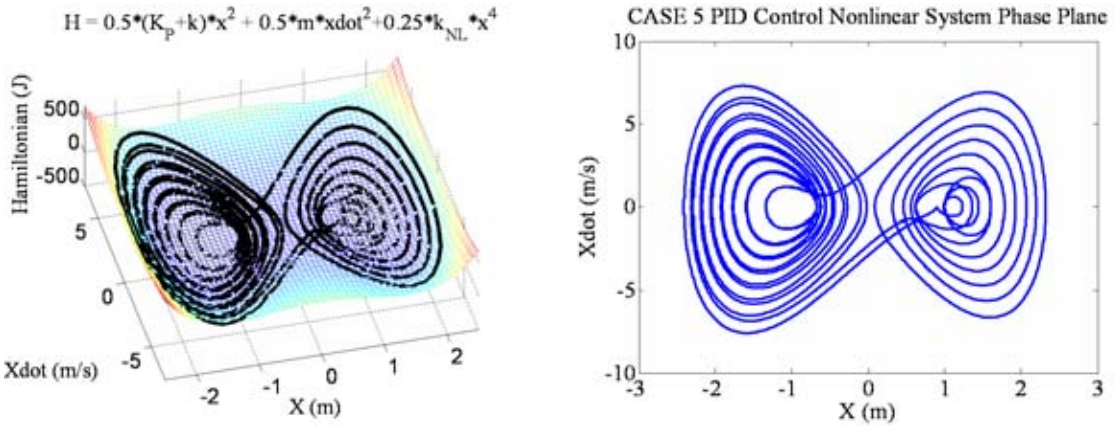

Figure D.11. Case 5 Hamiltonian 3D surface plots (left) and corresponding 2D phase plane plots (right)

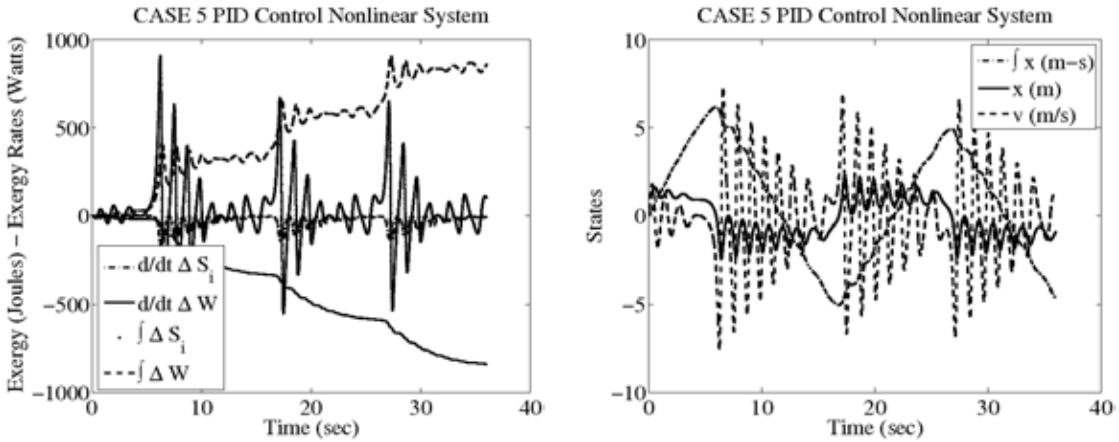

Figure D.12. Case 5 exergy and exergy-rate responses (left) and system responses (right)

reduction in K_I that the responses are slower, in comparison to the previous Case 5.

In Case 7 (see Fig. D.15) the K_I again is reduced resulting in the appearance that the system decays down to a point in the right well. Also note that in Fig. D.16 that the dissipative term

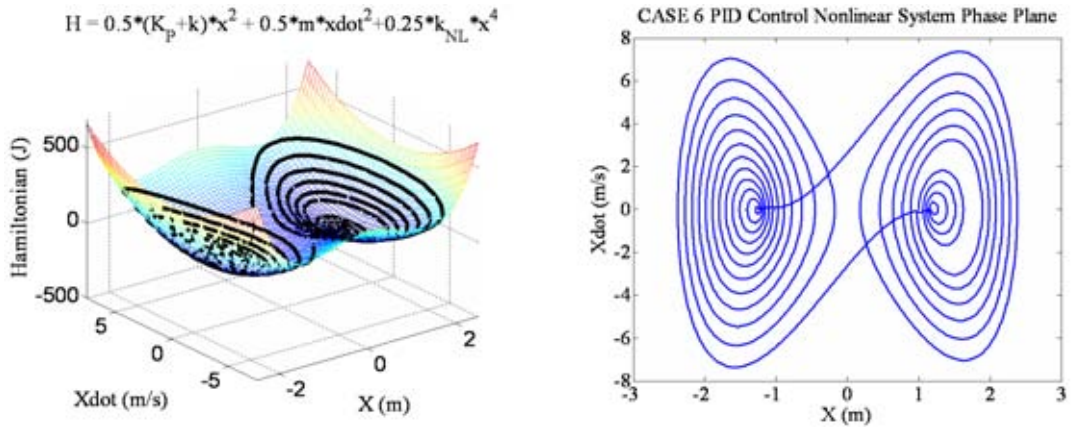

Figure D.13. Case 6 Hamiltonian 3D surface plots (left) and corresponding 2D phase plane plots (right)

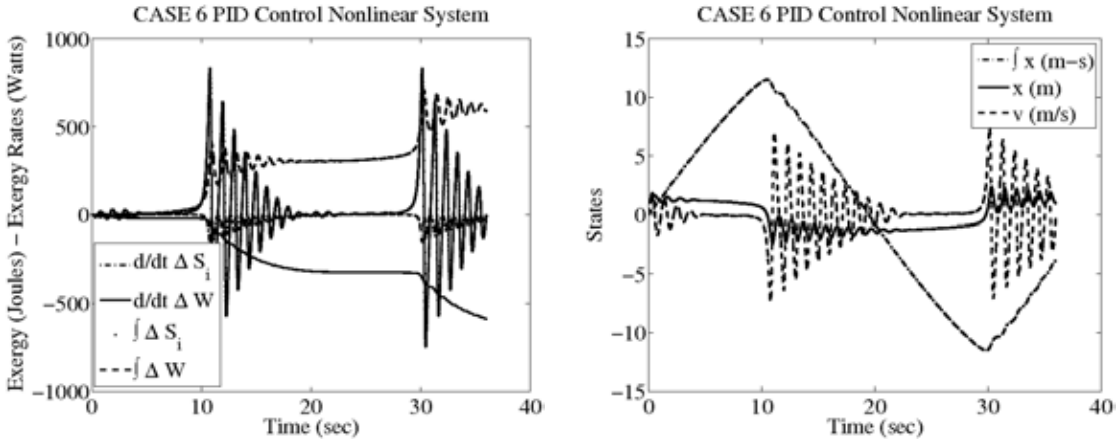

Figure D.14. Case 6 exergy and exergy-rate responses (left) and system responses (right)

is greater than the generator term (left) with corresponding decaying responses in Fig. D.16 (right) for both the position and velocity, respectively. Case 7 is building up slower than previous cases, since K_I is reduced. However, in Case 7 and 8, given enough simulation time, ($t_f = 100$ sec) the generator term eventually builds up enough energy to move out of the right well, but again overshoots (see Fig. D.17) the $(0,0)$ regulator point and spirals down into the left well. The exergy and exergy-rate responses are given in Fig. D.18 (left) along with the corresponding state responses (Fig. D.18 - right).

For Case 9, K_I is increased such that the system traverses around both left and right wells and approaches another higher energy level, nonlinear limit cycle (see Fig. D.19 along with Fig. D.20). In this case the generator term maintains a balance with the opposing damping terms subject to the nonlinear spring effect (refer to Fig. D.10).

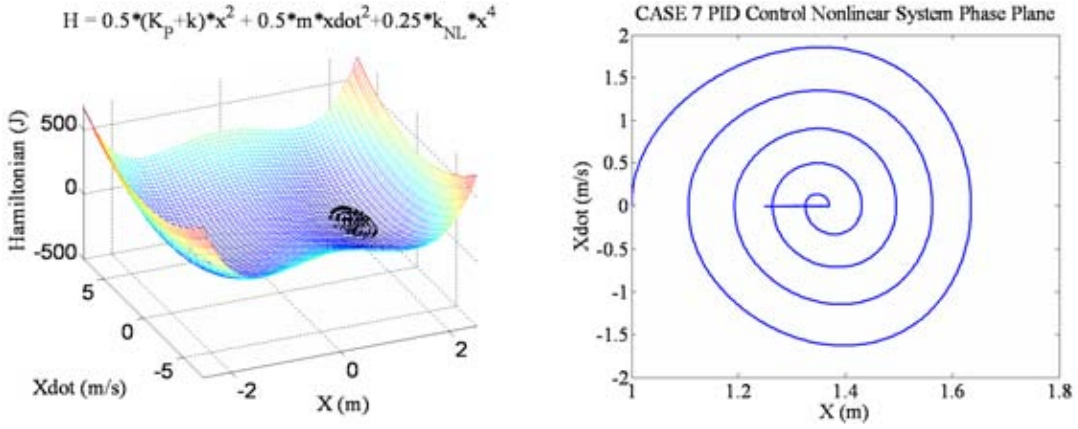

Figure D.15. Case 7 Hamiltonian 3D surface plots (left) and corresponding 2D phase plane plots (right)

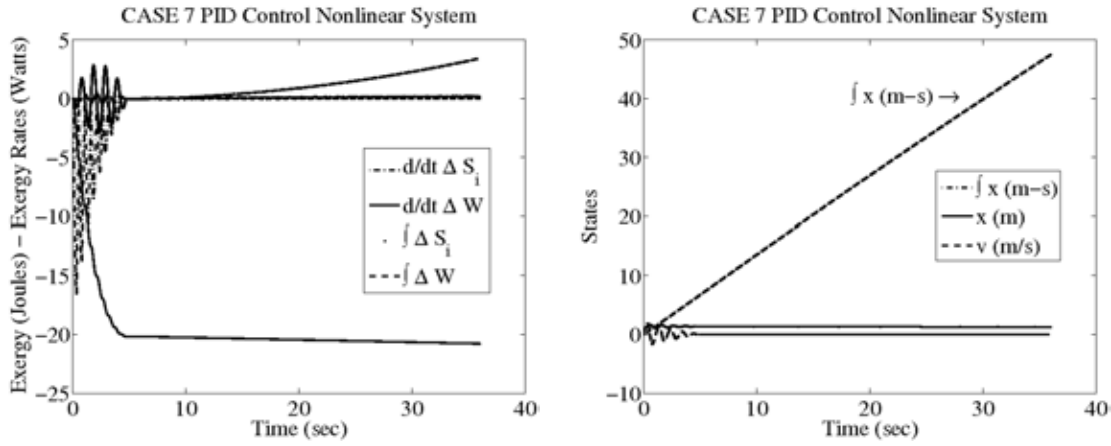

Figure D.16. Case 7 exergy and exergy-rate responses (left) and system responses (right)

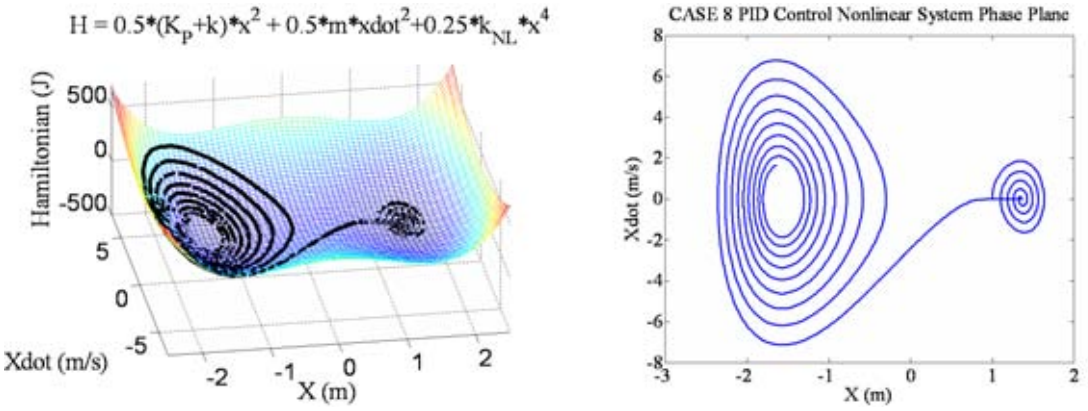

Figure D.17. Case 8 Hamiltonian 3D surface plots (left) and corresponding 2D phase plane plots (right)

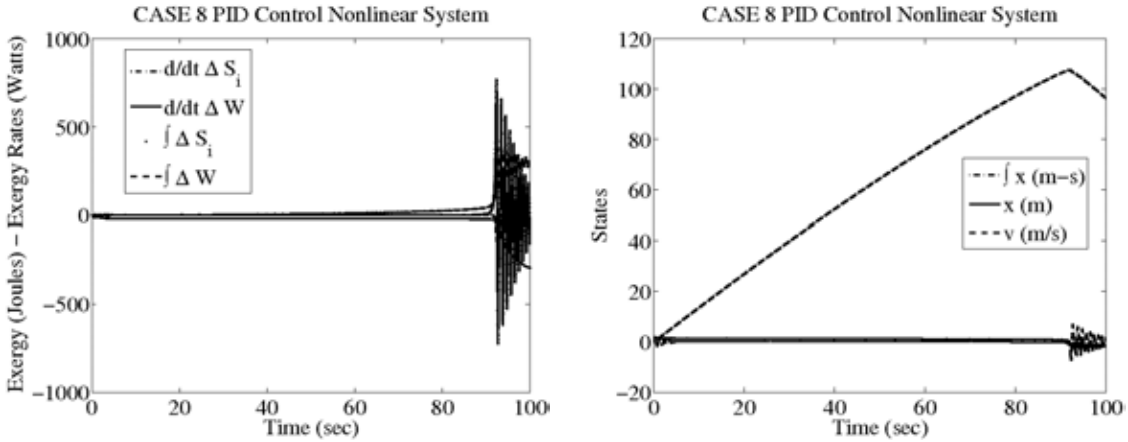

Figure D.18. Case 8 exergy and exergy-rate responses (left) and system responses (right)

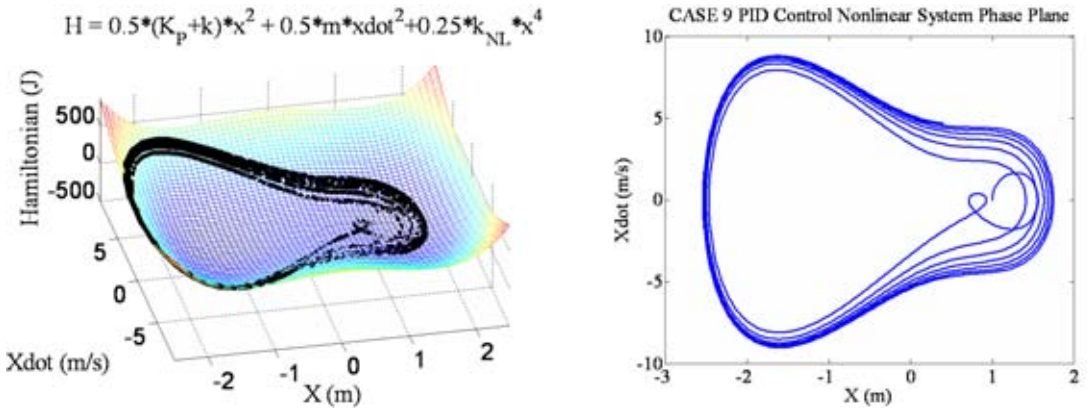

Figure D.19. Case 9 Hamiltonian 3D surface plots (left) and corresponding 2D phase plane plots (right)

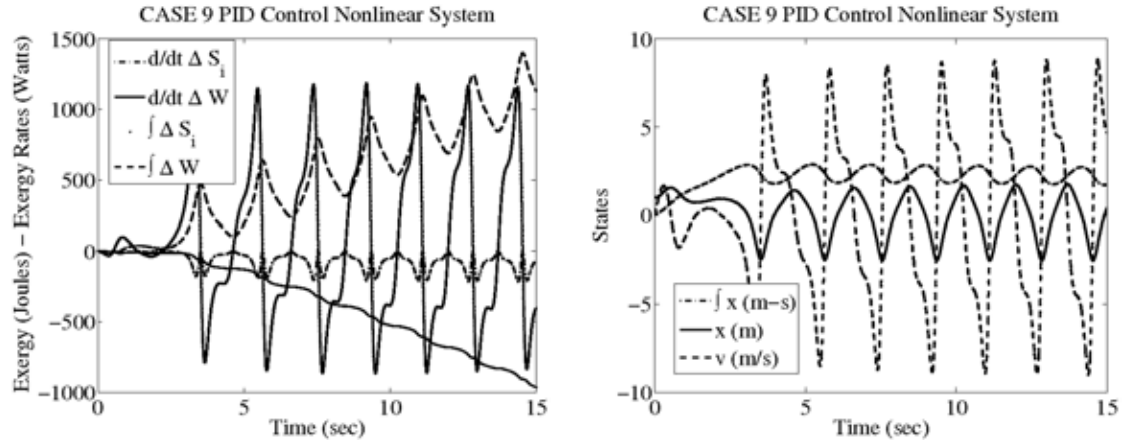

Figure D.20. Case 9 exergy and exergy-rate responses (left) and system responses (right)

Case 10 demonstrates a reduction in K_I and also starts in the left well, builds up enough energy to move over to the right well and eventually comes back to another stable energy state, nonlinear limit cycle, (see Figs. D.21 and D.22).

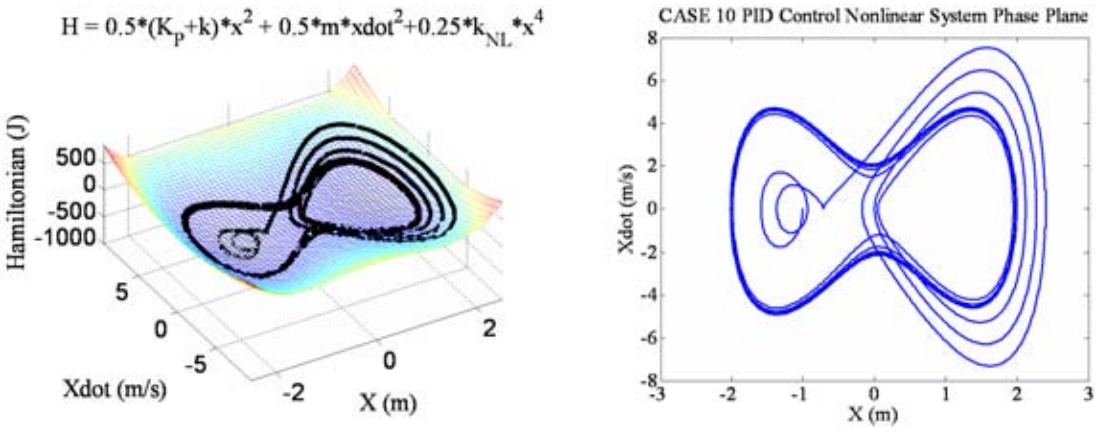

Figure D.21. Case 10 Hamiltonian 3D surface plots (left) and corresponding 2D phase plane plots (right)

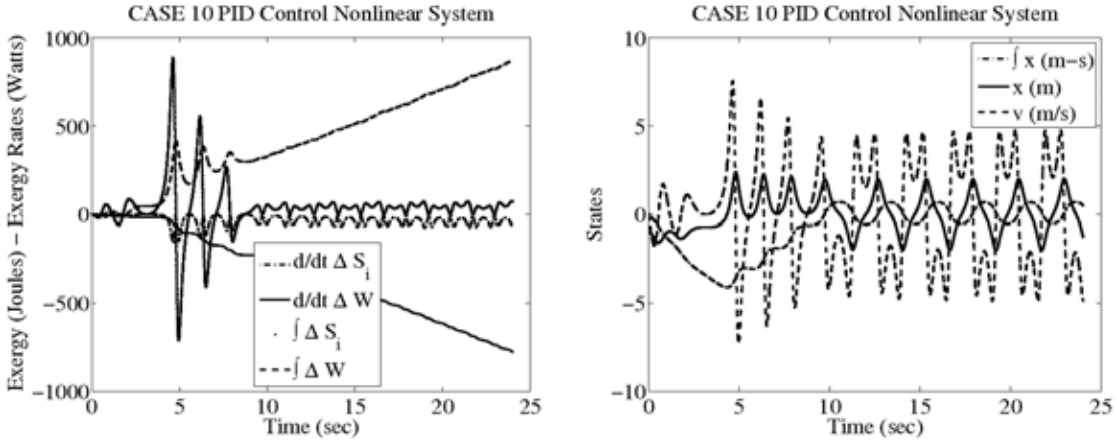

Figure D.22. Case 10 exergy and exergy-rate responses (left) and system responses (right)

For the last two cases (Cases 11 and 12), the PID regulator is converted to a tracking controller for which

$$u = -K_P(x - x_r) - K_I \int (x - x_r) d\tau - K_D(\dot{x} - \dot{x}_r) \tag{D.40}$$

where for this discussion, x_r is a reference step input and the reference velocity is $\dot{x}_r = 0$. The corresponding Hamiltonian becomes

$$\mathcal{H} = \frac{1}{2}m\dot{x}^2 + \frac{1}{4}k_{NL}x^4 + \frac{1}{2}kx^2 + \frac{1}{2}K_P(x - x_r)^2. \tag{D.41}$$

In Case 11, the system is given a unity reference step input for which after moving from $(0,0)$ the system spirals into and converges into the right well at $(1,0)$ (see Figs. D.23 and D.24).

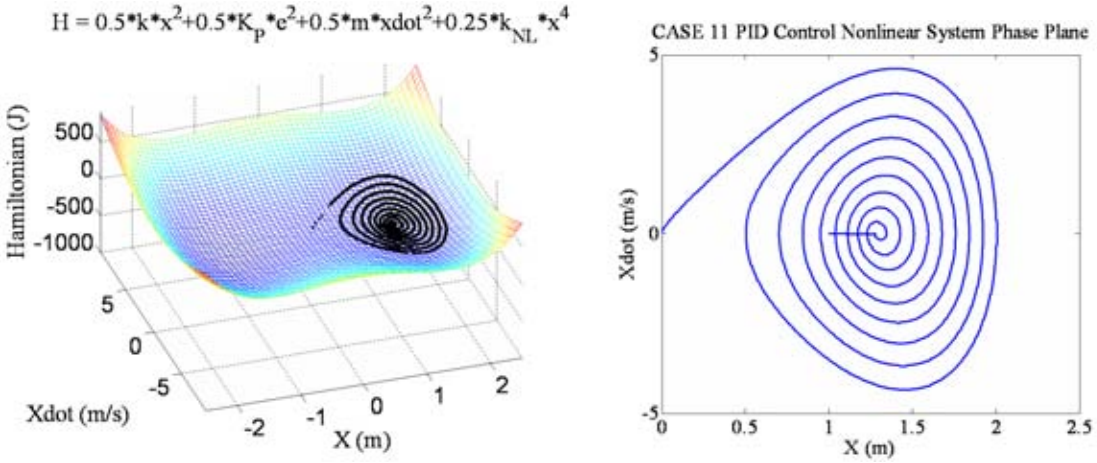

Figure D.23. Case 11 Hamiltonian 3D surface plots (left) and corresponding 2D phase plane plots (right)

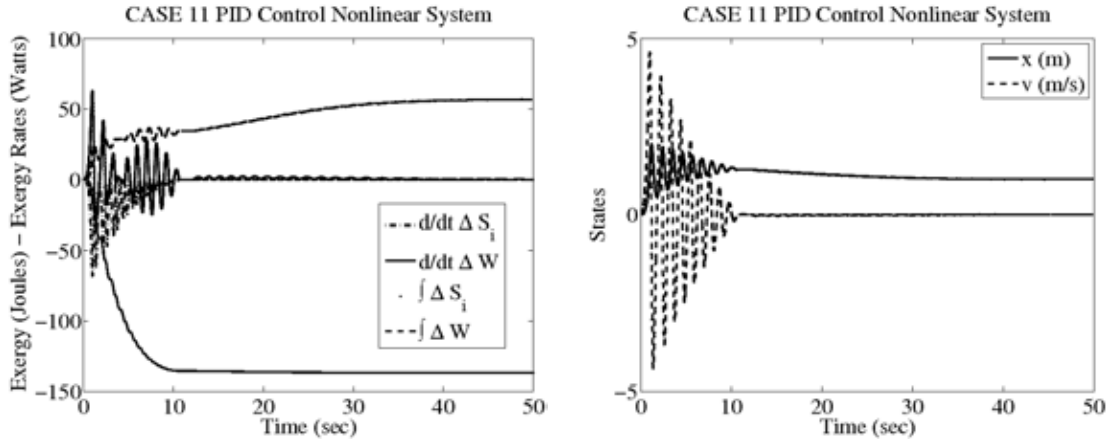

Figure D.24. Case 11 exergy and exergy-rate responses (left) and system responses (right)

In Case 12, the system also starts at $(0,0)$ and is commanded to step into the left well at $(-1,0)$ for which the results also spiral and converge to the appropriate final condition (see Figs. D.25 and D.26). In addition, for comparative purposes without simulation plots, the reference operating point was set to $(x_r, \dot{x}_r) = (0,0)$ (the unstable node) and for nonzero initial conditions, the tracking controller still eventually overshoots the set point with very similar results to the previous cases.

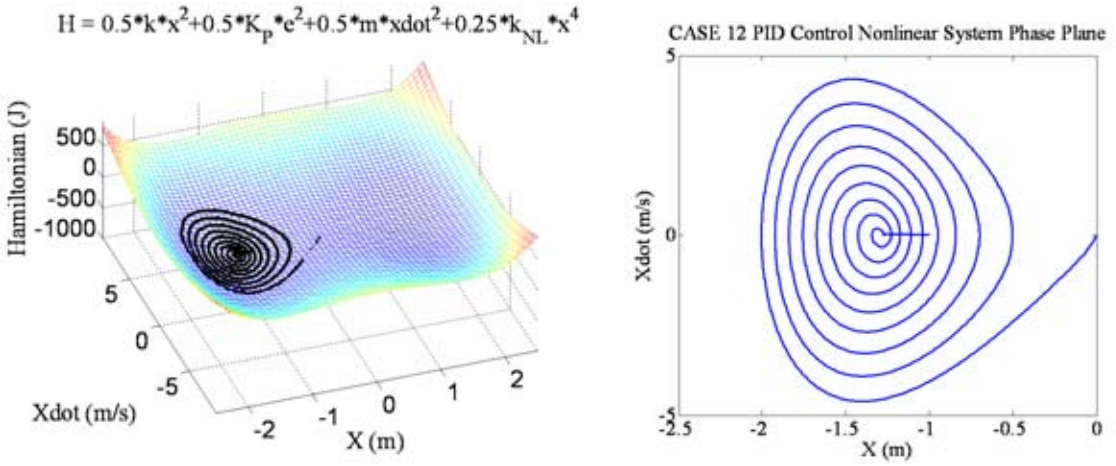

Figure D.25. Case 12 Hamiltonian 3D surface plots (left) and corresponding 2D phase plane plots (right)

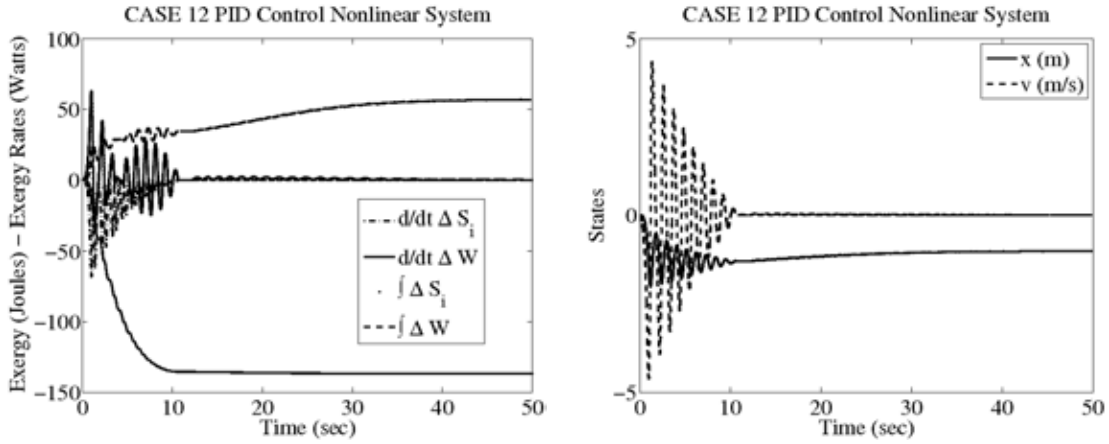

Figure D.26. Case 12 exergy and exergy-rate responses (left) and system responses (right)

This exergy/entropy control analysis and design has provided insight for the investigation of forced nonlinear systems. Both stability and performance can be further characterized and synthesized with a better understanding of limit cycles and their relationship and role played with respect to the nonlinear system.

The last example is a generalization of (D.23). Sabatini [39] discusses the uniqueness of limit cycles for a class of plane differential systems defined by

$$\begin{aligned} x' &= \beta(x)\,[\phi(y) - F(x,y)] \\ y' &= -\alpha(y)g(x). \end{aligned} \tag{D.42}$$

The system (D.42) contains the particular cases of Lotka-Volterra systems, the Rayleigh equation, the Liénard equation, the van der Pol equation, and more general second order equations.

In particular, if one chooses $\beta(x) = \alpha(y) = 1, F(x,y) \equiv F(x)$, and $\phi(y) = y$ then the Liénard equation results

$$x'' + f(x)x' + g(x) = 0. \tag{D.43}$$

where $f(x) = \partial F(x)/\partial x$ which leads to the van der Pol equation for $g(x) = x$ and $f(x) = -\mu(1-x^2)$

$$x'' - \mu(1-x^2)x' + x = 0. \tag{D.44}$$

Additionally, if one chooses $\beta(x) = \alpha(y) = 1, F(x,y) = F(x), g(x) = x$ then the Rayleigh equation results in

$$y'' - F(-y') + \phi(y) = 0. \tag{D.45}$$

In this example, the Liénard systems,

$$x' = y - F(x), \quad y' = -g(x) \tag{D.46}$$

will be investigated, where a unique limit cycle exists when

$$\int_0^T F(x)g(x)dt = 0 \tag{D.47}$$

for every cycle [39]. The goal is to show that (D.47) is equivalent to (D.27). The first step is to rewrite (D.46) in second order form

$$\begin{aligned} \dot{x} &= y - F(x), \quad \dot{y} = -g(x) \\ \ddot{x} &= \dot{y} - \tfrac{d}{dt}\,(F(x)) = -g(x) - f(x)\dot{x} \end{aligned}$$

and simplifying gives

$$\ddot{x} + f(x)\dot{x} + g(x) = 0. \tag{D.48}$$

The second step is to formulate the Hamiltonian for (D.48)

$$\mathcal{H} = \frac{1}{2}\dot{x}^2 + \mathcal{V}(x) \tag{D.49}$$

where $m = 1$ and $\partial \mathcal{V}(x)/\partial x = g(x)$. Next take the time derivative of the Hamiltonian (D.49) or

$$\dot{\mathcal{H}} = [\ddot{x} + g(x)]\,\dot{x} = -f(x)\dot{x}^2 = -\frac{d}{dt}\left(F(x)\right)\dot{x} \tag{D.50}$$

which leads to a limit cycle

$$\mathcal{H}_{cyclic} = 0 = \oint_\tau [\ddot{x} + g(x)]\,\dot{x}dt = \oint_\tau \left[-f(x)\dot{x}^2\right] dt = \oint_\tau \left[-\frac{d}{dt}\left(F(x)\right)\dot{x}\right] dt. \tag{D.51}$$

The third step is to rewrite (D.47) as

$$\begin{array}{rcl} \int_0^T F(x)g(x)dt & = & \oint_\tau F(x)g(x)dt = \int_0^T [y - \dot{x}]\, g(x)dt = \int_0^T \left[-y\dot{y} - \frac{\partial \mathcal{V}(x)}{\partial x}\dot{x}\right] dt \\ & = & -\frac{1}{2}y^2|_0^T - \mathcal{V}(x)|_0^T. \end{array} \tag{D.52}$$

The fourth step is to rewrite (D.51) as

$$\begin{array}{rcl} \int_0^T f(x)\dot{x}^2 dt & = & \int_0^T \frac{d}{dt}\left(F(x)\right)\dot{x}dt = \int_0^T \dot{F}\,[y - F]\,dt = -\frac{1}{2}F^2|_0^T + \int_0^T \dot{F}ydt \\ & = & -\frac{1}{2}F^2|_0^T + Fy|_0^T + \int_0^T Fgdt = \left[\frac{1}{2}y^2 - \frac{1}{2}\dot{x}^2\right]_0^T + \int_0^T F(x)g(x)dt \end{array} \tag{D.53}$$

which upon substitution of (D.52) gives

$$\oint_\tau f(x)\dot{x}^2 dt = \int_0^T f(x)\dot{x}^2 dt = -\left[\frac{1}{2}\dot{x}^2 + \mathcal{V}(x)\right]_0^T = -\mathcal{H}_{cyclic} = 0. \tag{D.54}$$

This example demonstrates the applicability of the Hamiltonian-based approach to a "large class" of nonlinear systems.

Finally, Appendix B provides the connections between Hamiltonian mechanics, irreversible thermodynamics, and nonlinear control theory to develop necessary and sufficient conditions for stability of nonlinear systems including the generalized stability boundary: *the limit cycle*.

D.4 The Power Flow Principle of Stability for Nonlinear Systems

A familiar eigenvalue problem results from (D.5) with $\dot{H} = 0$ and $[-c\dot{x} + u] = 0$ as

$$\begin{array}{lcl} m\ddot{x} + kx & = & 0 \\ \left[s^2 + \frac{k}{m}\right] x(s) & = & 0 \\ s^2 + \frac{k}{m} & = & 0 \end{array}$$

which is the undamped natural frequency.

A second eigenvalue problem is discussed in Reference [13] with respect to (D.12) as

$$\begin{array}{ll} m\ddot{x} + (k + K_P)x = 0 & -(c + K_D)\dot{x} - K_I \int x dt = 0 \\ \left[s^2 + \frac{1}{m}(k + K_P)\right] x(s) = 0 & [(c + K_D)s + K_I/s] x(s) = 0 \\ s^2 + (k + K_P)/m = 0 & \left[s^2 + K_I/(c + K_D)\right] x(s) = 0 \\ & s^2 + K_I/(c + K_D) = 0 \end{array}$$

which leads to a result of

$$\frac{(k + K_P)}{m} = \frac{K_I}{(c + K_D)} = \omega^2$$

for the existence of a linear limit cycle. This result is verified using the Routh-Hurwitz analysis in [13].

Now, a nonlinear extension to the previous eigenvalue problems can be discussed with respect to (D.51)

$$\oint_\tau [\ddot{x} + g(x)]\dot{x} dt = \oint_\tau \left[-f(x)\dot{x}^2\right] dt = 0.$$

The first term describes the nonlinear frequency content [40] of the undamped/undriven system

$$\ddot{x} + g(x) = 0$$

which effectively extends the undamped natural frequency to nonlinear systems and defines the Hamiltonian surface as well as the static stability of the system. The second term describes the dynamic stability of the nonlinear system and the existence of a limit cycle

$$\oint_\tau \left[-f(x)\dot{x}^2\right] dt \overset{>}{<} 0 \qquad \text{and} \qquad \oint_\tau \left[-f(x)\dot{x}^2\right] dt = 0$$

which is an extension of the real part of the eigenvalue (D.13) to nonlinear systems.

For example, equation (D.38) shows a nonlinear frequency content (amplitude dependent) and a resulting coupling into the effective damping which produces initial condition dependent limit cycle behavior (refer to Figures D.8 and D.10).

DISTRIBUTION:

1 MS 1202
Timothy M. Berg, 05624

1 MS 1003
John T. Feddema, 06473

1 MS 1137
Robert J. Glass, Jr., 06326

1 MS 1235
Steven Y. Goldsmith, 05633

1 MS 1137
Randall A. Laviolette, 06326

10 MS 1104
Rush D. Robinett, III, 06330

1 MS 1002
Stephen C. Roehrig, 06300

1 MS 1002
Jason E. Stamp, 06332

1 MS 1104
Marjorie L. Tatro, 06200

2 MS 0755
Juan J. Torres, 06332

2 MS 1108
David G. Wilson, 06332

2 MS 9018
Central Technical Files, 8944

2 MS 0899
Technical Library, 4536

1 MS 0161
Legal Intellectual Property, 11500